BNL-21638

Perovskites and Garnets

C. P. Khattak
Physics Department
Brookhaven National Laboratory*
Upton, New York 11973

and

F. F. Y. Wang
Department of Materials Science
State University of New York
Stony Brook, New York 11794

*Work at Brookhaven performed under the auspices of the U. S. Energy Research and Development Administration.

CONTRACT NO. E(30-1)-16

DISCLAIMER

Chapter 30

Perovskites and Garnets

List of Figures

30.1. Introduction

The extensive research devoted to the physics and chemistry of solids during the last quarter of a century has led to great advances in the understanding of the properties of solids in general. One area of very active research has been mixed oxide systems. These have been of particular interest because of their stability and the fact that a wide range of properties can be obtained by substitution of one ion for another. Two of the most extensively studied groups of compounds are the perovskites and garnets.

Ever since the discovery of the ferroelectric properties of barium titanate, perovskite compounds of the type ABO_3 have been widely studied. They now constitute a large group of materials of great importance in solid state physics and chemistry. For example, the electrical conductivity of perovskites varies over many orders of magnitude. Many such as $BaTiO_3$ and $SrTiO_3$ are noted for their high resistivities, which makes them useful as dielectric materials, while others such as $CaMoO_3$ and $LaTiO_3$ are fairly good conductors or semiconductors. Strontium-doped $LaCrO_3$ is currently a possible candidate for high temperature electrodes. A novel property recently reported is the insulator-metal transition in Sr-doped $LaVO_3$. Lead zirconate-lead titanate solid solutions have been used in solid state devices because of their piezoelectric properties. Various perovskites have been utilized for their optical properties such as electro-optic effect, coloration by light, application in laser host materials, etc. In addition to these applications, certain perovskite oxides have catalytic properties comparable to those of platinum in the oxidation of carbon monoxide and hydrocarbons. This is of obvious significance in

the area of automobile emission control. The catalytic properties have also been utilized for making ethanol sensors (Obayaski et al, 1976).

The discovery of ferrimagnetism in yttrium iron garnet has attracted attention to the use of these materials for microwave device applications. To date garnets are the most useful materials in the microwave industry because of their magnetization, linewidth, Curie temperature and g-factor properties. With the advent of solid state lasers, yttrium aluminium garnet was soon found to be an excellent laser host material for room temperature and high power applications.

Current research on weakly ferromagnetic materials, such as garnets and orthoferrites, for magnetic bubble domain devices has stimulated further interest in the magnetic properties of these compounds. These devices will be used for integrated circuit memory and charged coupled devices in the next generation of computer memory technology.

30.2. Perovskites

30.2.1 Preparation

The perovskite structure is a close-packed lattice with the general formula ABX_3. Almost all the known rare-earth perovskites are oxides with the rare-earth ion occupying the A sites and the present discussion will hence be restricted to ABO_3 type compounds. Since most of the rare-earth ions are stable only in the trivalent state the valence relationship is $A^{3+}B^{3+}O_3$. It is much easier to obtain the compounds in polycrystalline than in single crystal form; however in some instances crystals have been prepared for special applications.

A. Powder Synthesis

Many of the perovskite compounds can be prepared by high temperature solid state reaction of binary oxides or peroxides. However, some of these tend to be refractory and hence unreactive. Others have a tendency to hydrate or oxidise and are inconvenient to use. Therefore, it is preferable to use carbonates, oxalates, or other easily decomposable compounds, assuming they can be obtained with suitable purity. These materials are usually in the form of fine powders and decompose in the initial stages of the reaction so that faster reaction rates are obtained. In some cases fine powders may be obtained by evaporation of solutions. The rare-earth raw materials are generally sesquioxides. Since solid state reactions often do not proceed to completion on the first firing, repeated regrinding and reheating is usually necessary. The reaction is conveniently followed by weight loss measurements and by x-ray analysis. The reaction is generally carried out in alumina, zirconia or platinum crucibles which are fairly inert towards these compounds. However, if necessary, reaction of the crucible is avoided by placing the reactants on top of compacts of the same material.

In a typical preparation of $LaCoO_3$ powder, an equimolar mixture of the appropriate oxalates was decomposed by slow heating to 600°C. The resultant material was pressed into pellets and fired at 1000 to 1200°C for two days. Repeated grinding and firing was necessary to eliminate the unreacted material (Raccah and Goodenough, 1967).

If one of the constituent materials is volatile special precautions need to be taken. Problems of this nature are frequently encountered in the synthesis of lead-containing perovskites due to the volatility of lead oxide. Under these circumstances the reaction is carried out in a lead oxide atmosphere, by using excess lead oxide, or in a closed system such as an evacuated silica tube.

In some instances the valence state of an ion may be different in the final compound from that in an available raw material. For example, in $LaVO_3$ the vanadium is in the trivalent state whereas it is in a pentavalent state in V_2O_5. Thus $LaVO_3$ was synthesized by reacting La_2O_3 and V_2O_5 in a vacuum of 10^{-4} mm (Shin-ike et al, 1976). In the case of $LaNiO_3$, the compound was prepared by reacting the appropriate oxalates in oxygen (Goodenough and Raccah, 1965).

In general, conditions which are ideal for the formation of one compound may be unsuitable for another similar material. Hence the proper equilibrium conditions for the synthesis of each compound under study must be determined.

B. Crystal Growth

Although single crystals of some perovskite compounds have been grown in large sizes, those containing rare-earths have generally been rather small. This may be because they have high melting points and suitable fluxes are not known. Furthermore, most of the rare-earth perovskites undergo phase transi-

tions at elevated temperatures which present problems in the preparation of single crystals by many of the usual techniques.

A majority of the rare-earth perovskites have been grown from a fluxed melt. The most commonly used fluxes are lead oxide and lead fluoride. Boron oxide is generally added to increase the solubility. Single crystals are grown by heating the solute and flux to sufficiently high temperatures followed by either slow cooling or evaporation of the flux. A problem commonly encountered in the use of such a technique is the entrapment of lead into the perovskite lattice. It has been found that the growth of $LaCrO_3$ crystals by evaporation of a PbF_2-B_2O_3 flux at 1250°C, resulted in the incorporation of about 7 atomic percent of lead in the compound (Khattak, 1974).

In a fluxed solution there are generally a number of constituents. Under these circumstances the possibility of a competing phase forming instead of the perovskite phase must be considered. For example, it has been found that for $RAlO_3$ (R = Eu to Er) the garnet phase, $R_3Al_5O_{12}$, has an increasing tendency to form as the radius of the rare earth ion decreases (Wanklyn et al, 1975). Flicstein and Schieber (1973) found that the ratio of Dy_2O_3:Al_2O_3:PbF_2 was decisive in the formation of the perovskite, garnet or oxyfluoride phase.

The problems associated with flux growth have been overcome by the growth from the melt as in the case of $LaVO_3$ (Rogers et al, 1966). Another method developed recently is the accelerated crucible rotation technique (ACRT) which greatly reduces the problems of diffusion and homogenization in conventional fluxed melts (Scheel, 1972). In other cases high pressure has been utilized for growth of the perovskite phase. Another method developed for orthoferrites for use in bubble domain devices involves the growth of thin films of

these compounds. Shick and Nielsen (1971) have utilized the liquid phase homo-epitaxial growth technique for this purpose.

Some excellent reviews of single crystal growth techniques have been given by Laudise (1970), Goodenough et al (1972), Wanklyn (1972), Elwell and Scheel (1975). Details of single crystal growth of a number of rare-earth perovskites are given in Table 30.1.

Table 30.1. Crystal Growth Details for Some of the Rare-Earth Perovskite Oxides

Abbrieviations used:

ACRT - Accelerated Crucible Rotation Technique
CZG - Czochralski Growth
EV - Evaporation
HEG - Homo-epitaxial Growth
HPS - High-pressure Solution Growth
HYG - Hydrothermal Growth
LPE - Liquid Phase Epitaxy

Crystal	Technique	Flux	Temp. Range (°C)	Cooling Rate (°C/hr)	Approximate Dimensions (mm)	References
$LaAlO_3$(Mn)	EV	$Pb_7O_2F_{10}$	1200	-	3 x 3 x 0.4	Tsushima (1966)
$LaAlO_3$	SC	PbO-PbF_2	1200 - 800	1.5 - 2	10	Zonn & Jaffe (1968)
$LaAlO_3$(^{17}O)	EV	PbO-PbF_2	1280	-	3	Garton et al (1972)
$LaAlO_3$	SC	PbO-PbF_2-V_2O_5	1300 - 930	0.5	11 x 9 x 6	Kjems et al (1973a)
$LaCoO_3$	EV	PbO-PbF_2	1250	-	2 x 1 x 1	Wanklyn (1972)
$LaCrO_3$	EV	PbF_2-B_2O_3	1240	-	5 x 4 x 4	Wanklyn (1969)
(La,Pb)MnO_3	SC	PbF_2-PbO	1250	1	-	Morrish et al (1969)
(La,Pb)MnO_3	SC	PbF_2-PbO	1150	-	1 - 5	Janes and Bodnar (1971)
$La_{0.69}Pb_{0.31}MnO_3$	SC	PbO-B_2O_3	1010 - 850	50	5	Vogel and Fleming (1975)
$LaVO_3$	SC	from melt	1280	5	-	Rogers et al (1966)
$Ba(La_{0.5}Ta_{0.5})O_3$	SC	BaF_2	-	-	0.5	Galasso et al (1966)

Table 30.1 (Cont'd)

Crystal	Technique	Flux	Temp. Range (°C)	Cooling Rate (°C/hr)	Approximate Dimensions (mm)	References
$Ba(Gd_{0.5}Ta_{0.5})O_3$	SC	BaF_2	-	-	0.5	Gallasso et al (1966)
$Ba(Lu_{0.5}Ta_{0.5})O_3$	SC	BaF_2	-	-	0.5	Gallasso et al (1966)
$BaLaLiWO_6$	CZG	-	-	-	5-10 mm/hr	Brixner (1974)
$BaLaLiMoO_6$	HPS	-	-	-	-	Brixner (1974)
$CeAlO_3$	SC	KF	1300 - 840	4 - 5	0.05	Zonn (1965)
$PrAlO_3$	SC	$PbO-PbF_2$	1285 - 960	3.5	3	Garton and Wanklyn (1967)
$PrAlO_3$	SC	$PbO-PbF_2$	1300 - 800	4.5	5	Zonn and Jaffe (1968)
$PrAlO_3$	SC	$PbO-PbF_2-B_2O_3$	1300 - 950	0.5	20 x 20 x 10	Bergeneau et al (1974)
$(Pr,Pb)MnO_3$	SC	$PbO-PbF_2$	1150	-	5	Janes and Bodner (1971)
$NdAlO_3$	SC	$PbO-PbF_2$	1300 - 800	4.5	5	Zonn and Jaffe (1968)
$NdAlO_3$	SC	$PbO-PbF_2$	1280 - 910	0.7	7	Garton and Wanklyn (1967)
$(Nd,Pb)MnO_3$	SC	$PbO-PbF_2$	1150	-	5	Janes and Bodner (1971)
$TbAlO_3$	SC	$PbO-PbF_2-B_2O_3$	1300 - 900	2	-	Holmes et al (1968)
$TbAlO_3$	SC	$PbO-PbF_2-B_2O_3$	1280 - 950	2.5	3 x 2 x 1.5	Wanklyn (1969)
$TbAlO_3$	SC	$Bi_2O_3-B_2O_3-Tb_4O_7$	1315 - 815	2	3.5 x 2.5 x 2	Wanklyn (1969)
$SmAlO_3$	SC	$PbO-PbF_2$	1290 - 960	2.3	3	Garton and Wanklyn (1967)
$SmAlO_3$	SC	$PbO-PbF_2$	1200 - 800	1.5	10	Zonn and Jaffe (1968)

Table 3D.1 (Cont'd)

Crystal	Technique	Flux	Temp. Range (°C)	Cooling Rate (°C/hr)	Approximate Dimensions (mm)	References
$SmFeO_3$	SC	$PbO-PbF_2$	1280 - 900	-	-	Schieber (1964)
$(Sm,Tb)FeO_3$	SC	$PbO-PbF_2-B_2O_3$	1300 - 900	0.5	15	Van Uitert et al (1970a)
$(Sm_{0.55}Tb_{0.45}FeO_3$	HEG	$PbO-B_2O_3$	990 - 875	2 - 20	1	Shick and Nielsen (1971)
$Sm_{0.55}Tb_{0.45}FeO_3$	SC/EV	$PbO-PbF_2-B_2O_3$	1300 - 970	0.5	-	Quon et al (1971)
$Sm_{0.55}Tb_{0.45}FeO_3$	SC	$PbO-PbF_2-B_2O_3$	1280 - 950	1.25	10 x 10 plate	Nakada et al (1972)
$(Sm,Dy)FeO_3$	SC	$PbO-PbF_2-B_2O_3$	1300 - 900	0.5	-	Pierce et al (1969)
$EuAlO_3$	SC	$PbO-PbF_2-B_2O_3-MoO_3$	1295 - 900	1	2	Wanklyn et al (1975)
$EuFeO_3$	SC	PbO	1250 - 1000	6	5 x 5 x 1	Drofenik et al (1973)
$GdAlO_3$	SC	$PbO-PbF_2-B_2O_3$	1290 - 800	2	6	Wanklyn (1969)
$GdAlO_3$	ACRT	$PbO-PbF_2-B_2O_3$	1300 - 900	0.3 - 0.6	35 x 30 x 25	Scheel and Schulz-Dubois (1971); Scheel (1972)
$GdMnO_3$	SC	PbF_2	1280 - 900	1	3 x 3 x 2	Wanklyn (1972)
$TbAlO_3$	EV	$PbO-PbF_2$	1207	-	3	Garton and Wanklyn (1967)
$TbAlO_3$	SC	$PbO-PbF_2-B_2O_3-MoO_3$	1295 - 900	1 - 2	4.5 x 2.5 x 2	Wanklyn et al (1975)
$TbFeO_3$	HEG	$PbO-B_2O_3$	990 - 875	2 - 20	1	Schick and Nielsen (1971)
$TbFeO_3(Cr)$	EV	$PbF_2-B_2O_3$	1300	-	5	Van Uitert et al (1970b)
$DyAlO_3$	EV	PbO	1260	-	3	Garton and Wanklyn (1967)

Table 30.1 (Cont'd)

Crystal	Technique	Flux	Temp. Range (°C)	Cooling Rate (°C/hr)	Approximate Dimensions (mm)	References
$DyAlO_3$	EV	$PbO-PbF_2-B_2O_3$	1220	-	7 x 3 x 2	Wanklyn (1969)
$DyAlO_3$	HPS	NaOH	1200	-	-	Dernier and Maines (1971)
$DyAlO_3$	SC	$PbO-PbF_2$	1290	-	-	Flicstein and Schieber (1973)
$DyAlO_3$	SC	$PbO-PbO_2-B_2O_3-MoO_3$	1245 - 900	1 - 2	3.5 x 2 x 1.5	Wanklyn et al (1975)
$DyFeO_3$	SC	$PbO-PbF_2-B_2O_3-MoO_3$	1240 - 900	1 - 1.5	-	Wanklyn et al (1975)
$HoAlO_3$	HPS	NaOH	1200	-	-	Dernier and Maines (1971)
$HoAlO_3$	SC	$PbO-PbF_2-B_2O_3-MoO_3$	1290 - 900	3	4 x 2 x 1.5	Wanklyn et al (1975)
$HoFeO_3$(Cr)	SC	$PbO-PbF_2-B_2O_3$	1300 - 900	1	5	Van Uitert et al (1970b)
$ErAlO_3$	HPS	NaOH	1200	-	-	Dernier and Maines (1971)
$ErAlO_3$	SC	$PbF_2-PbO-B_2O_3-MoO_3$	1290 - 900	1 - 1.3	2	Wanklyn et al (1975)
$ErMnO_3$	SC	$PbF_2-PbO-B_2O_3$	1280 - 900	1	-	Wanklyn (1972)
$TmAlO_3$	HPS	NaOH	1200	-	-	Dernier and Maines (1971)
$TmFeO_3$	HYG	KOH	385 - 390	-	-	Kolb and Laudise (1971)
$TmFeO_3$	SC	Bi_2O_3	1300 - 950	0.5 - 1	3 x 12	Gendelev and Titova (1971)
$YbAlO_3$	HPS	NaOH	1200	-	-	Dernier and Maines (1971)
$YbCrO_3$	EV	$PbF_2-B_2O_3-PbO_2$	1260	-	3 x 3 x 2	Wanklyn (1972)

Table 30.1 (Cont'd)

Crystal	Technique	Flux	Temp. Range (°C)	Cooling Rate (°C/hr)	Approximate Dimensions (mm)	References
$YbFeO_3$	SC/EV	$PbO-PbF_2-B_2O_3$	1300 - 950	0.5	-	Quon et al (1971)
$YbFeO_3$	HEG	$PbO-B_2O_3$	900 - 875	2 - 20	1	Shick and Nielsen (1971)
$YbFeO_3$	SC	$PbF_2-PbO-B_2O_3$	1300 - 1100	3	12 x 9	Damen and Robertson (1972)
$LuAlO_3$	HPS	NaOH	120C	-	-	Dernier and Maines (1971)
$LuCrO_3$	EV	$PbF_2-PbO_2-B_2O_3$	126G	-	3 x 2 x 2	Wanklyn (1972)
$LuMnO_3$	SC	Bi_2O_3	1200	50 - 100	1	Yakel et al (1963)
$RAlO_3$	SC	PbO	1300 - 850	30	-	Remeika (1956)
$RAlO_3$	SC	Pb_2OF_2	1260 - 1000	3	6 x 6 x 3	Linares (1962)
$RAlO_3$	SC	$PbO-PbF_2-B_2O_3$	1290 - 900	2	3 - 6	Wanklyn (1969)
$RAlO_3$	SC	$Bi_2O_3-B_2O_3$	1315 - 315	2	3 - 6	Wanklyn (1969)
$RCoO_3$	SC	PbO	1300 - 350	30	1	Remeika (1956)
$RCrO_3$	SC	Bi_2O_3	1300 - 350	30	-	Remeika (1956)
$RCrO_3$	EV	$PbF_2-B_2O_3$	1240	-	5	Wanklyn (1969)
$RCrO_3$	EV	$PbF_2-Bi_2O_3$	1230	-	-	Subba Rao et al (1971)
$RFeO_3$	SC	PbO	1300 - 850	30	-	Remeika (1956)
$RFeO_3$	SC	$PbO-B_2O_3$	1300 - 950	2	10 x 5 x 2	Remeika and Kometani (1968)

Table 30.1 (Cont'd)

Crystal	Technique	Flux	Temp. Range (C°)	Cooling Rate (°C/hr)	Approximate Dimensions (mm)	References
$RFeO_3$	HYG	KOH	375	-	10	Kolb et al (1968)
$RFeO_3$	SC	$PbO-PbF_2-B_2O_3$	1290 - 850	2	5	Wanklyn (1969)
$RFeO_3$	SC	$PbO-PbF_2-B_2O_3$	1300 - 850	2 - 4	10	Giess et al (1970)
$RFeO_3$	SC	$PbO-PbF_2-B_2O_3$	1300 - 950	0.5 - 1	18	Gendelev and Titova (1971)
$RFeO_3$	LPE/SC	$PbO-B_2O_3$	1150 - 1100	2 - 20	-	Shick and Nielsen (1971)
$RFeO_3$	SC	$PbO-B_2O_3$	1300 - 1000	2	5 x 5 x 5	I. Mikami (1973); I. Mikami et al (1973)
$RFeO_3$	SC	$PbO-PbF_2-B_2O_3$	1280 - 950	1.25 - 5	-	Akaba (1974)
$RFeO_3$(Bi)	SC	$PbO-Bi_2O_3-B_2O_3$	1300 - 950	1 - 4	10	Remeika et al (1969)
$RFeO_3$(Ni,Cr, Mn)	EV	$PbO-PbF_2-B_2O_3$	1300	-	-	Van Uitert et al (1970b)
$RFeO_3$(Ni,Cr,Mn)	SC	$PbO-PbF_2-B_2O_3$	900	-	-	Van Uitert et al (1970b)
$RGaO_3$	SC	PbO	1300 - 850	30	-	Remeika (1956)
$RGaO_3$	HPS	NaOH	1000	-	-	Marezio et al (1966)
$RGaO_3$	HPS	NaOH	1000	-	-	Marezio et al (1968)
$RGaO_3$	SC	$PbO-B_2O_3$	1300	1 - 5	-	Marezio et al (1968)
$RMnO_3$	SC	Bi_2O_3	1400 - 1000	-	plate	Bertaut et al (1963)
$RMnO_3$	EV	Bi_2O_3	1450	-	plate	Bertaut et al (1963)

Table 30.1 (Cont'd)

Crystal	Technique	Flux	Temp. Range (°C)	Cooling Rate (°C/hr)	Approximate Dimensions (mm)	References
$R_{2/3}Pb_{1/3}MnO_3$	SC	Pb_2OF_2	1150	-	5	Janes and Bodnar (1971)
$RScO_3$	SC	PbO	1300 - 850	30	-	Remeika (1956)

30.2.2 Crystal Chemistry

The perovskite family of compounds is one of the most widely studied groups of materials and some of the earliest concepts of modern crystal chemistry were developed in the study of these compounds. The group derives its name from the atomic arrangement first found in the rare mineral perovskite, $CaTiO_3$. The structure was originally thought to be cubic but the true symmetry was later shown to be orthorhombic (Megaw, 1946). However, the name "perovskite" was retained for the structure type. The truly cubic structure is referred to as "ideal perovskite", and has a unit cell edge of about 4Å containing one ABO_3 formula unit. In this structure the B ion is in octahedral coordination and the A cation in twelvefold coordination with the oxygen ions. The simple cubic structure is shown in Fig. 30.1a. Alternatively, the A cation may be thought of as being in the body center position and the B cation at the corners, in which case oxygens would occupy the center of the edges of the cube, as shown in Fig. 30.1b. The basic building blocks of the perovskite structure are the oxygen octahedra. When these octrahedra share corners cubic stacking is obtained, while the sharing of faces leads to hexagonal stacking. Thus the prerequisites for a perovskite structure are corner-shared octahedra containing a small B cation in octahedral coordination with a relatively large A cation in the interstices of the framework of octahedra. The stability of the structure arises mainly from the electrostatic (Madelung) energy, so that the relative sizes of the A and B cations are important. In order to have contact between the ions, $(R_A + R_O)$ should equal $\sqrt{2}(R_B + R_O)$, where (R_A, R_B and R_O are the respective ionic radii. Goldschmidt (1926) defined a tolerance factor, t, to define the limits of stability of the structure:

$$t = (R_A + R_O)/\sqrt{2}\,(R_B + R_O) \qquad (30.1)$$

The perovskite structure is stable within the range $0.75 < t < 1.00$ with t lying between 0.8 and 0.9 in most cases. The necessity for octahedral coordination sets a lower limit of 0.51 Å on the size of the B cation in oxide systems, since an ion smaller than this does not achieve optimum B-O separation and stabilizes a structure with lower coordination. The tolerance factor and the minimum size of the B ion set a lower bound on the size of the A cation of 0.90 Å.

An alternative way of viewing the perovskite structure is as a close-packing of oxygen anions, one quarter of which have been replaced by a large A cation, or as a close-packing of ordered AO_3 layers as illustrated in Fig. 30.2. The A cation may be thought of as lying at the corners of the basal plane of a hexagonal cell with oxygens at the edge-centers and the face-centered position. Close-packed stacking of these layers leads to the formation of one octahedron of oxygens for each AO_3 unit.

In the rare earth perovskite oxides, the rare-earth ion, R, is a relatively large ion and is hence generally the A ion in the ABO_3 structure. Most of the examples in the literature are RBO_3 type compounds but compounds of the type ARO_3 are also known and some examples of these are listed later. In some instances the rare-earth ion may substitute for some fraction of the A or B ions leading to the formation of systems of the type $(R,A)BO_3$ or $A(R,B)O_3$ respectively.

Early exploratory studies (Wood, 1951; Roy, 1954; Keith and Roy, 1954; Yakel, 1955; Roth, 1957) involved a search for perovskite phases in a number of metal oxide systems. Later, more systematic investigations were carried out in a series of compounds in which one of the cations was kept the same and the

other varied (Brous et al, 1953; Geller and Wood, 1956; Geller and Bala, 1956; Gilleo, 1957; Koehler and Wollan, 1957; Geller 1957a; Yakel et al, 1963; Eibschütz, 1965). Meanwhile the correlation of the relative ionic radii (Geller, 1957b) and covalent character (Dalziel, 1959) with the crystallography of perovskite compounds was studied. Recently a number of studies have treated perovskite oxides in terms of the basic building blocks of the structure. Some of these studies have discussed perovskite compounds in terms of the displacement parameters from an idealized model (Megaw, 1968a) and changes in the shape and size of the octahedra (Megaw, 1968b, 1968c; Marezio et al, 1970; Glazer, 1972). Review articles dealing with these factors aimed at an understanding of the perovskite structure (Megaw, 1972; Megaw and Darlington, 1975) are of particular interest. Fukunaga and Fujita (1973) have developed a relation between the ionic radii and cell volumes in perovskite compounds by using values for over 200 oxides. This equation of state is useful in predicting the molar volume of a perovskite obtained from a particular combination of elements. Sakhnenko et al (1972) have developed a method of calculating the interatomic distance in crystals, based on the idea of deformation of the unstressed lengths of cation-anion bonds. These procedures were adopted by Fesenko and Geguzina (1973) to compare the calculated mean unit cell size of 675 compounds with the experimentally observed value. They found that agreement was within 1% in 646 of these compounds. McCarthy and Greedan (1975) and Greedan et al (1975) have suggested guidelines to predict new phases of compounds containing Eu. Glazer (1975) has described simple ways of determining the symmetry of perovskite structure, using trial models based on tilting of rigid octrahedra.

Crystallographic details for some of the rare-earth perovskites are listed in Table 30.2. Wherever possible the data are taken from the same source for a

particular series of compounds such as manganites, vanadites, etc. Structural details of other perovskites can be found in the literature (Galasso, 1969; Goodenough and Longo, 1970; Müller and Roy, 1974).

30.2.3 Crystal Structure

Although many of the crystal chemistry concepts developed in the early days can be understood in terms of the ideal cubic structure, investigations in the past two decades have shown a variety of deviations from cubic symmetry, especially in rare-earth perovskite oxides. Even though distortions from the simple cubic structure are very frequently observed, such compounds nevertheless exhibit a strong pseudocubic nature. In many previous studies the distortions were very small and the true symmetry was not determined at that time. In such cases the descriptions of the structure were given in terms of a pseudocell. The discussion of perovskite systems in the literature involves many assumptions, revisions, redeterminations and controversies, some of which have not been resolved to date. Even though the distorted structure may exist at room temperature it may transform to the ideal perovskite structure at high temperature. This transition may proceed in several stages via other distorted phases. Deviations from the ideal perovskite structure may occur as a simple distortion of the primitive unit cell, or an enlargement of the primitive cell, or a combination of both.

The space group of the simple cubic structure is $Pm3m\text{-}O_h^1$ with atoms in the following positions (Fig. 30.1): A in 1(b) sites at (1/2, 1/2, 1/2); B in 1(a) sites at (0, 0, 0) and O in 3(d) sites at (1/2, 0, 0). There is one formula unit per unit cell. An example of such an arrangement is provided by $EuTiO_3$. This compound was first reported by Brous et al (1953) and recently studied by McCarthy and Greedan (1975).

A modification of the simple perovskite structure is obtained when two types of B ions with suitably different ionization and size are incorporated. In the case of equiatomic proportions of the two types, the general formula of

the perovskite is now $A(B_{0.5}\ B'_{0.5})O_3$ or $A_2BB'O_6$. It was postulated (Galasso et al, 1959) that an ordered distribution of the two types of B ions along alternate (111) planes is most probable when a large difference exists in either their charges or ionic radii. A completely ordered structure of such a perovskite is shown in Fig. 30.3. It can be seen that the unit cell is doubled along all three axes, compared to a primitive unit cell. In the ordered structure the oxygens are slightly shifted towards the more highly charged cation but the octahedral symmetry of the B and B' cations is retained (Steward and Rooksby, 1951; Cox et al, 1967; Khattak, et al, 1973, 1975, 1976). The symmetry now becomes face-centered cubic and the space group $Fm3m\text{-}O_h^5$ with A in 8(c) sites at (1/4, 1/4, 1/4); B in 4(a) sites at (0, 0, 0); B' in 4(b) sites at (1/2, 1/2, 1/2); and O in 24(e) sites at (1/4, 0, 0). There are four formula units of $A_2BB'O_6$ per unit cell.

Distortions from the ideal ABO_3 cubic symmetry occur frequently and structures with tetragonal, orthorhombic, rhombohedral, monoclinic and triclinic symmetry are known. The number of compounds reported to have tetragonal, monoclinic or triclinic structures is few and detailed structural characterizations have not been carried out in most of these cases. On the other hand, examples of the orthorhombic and rhombohedral structures are numerous.

In the rare earth perovskites, compounds with an orthorhombic distortion are the most common. This structure was first observed in a single crystal of $GdFeO_3$ (Geller, 1956) and later by Coppens and Eibschütz (1965) and is hence sometimes typified as the $GdFeO_3$ structure. The cell constants of the distorted perovskite are related to the cubic pseudocell, a_o, as follows:

$$a_{ortho} \approx b_{ortho} \approx \sqrt{2}\ a_o$$

and $c_{ortho} \approx 2a_o$

In many early publications this cell was indexed in terms of a monoclinic pseudocell with $a = b \approx c \approx a_o$ and $\beta \approx 90°$ to emphasize the distortion from the ideal perovskite cell. The true orthorhombic space group Pbnm - D_{2h}^{16} has four formula units per unit cell with atoms in the following positions: A in 4(c) sites at $\pm(x, y, 1/4; 1/2 - x, 1/2 + y, 1/4)$; B in 4(b) sites at (1/2, 0, 0; 1/2, 0, 1/2; 0, 1/2, 0; 0, 1/2, 1/2) and O in 8(d) sites at $\pm(x, y, z; 1/2 - x, 1/2 + y, 1/2 - z; \bar{x}, \bar{y}, 1/2 + z; 1/2 + x, 1/2 - y, \bar{z})$ and 4(c) sites. This distorted perovskite form, shown in Fig. 30.4, is obtained by tilting of the oxygen octahedra in such a way that the A atoms are displaced along $<1\bar{1}0>$ pseudocubic directions, or <010> directions in the orthorhombic cell (Glazer, 1975).

The Pbnm space group is a centric one. In some materials, such as $LaYbO_3$, non-centric symmetry has been found, described by the space group $Pbn2_1$ - C_{2v}^9 (Müller-Buschbaum and Teske, 1968). However, the deviations from the centric structure are very small.

An interesting feature of the RBO_3 type compounds with an orthorhombic structure is the variation of the cell parameters with the rare earth ionic radius. It has been found that while the lattice parameters a and c, and volume of the cell, V, decrease smoothly with the radius of the rare earth ion, the lattice parameter b increases and sometimes goes through a maximum. Such behavior has been reported for $RAlO_3$ (Dernier and Maines, 1971), $RTiO_3$ (McCarthy et al, 1969), RVO_3 (McCarthy et al, 1974), $RCrO_3$ (Quezel-Ambrunaz and Mareschal, 1963), $RMnO_3$ (McCarthy et al, 1973), $RFeO_3$ (Eibschütz, 1965), $RCoO_3$ (Demazeau et al, 1974) and $RGaO_3$ (Geller et al, 1974).

In early work, rhombohedral distortions were considered in terms of deviations from the primitive cell, a_o, so that a rhombohedral cell was specified with one formula unit per cell. Subsequent investigations showed that in many cases the anions were displaced so as to require a larger unit cell, and a face-centered rhombohedral cell containing eight formula units with a cell size $a_f \approx 2a_o$ and $\alpha \approx 90°$ was used. Another way of describing such a rhombohedral cell is with a primitive cell containing two formula units with cell edge $a_p \approx \sqrt{2}a_o$ and $\alpha \approx 60°$. The relations (Geller and Bala, 1956) between the face-centered and primitive rhombohedral cells are as follows:

$$a_p = 1/2\ a_f \sqrt{[2(1 + \cos \alpha_f)]} \tag{30.2}$$

$$\cos \alpha_p = 1/2\ \frac{3\cos \alpha_f + 1}{\cos \alpha_f + 1} \tag{30.3}$$

or

$$a_f = a_p \sqrt{(3 - 2 \cos \alpha_p)} \tag{30.4}$$

$$\cos \alpha_f = \frac{2\cos \alpha_p - 1}{3 - 2\cos \alpha_p} \tag{30.5}$$

Figure 30.5a shows the primitive rhombohedral cell and its relation to the ideal cubic structure. Figure 30.5b indicates how the primitive unit cell is derived from the face-centered rhombohedral cell. Megaw and Darlington (1975) have discussed the geometrical and structural relationship between the various space groups in such distorted perovskites.

The rhombohedral structure is sometimes typified as the $LaAlO_3$ structure. Although in early investigations $LaAlO_3$ was described as monoclinic (Ruggiero and Ferro, 1955) and tetragonal (Bertaut and Forrat, 1956) it was finally established to have a rhombohedral structure (Geller and Bala, 1956). However, they

described it with the space group $R\bar{3}m$ - D_{3d}^5. It was later found to have $R\bar{3}c$ - D_{3d}^6 symmetry (Derighetti et al, 1965; Rango et al, 1966), and this assignment was confirmed by detailed neutron scattering data (Kjems et al, 1973a).

Table 30.2. Crystallographic Properties of Some Rare-Earth Perovskite Oxides

Abbreviations used for Symmetry:
- C - Cubic
- H - Hexagonal
- M - Monoclinic
- O - Orthorhombic
- R - Rhombohedral
- T - Tetragonal

Compound	Sym.	a ° Å	b ° Å	c ° Å	Angle	Space Group	Remarks	References
$LaAlO_3$	R	5.357			α=60°06'	$R\bar{3}m$		Geller and Bala (1956)
	R	3.790			α=90°05'	$R\bar{3}m$		
	H	5.365		13.11		$R\bar{3}m$		
	C	3.818				Pm3m	T = 650°C, Cubic T > 435°C	
	R					$R\bar{3}c$		Derighetti et al (1965); Rango et al (1966)
						Pm3m	T > 489°C	Kjems et al (1973a)
$CeAlO_3$	R	3.716			α=90°12'			Roth (1957)
	R	5.327			α=60°15'			Kim (1968)
$PrAlO_3$	R	5.327			α=60°22'	$R\bar{3}m$		Geller and Bala (1956)
	R	7.539			α=90°21'	$F\bar{3}2/c$	T = 239 K	Burbank (1970)
	R	3.76			α=90.25°	$R\bar{3}c$	205<T<1320 K	Birgeneau et al (1974)
	O	5.347	7.481	5.322		I112/m	T = 172 K	Burbank (1970)
	O						151<T<205 K	Birgeneau et al (1974)

Table 30.2 (Cont'd)

Compound	Sym.	a	b	c	Angle	Space Group	Remarks	References
	M	5.335	7.477	5.317	β=90°40'	$I\bar{1}$	T = 135 K	Burbank (1970)
	M	3.74	3.74	3.79	β=90.07°	D_{4h}^{18}	T=4.2 K, Almost tetragonal	Birgeneau et al (1974)
$NdAlO_3$	R	5.286			β=60°25'	$R\bar{3}m$		Geller and Bala (1956)
	R	3.750			β=90°22'	$R\bar{3}m$		
$SmAlO_3$	O	5.285	5.290	7.473		Pbnm		Geller and Bala (1956)
	O	5.2912	5.2904	7.4740		Pbnm	High Pressure preparation	Dernier and Maines (1971)
	R	5.316			α=60°19'	$R\bar{3}m$	T=850°C, rhombohedral	Geller (1957a)
	R	3.768			α=90°16'	$R\bar{3}m$	T>800°C	
$EuAlO_3$	O	5.271	5.292	7.458		Pbnm		Geller and Bala (1956)
	O	5.267	5.294	7.459		Pbnm	High Pressure Preparation	Dernier and Maines (1971)
$GdAlO_3$	O	5.247	5.304	7.447		Pbnm		Geller and Bala (1956)
	O	5.250	5.302	7.447		Pbnm	High Pressure Preparation	Dernier and Maines (1971)
$TbAlO_3$	O	5.22	5.28	7.41		Pbnm		Garton and Wanklyn (1967)
	O	5.2317	5.3097	7.4196		Pbnm	High Pressure Preparation	Dernier and Maines (1971)
$DyAlO_3$	O	5.23	5.31	7.40		Pbnm		Gilleo (1956)
	O	5.2053	5.3172	7.3950		Pbnm	High Pressure Preparation	Dernier and Maines (1971)

Table 30.2 (Cont'd)

Compound	Sym.	a	b	c	Angle	Space Group	Remarks	References
$HoAlO_3$	O	5.18	5.33	7.36		Pbnm		Schneider et al (1961)
	O	5.1811	5.3229	7.3741		Pbnm	High Pressure Preparation	Dernier and Maines (1971)
$ErAlO_3$	O	5.16	5.32	7.33		Pbnm		Schneider et al (1961)
	O	5.1595	5.3271	7.3539		Pbnm	High Pressure Preparation	Dernier and Maines (1971)
$TmAlO_3$	O	5.15	5.33	7.29		Pbnm		Schneider et al (1961)
	O	5.1435	5.3277	7.3335		Pbnm	High Pressure Preparation	Dernier and Maines (1971)
$YbAlO_3$	O	5.12	5.33	7.31		Pbnm		Garton and Wanklyn (1967)
	O	5.1251	5.3310	7.3146		Pbnm	High Pressure Preparation	Dernier and Maines (1971)
$LuAlO_3$	O	5.1012	5.3317	7.3000		Pbnm	High Pressure Preparation	Dernier and Maines (1971)
$YAlO_3$	O	5.179	5.329	7.370		Pbnm		Geller and Wood (1956)
$LaScO_3$	O	5.678	5.787	8.098		Pbnm		Geller (1957a)
$CeScO_3$	O						No lattice parameter given	Keith and Roy (1954)
$PrScO_3$	O	5.615	5.776	8.027		Pbnm		Geller (1957a)
$NdScO_3$	O	5.574	5.771	7.998		Pbnm		Geller (1957a)

Table 30.2 (Cont'd)

Compound	Sym.	a	b	c	Angle	Space Group	Remarks	References
$SmScO_3$	O	5.53	5.76	7.95		Pbnm		Schneider et al (1961)
$EuScO_3$	O	5.502	5.752	7.954		Pbnm		Faucher and Caro (1975)
$GdScO_3$	O	5.487	5.756	7.925		Pbnm		Geller (1957a)
$DyScO_3$	O	5.43	5.71	7.89		Pbnm		Schneider et al (1961)
$HoScO_3$	O	5.42	5.71	7.87		Pbnm		Schneider et al (1961)
$YScO_3$	O	5.431	5.712	7.894		Pbnm		Geller (1957a)
$SmTiO_3$	O	5.468	5.665	7.737		Pbnm		McCarthy et al (1969)
$EuTiO_3$	C	3.904				Pm3m		McCarthy and Greedan (1975)
$GdTiO_3$	O	5.407	5.667	7.692		Pbnm		McCarthy et al (1969)
$TbTiO_3$	O	5.388	5.648	7.676		Pbnm		McCarthy et al (1969)
$DyTiO_3$	O	5.361	5.659	7.647		Pbnm		McCarthy et al (1969)
$HoTiO_3$	O	5.339	5.665	7.626		Pbnm		McCarthy et al (1969)
$ErTiO_3$	C	5.340	5.665	7.624		Pbnm		McCarthy et al (1969)
$TmTiO_3$	C	5.318	5.657	7.613		Pbnm		McCarthy et al (1969)
$YbTiO_3$	C	5.306	5.647	7.607		Pbnm		McCarthy et al (1969)
$LuTiO_3$	C	5.293	5.633	7.598		Pbnm		McCarthy et al (1969)
$YTiO_3$	O	5.274	5.633	7.580		Pbnm		McCarthy et al (1969)
$LaVO_3$	T	5.535		7.830		Pbnm		McCarthy et al (1974)

Table 30.2 (Cont'd)

Compound	Sym.	a	b	c	Angle	Space Group	Remarks	References
$CeVO_3$	T	5.519		7.809		Pbnm		McCarthy et al (1974)
$PrVO_3$	O	5.472	5.529	7.774		Pbnm		McCarthy et al (1974)
$NdVO_3$	O	5.451	5.575	7.740		Pbnm		McCarthy et al (1974)
$SmVO_3$	O	5.394	5.581	7.684		Pbnm		McCarthy et al (1974)
$EuVO_3$	O	5.362	5.599	7.651		Pbnm		McCarthy et al (1974)
$GdVO_3$	O	5.342	5.604	7.637		Pbnm		McCarthy et al (1974)
$TbVO_3$	O	5.325	5.606	7.614		Pbnm		McCarthy et al (1974)
$DyVO_3$	O	5.299	5.594	7.593		Pbnm		McCarthy et al (1974)
$HoVO_3$	O	5.276	5.592	7.576		Pbnm		McCarthy et al (1974)
$ErVO_3$	O	5.256	5.581	7.559		Pbnm		McCarthy et al (1974)
$TmVO_3$	O	5.237	5.573	7.545		Pbnm		McCarthy et al (1974)
$YbVO_3$	O	5.223	5.564	7.534		Pbnm		McCarthy et al (1974)
$LuVO_3$	O	5.214	5.561	7.530		Pbnm		McCarthy et al (1974)
YVO_3	O	5.274	5.590	7.574		Pbnm		McCarthy et al (1974)
$LaCrO_3$	O	5.477	5.514	7.755		Pbnm		Geller (1957a)
	H	5.51		13.34			T=550 K, Rhombohedral	
	C	3.92					550<T<1300 K T=1500 K	Ruiz et al (1967)

Table 30.2 (Cont'd)

Compound	Sym.	a	b	c	Angle	Space Group	Remarks	References
$LaCrO_3$	O	5.515	5.479	7.753		Pbnm		Quezel-Ambrunaz and Mareschal (1963)
$CeCrO_3$	O	5.475	5.475	7.740		Pbnm		Quezel-Ambrunaz and Mareschal (1963)
$PrCrO_3$	O	5.448	5.479	7.718		Pbnm		Quezel-Ambrunaz and Mareschal (1963)
$NdCrO_3$	O	5.425	5.478	7.694		Pbnm		Quezel-Ambrunaz and Mareschal (1963)
$SmCrO_3$	O	5.367	5.508	7.643		Pbnm		Quezel-Ambrunaz and Mareschal (1963)
$EuCrO_3$	O	5.340	5.515	7.622		Pbnm		Quezel-Ambrunaz and Mareschal (1963)
$GdCrO_3$	O	5.312	5.525	7.606		Pbnm		Quezel-Ambrunaz and Mareschal (1963)
$TbCrO_3$	O	5.291	5.618	7.576		Pbnm		Quezel-Ambrunaz and Mareschal (1963)
$DyCrO_3$	O	5.263	5.520	7.552		Pbnm		Quezel-Ambrunaz and Mareschal (1963)
$HoCrO_3$	O	5.243	5.519	7.538		Pbnm		Quezel-Ambrunaz and Mareschal (1963)
$ErCrO_3$	O	5.223	5.516	7.519		Pbnm		Quezel-Ambrunaz and Mareschal (1963)
$TmCrO_3$	O	5.209	5.508	7.500		Pbnm		Quezel-Ambrunaz and Mareschal (1963)

Table 30.2 (Cont'd)

Compound	Sym.	a	b	c	Angle	Space Group	Remarks	References
$YbCrO_3$	O	5.195	5.510	7.490		Pbnm		Quezel-Ambrunaz and Mareschal (1963)
$LuCrO_3$	O	5.176	5.497	7.475		Pbnm		Quezel-Ambrunaz and Mareschal (1963)
$YCrO_3$	O	5.241	5.521	7.532		Pbnm		Quezel-Ambrunaz and Mareschal (1963)
$LaMnO_3$	O	5.536	5.726	7.697		Pbnm	2%Mn is as Mn^{4+}	Voorhoeve et al (1975b)
$CeMnO_3$	O	5.537	5.557	7.812		Pbnm		Quezel-Ambrunaz (1968)
$PrMnO_3$	O	5.545	5.787	7.575		Pbnm		Quezel-Ambrunaz (1968)
$NdMnO_3$	O	5.380	5.854	7.557		Pbnm		Quezel-Ambrunaz (1968)
$SmMnO_3$	O	5.359	5.843	7.482		Pbnm		Quezel-Ambrunaz (1968)
$EuMnO_3$	O	5.338	5.842	7.453		Pbnm		Quezel-Ambrunaz (1968)
$GdMnO_3$	O	5.313	5.853	7.432		Pbnm		Quezel-Ambrunaz (1968)
$TbMnO_3$	O	5.297	5.831	7.403		Pbnm		Quezel-Ambrunaz (1968)
$DyMnO_3$	O	5.275	5.828	7.375		Pbnm		Quezel-Ambrunaz (1968)
$HoMnO_3$	O	5.27	5.84	7.36		Pbnm	High Pressure and High Temperature Preparation	Waintal et al (1966)
$ErMnO_3$	O	5.26	5.84	7.35			High Pressure Preparation	Waintal and Chenavas (1967)

Table 30.2 (Cont'd)

Compound	Sym.	a	b	c	Angle	Space Group	Remarks	References
$TmMnO_3$	O	5.24	5.82	7.335			High Pressure Preparation	Waintal and Chenavas (1967)
$YbMnO_3$	O	5.23	5.81	7.32			High Pressure Preparation	Waintal and Chenavas (1967)
$LuMnO_3$	O	5.22	5.80	7.30			High Pressure Preparation	Waintal and Chenavas (1967)
$YMnO_3$	O	5.205	5.79	7.31			High Pressure Preparation	Waintal and Chenavas (1967)
$LaFeO_3$	O	5.556	5.565	7.862		Pbnm	Rhombohedral above 980°C	Geller and Wood (1956); Dalziel (1959)
$CeFeO_3$	O	5.541	5.577	7.809				Robbins et al (1969)
$PrFeO_3$	O	5.482	5.578	7.786		Pbnm		Marezio et al (1970)
$NdFeO_3$	O	5.453	5.584	7.768		Pbnm		Marezio et al (1970)
$SmFeO_3$	O	5.400	5.597	7.711		Pbnm		Marezio et al (1970)
$EuFeO_3$	O	5.372	5.606	7.685		Pbnm		Marezio et al (1970)
$GdFeO_3$	O	5.349	5.611	7.669		Pbnm		Marezio et al (1970)
$TbFeO_3$	O	5.326	5.602	7.635		Pbnm		Eibschutz (1965)
$DyFeO_3$	O	5.302	5.598	7.623		Pbnm		Eibschutz (1965)

Table 30.2 (Cont'd)

Compound	Sym.	a	b	c	Angle	Space Group	Remarks	References
$HoFeO_3$	O	5.278	5.591	7.602		Pbnm		Eibschutz (1965)
$ErFeO_3$	O	5.263	5.582	7.591		Pbnm		Eibschutz (1965)
$TmFeO_3$	O	5.251	5.576	7.584		Pbnm		Eibschutz (1965)
$YbFeO_3$	O	5.233	5.557	7.570		Pbnm		Eibschutz (1965)
$LuFeO_3$	O	5.213	5.547	7.765		Pbnm		Eibschutz (1965)
$YFeO_3$	O	5.283	5.592	7.603		Pbnm		Eibschutz (1965)
$LaCoO_3$	R	5.436			α=60°48'	$R\bar{3}c$	T<375°C;	Wold et al (1957); Raccah and Goodenough (1967);
	R	5.52			α=60°0'	$R\bar{3}$	T = 937°C	Raccah and Goodenough (1967)
$LaCoO_{2.75}$	M	5.4	5.42	7.48	∃=88°			Sis et al (1973)
$PrCoO_3$	O	5.331	5.373	7.587				Bertant and Forrat (1956)
$NdCoO_3$	O	5.345	5.345	7.560		Pbnm	High Pressure Preparation	Demazeau et al (1974)
$SmCoO_3$	O	5.294	5.352	7.504		Pbnm	High Pressure Preparation	Demazeau et al (1974)
$EuCoO_3$	O	5.261	5.369	7.488		Pbnm	High Pressure Preparation	Demazeau et al (1974)

Table 30.2 (Cont'd)

Compound	Sym.	a	b	c	Angle	Space Group	Remarks	References
$GdCoO_3$	O	5.228	5.387	7.465		Pbnm	High Pressure Preparation	Demazeau et al (1974)
$TbCoO_3$	O	5.209	5.402	7.425		Pbnm	High Pressure Preparation	Demazeau et al (1974)
$DyCoO_3$	O	5.180	5.417	7.407		Pbnm	High Pressure Preparation	Demazeau et al (1974)
$HoCoO_3$	O	5.147	5.417	7.375		Pbnm	High Pressure Preparation	Demazeau et al (1974)
$ErCoO_3$	O	5.122	5.421	7.357		Pbnm	High Pressure Preparation	Demazeau et al (1974)
$TmCoO_3$	O	5.104	5.417	7.325		Pbnm	High Pressure Preparation	Demazeau et al (1974)
$YbCoO_3$	O	5.086	5.419	7.310		Pbnm	High Pressure Preparation	Demazeau et al (1974)
$LuCoO_3$	O	5.065	5.418	7.290		Pbnm	High Pressure Preparation	Demazeau et al (1974)
$YCoO_3$	O	5.137	5.418	7.366		Pbnm	High Pressure Preparation	Demazeau et al (1974)

Table 30.2 (Cont'd)

Compound	Sym.	a	b	c	Angle	Space Group	Remarks	References
$LaNiO_3$	R	5.461			α=60°49'	$R\bar{3}m$		Wold et al (1957)
	R	7.676			α=90°43'	$R\bar{3}m$		
$LaGaO_3$	O	5.519	5.494	7.770		Pbnm		Geller et al (1974)
	R	5.544			α=60°25'	$R\bar{3}m$	T=900°C, Rhombohedral T>875°C	Geller (1957a)
	R	3.933			α=90°22'	$R\bar{3}m$		
$CeGaO_3$	T	5.490		7.749			Predicted	Geller et al (1974)
$PrGaO_3$	O	5.458	5.490	7.733		Pbnm		Marezio et al (1968)
	O	5.460	5.490	7.726		Pbnm		Geller et al (1974)
$NdGaO_3$	O	5.431	5.499	7.710		Pbnm		Marezio et al (1968)
	O	5.427	5.500	7.705		Pbnm		Geller et al (1974)
$SmGaO_3$	O	5.369	5.520	7.650		Pbnm	High Pressure Preparation	Marezio et al (1968)
	O	5.377	5.513	7.654		Pbnm	Quenched from molten state	Geller et al (1974)
$EuGaO_3$	O	5.351	5.528	7.628		Pbnm	High Pressure Preparation	Marezio et al (1968)
	O	5.351	5.528	7.628		Pbnm	Quenched from molten state	Geller et al (1974)
$GdGaO_3$	O	5.322	5.537	7.606		Pbnm	High Pressure Preparation	Marezio et al (1968)

Table 30.2 (Cont'd)

Compound	Sym.	a	b	c	Angle	Space Group	Remarks	References
	O	5.325	5.535	7.507		Pbnm	Quenched from molten state	Geller et al (1974)
$TbGaO_3$	O	5.307	5.531	7.578		Pbnm	High Pressure Preparation	Marezio et al (1968)
	O	5.307	5.528	7.577		Pbnm	Quenched from molten state	Geller et al (1974)
$DyGaO_3$	O	5.282	5.534	7.556		Pbnm	High Pressure Preparation	Marezio et al (1968)
	O	5.821	5.533	7.555		Pbnm	Quenched from molten state	Geller et al (1974)
$HoGaO_3$	O	5.251	5.231	7.536		Pbnm	High Pressure Preparation	Marezio et al (1968)
	O	5.256	5.530	7.536		Pbnm	Quenched from molten state	Geller et al (1974)
$ErGaO_3$	O	5.239	5.527	7.522		Pbnm	High Pressure Preparation	Marezio et al (1968)
	O	5.237	5.522	7.517		Pbnm	Quenched from molten state	Geller et al (1974)
$TmGaO_3$	O	5.224	5.515	7.505		Pbnm	High Pressure Preparation	Marezio et al (1968)

Table 30.2 (Cont'd)

Compound	Sym.	a	b	c	Angle	Space Group	Remarks	References
$YbGaO_3$	O	5.208	5.510	7.490		Pbnm	High Pressure Preparation	Marezio et al (1968)
$LuGaO_3$	O	5.188	5.505	7.484		Pbnm	High Pressure Preparation	Marezio et al (1968)
$YGaO_3$	O	5.257	5.536	7.533		Pbnm	High Pressure Preparation	Marezio et al (1968)
$LaYO_3$	O	6.09	5.885	8.505		Pbnm	High Pressure Preparation	Coutures and Foex (1974)
	M	14.54	3.73	9.10	β=101°53'		T=1600°C; 1550<T<1750°C	Coutures and Foex (1974)
	H	3.91		6.245			T=1860°C; 1750<T<1975°C	Coutures and Foex (1974)
	C	4.31					T=2050°C; 1975<T<2225°C	Coutures and Foex (1974)
$EuZrO_3$	C	4.18				Pm3m		Shafer (1965)
$EuNbO_3$	C	4.008				Pm3m		McCarthy and Greedan (1975)
$LaRhO_3$	O	5.524	5.679	7.900		Pbnm		Wold et al (1957)
$PrRhO_3$	O	5.4143	5.7473	7.8026		Pbnm	High Pressure Preparation	Shannon (1970)
$NdRhO_3$	O	5.402	5.772	7.816		Pbnm		Wold et al (1963)
	O	5.3778	5.7551	7.7745		Pbnm	High Pressure Preparation	Shannon (1970)

Table 30.2 (Cont'd)

Compound	Sym.	a	b	c	Angle	Space Group	Remarks	References
$SmRhO_3$	O	5.3211	5.7613	7.7083		Pbnm	High Pressure Preparation	Shannon (1970)
$EuRhO_3$	O	5.2985	5.7607	7.6802		Pbnm	High Pressure Preparation	Shannon (1970)
$GdRhO_3$	O	5.2774	5.7605	7.6584		Pbnm	High Pressure Preparation	Shannon (1970)
$TbRhO_3$	O	5.2541	5.7492	7.6226		Pbnm	High Pressure Preparation	Shannon (1970)
$DyRhO_3$	O	5.2449	5.7314	7.6002		Pbnm	High Pressure Preparation	Shannon (1970)
$HoRhO_3$	O	5.2299	5.7257	7.5823		Pbnm	High Pressure Preparation	Shannon (1970)
$ErRhO_3$	O	5.2160	5.7117	7.5610		Pbnm	High Pressure Preparation	Shannon (1970)
$TmRhO_3$	O	5.2028	5.6974	7.5428		Pbnm	High Pressure Preparation	Shannon (1970)
$LuRhO_3$	O	5.1861	5.6700	7.5125		Pbnm	High Pressure Preparation	Shannon (1970)

Table 30.2 (Cont'd)

Compound	Sym.	a	b	c	Angle	Space Group	Remarks	References
$LaInO_3$	O	5.723	5.914	8.207				Roth (1957)
$NdInO_3$	O	5.627	5.891	8.121				Roth (1957)
$SmInO_3$	O	5.589	5.886	8.082				Roth (1957)
$EuInO_3$	O	5.567	5.835	8.078			High Pressure Preparation	Shannon (1967)
$GdInO_3$	O	5.548	5.842	8.071			High Pressure Preparation	Shannon (1967)
$DyInO_3$	O	5.519	5.751	8.041			High Pressure Preparation	Shannon (1967)
$YInO_3$	O	5.500	5.787	8.053			High Pressure Preparation	Shannon (1967)
$LaHoO_3$	O	5.884	6.094	8.508			High Pressure Preparation	Berndt et al (1975)
$LaErO_3$	O	5.85	8.43	6.07			High Pressure Preparation	Schneider and Roth (1960)
$LaTmO_3$	O	5.85	8.42	6.06			High Pressure Preparation	Schneider and Roth (1960)
$CeTmO_3$	O	5.828	6.035	8.405				Berndt et al (1975)

Table 30.2 (Cont'd)

Compound	Sym.	a	b	c	Angle	Space Group	Remarks	References
$LaYbO_3$	O	5.82	8.37	6.02		$Pbn2_1$		Schneider and Roth (1960); Muller-Buschbaum and Teske (1968)
	C	4.325				Pm3m	T=2080°C	Traverse et al (1968)
$CeYbO_3$	O	5.806	6.009	8.373				Berndt et al (1975)
$PrYbO_3$	O	5.776	5.995	8.368				Berndt et al (1975)
$LaLuO_3$	O	5.832	6.013	8.387				Berndt et al (1975)
$CeLuO_3$	O	5.793	5.997	8.344				Berndt et al (1975)
$PrLuO_3$	O	5.768	5.991	8.340				Berndt et al (1975)
$NdLuO_3$	O	5.737	5.974	8.311				Berndt et al (1975)
$EuUO_3$	O	6.020	6.165	8.616				Berndt et al (1976)
$EuNpO_3$	O	6.001	6.150	8.579				Berndt et al (1976)
$La_{0.8}Na_{0.2}MnO_3$	H	5.506		13.317			Rhombohedral	Voorhoeve et al (1975b)
$La_{0.8}Rb_{0.2}MnO_3$	H	5.541		13.415			Rhombohedral	Voorhoeve et al (1975b)
$La_{0.95}K_{0.05}MnO_3$	O	5.538	5.521	7.789				Voorhoeve et al (1975b)
$La_{0.90}K_{0.1}MnO_3$	H	5.524		13.374			Rhombohedral	Voorhoeve et al (1975b)
$La_{0.8}K_{0.2}MnO_3$	H	5.519		13.381			Rhombohedral	Voorhoeve et al (1975b)
$La_{0.7}K_{0.3}MnO_3$	H	5.511		13.376			Rhombohedral	Voorhoeve et al (1975b)
$La_{0.6}K_{0.4}MnO_3$	H	5.511		13.380			Rhombohedral	Voorhoeve et al (1975b)

Table 30.2 (Cont'd)

Compound	Sym.	a	b	c	Angle	Space Group	Remarks	References
$La_{0.86}Sr_{0.16}CrO_3$	O	5.515	5.479	7.753		Pbnm		Meadowcroft (1968)
$La_{0.5}K_{0.5}TiO_3$	C	3.914				Pm3m		Roy (1954)
$Ce_{0.5}K_{0.5}TiO_3$	C	3.90				Pm3m		Roy (1954)
$Nd_{0.5}K_{0.5}TiO_3$	C	3.874				Pm3m		Roy (1954)
$La_{0.9}Bi_{0.1}CrO_3$	O	5.47	5.50	7.75				Iwahashi and Iida (1965)
$La_{0.5}Sr_{0.5}CoO_3$	C	7.754				Fm3m		Yakel (1955); Gai and Rao (1975)
$Eu_{0.80}NbO_3$	C	3.988						Fayolle et al (1975)
$Eu_{0.90}NbO_3$	C	3.994						Fayolle et al (1975)
$La_{0.69}Pb_{0.31}MnO_3$	R	3.893			α=90°11'			Vogel and Fleming (1975)
Eu_2EuTaO_6	C	8.309				Fm3m		Sato et al (1975)
Eu_2CaWO_6	C	8.18						Shafer (1965)
Eu_2SrWO_6	C	8.21						Shafer (1965)
La_2MgIrO_6	O	5.59	5.59	7.91				Blasse (1965)
La_2CoIrO_6	O	5.60	5.60	7.92				Blasse (1965)
La_2CuIrO_6	M	5.80	5.60	7.72	γ=86°56'			Blasse (1965)
$BaLaLiWO_6$	C	8.032						Brixner (1974)
$BaLaNaWO_6$	C	8.273						Brixner (1974)

Table 30.2 (Cont'd)

Compound	Sym.	a	b	c	Angle	Space Group	Remarks	References
$BaLaKWO_6$	C	8.512						Brixner (1974)
$SrLaLiWO_6$	C	7.908						Brixner (1974)
$BaLaLiMoO_6$	C	8.0119						Brixner (1974)
$Nd_{0.95}Ca_{0.05}Fe_{0.95}Sn_{0.05}O_3$	O	5.470	5.608	7.792				Lyubutin and Vishnyakov (1973)
$Nd_{0.90}Ca_{0.10}Fe_{0.90}Sn_{0.10}O_3$	O	5.476	5.614	7.804				Lyubutin and Vishnyakov (1973)
$Nd_{0.85}Ca_{0.15}Fe_{0.85}Sn_{0.15}O_3$	O	5.484	5.618	7.812				Lyubutin and Vishnyakov (1973)
$Nd_{0.80}Ca_{0.20}Fe_{0.80}Sn_{0.20}O_3$	O	5.490	5.624	7.828				Lyubutin and Vishnyakov (1973)
$Nd_{0.75}Ca_{0.25}Fe_{0.75}Sn_{0.25}O_3$	O	5.500	5.628	7.836				Lyubutin and Vishnyakov (1973)
$Nd_{0.70}Ca_{0.30}Fe_{0.70}Sn_{0.30}O_3$	O	5.504	5.634	7.844				Lyubutin and Vishnyakov (1973)
$BaCeO_3$	O	6.212	6.235	8.781		Pbnm		Jacobson et al (1972)
$BaPrO_3$	O	6.181	6.214	8.722		Pbnm		Jacobson et al (1972)
$BaTbO_3$	R	6.046			α=60°22'	$R\bar{3}c$		Jacobson et al (1972)
	R	8.573			α=90°17'	$R\bar{3}c$		Jacobson et al (1972)
$SrCeO_3$	O	6.094	6.132	8.638				Solov'eva and Gavrish (1974)
Ba_2DyTaO_3	C	8.454				Fm3m		Galasso et al (1966)

Table 30.2 (Cont'd)

Compound	Sym.	a	b	c	Angle	Space Group	Remarks	References
Ba_2HoTaO_6	C	8.442				Fm3m		Galasso et al (1966)
Ba_2ErTaO_6	C	8.423				Fm3m		Galasso et al (1966)
Ba_2TmTaO_6	C	8.406				Fm3m		Galasso et al (1966)
Ba_2YbTaO_6	C	8.390				Fm3m		Galasso et al (1966)
Ba_2LuTaO_6	C	8.372				Fm3m		Galasso et al (1966)
Ba_2YTaO_6	C	8.433				Fm3m		Galasso et al (1966)
Ba_2LaNbO_6	T	8.607		8.690				Galasso and Darby (1963)
Ba_2NdNbO_6	C	8.540				Fm3m		Galasso and Darby (1963)
Ba_2SmNbO_6	C	8.518				Fm3m		Galasso and Darby (1963)
Ba_2EuNbO_6	C	8.507				Fm3m		Galasso and Darby (1963)
Ba_2GdNbO_6	C	8.496				Fm3m		Galasso and Darby (1963)
Ba_2DyNbO_6	C	8.437				Fm3m		Galasso and Darby (1963)
Ba_2HoNbO_6	C	8.434				Fm3m		Galasso and Darby (1963)
Ba_2ErNbO_6	C	8.427				Fm3m		Galasso and Darby (1963)
Ba_2TmNbO_6	C	8.408				Fm3m		Galasso and Darby (1963)
Ba_2YbNbO_6	C	8.374				Fm3m		Galasso and Darby (1963)
Ba_2LuNbO_6	C	8.364				Fm3m		Galasso and Darby (1963)
Ba_2LaPaO_6	C	8.885				Fm3m		Keller (1965)

Table 30.2 (Cont'd)

Compound	Sym.	a	b	c	Angle	Space Group	Remarks	References
Ba_2CePaO_6	C	8.800				Fm3m		Keller (1965)
Ba_2PrPaO_6	C	8.862				Fm3m		Keller (1965)
Ba_2NdPaO_6	C	8.840				Fm3m		Keller (1965)
Ba_2SmPaO_6	C	8.792				Fm3m		Keller (1965)
Ba_2EuPaO_6	C	8.783				Fm3m		Keller (1965)
Ba_2GdPaO_6	C	8.774				Fm3m		Keller (1965)
Ba_2TbPaO_6	C	8.753				Fm3m		Keller (1965)
Ba_2DyPaO_6	C	8.740				Fm3m		Keller (1965)
Ba_2HoPaO_6	C	8.730				Fm3m		Keller (1965)
Ba_2ErPaO_6	C	8.716				Fm3m		Keller (1965)
Ba_2TmPaO_6	C	8.692				Fm3m		Keller (1965)
Ba_2YbPaO_6	C	8.678				Fm3m		Keller (1965)
Ba_2LuPaO_6	C	8.666				Fm3m		Keller (1965)
Ba_2YPaO_6	C	8.718				Fm3m		Keller (1965)
Ba_2CeUO_6	C	8.87				Fm3m		Awasthi et al (1967)
Ba_2NdUO_6	C	8.76				Fm3m		Awasthi et al (1967)
Ba_2SmUO_6	C	8.76				Fm3m		Awasthi et al (1967)
Ba_2EuUO_6	C	8.68				Fm3m		Awasthi et al (1967)

Table 30.2 (Cont'd)

Compound	Sym.	a	b	c	Angle	Space Group	Remarks	References
Ba_2GdUO_6	C	8.66				Fm3m		Awasthi et al (1967)
Ba_2DyUO_6	C	8.65				Fm3m		Awasthi et al (1967)
Ba_2HoUO_6	C	8.65				Fm3m		Awasthi et al (1967)
Ba_2YbUO_6	C	8.60				Fm3m		Awasthi et al (1967)
Ba_2LuUO_6	C	8.57				Fm3m		Awasthi et al (1967)
$Pb(Li_{0.25}La_{0.25}W_{0.5})O_3$	C	4.020						Viskov et al (1966)
$Ba(La_{0.5}Ta_{0.5})O_3$	O	8.611	8.639	8.764				Galasso et al (1966)
$Ba(Gd_{0.5}Ta_{0.5})O_3$	T	8.487		8.513				Galasso et al (1966)

30.2.4 Phase Transition

A very common feature of the distorted perovskites is the readiness with which they undergo phase transformations as a function of temperature. An example of this is provided by $LaAlO_3$, which undergoes a transition to a cubic phase at 489°C (Geller and Bala, 1956). The rhombohedral structure is retained to liquid helium temperature (Granicher et al, 1957; Kiro et al, 1963; Müller et al, 1968).

Rhombohedral $PrAlO_3$ undergoes a series of transformations and has been the subject of a detailed study. On heating this compound exhibits a transition to a cubic phase at 1320 K similar to that observed in $LaAlO_3$. On cooling it undergoes a first order transition to an orthorhombic phase at 205 K, followed by a second order transition at 151 K (Cohen et al, 1969). The 151 K transition has been investigated by x-ray studies (Burbank, 1970), neutron scattering techniques (Kjems et al, 1973b), Raman scattering and fluorescence (Harley et al, 1973), and EPR (Cohen et al, 1974) measurements.

Another interesting example of a rhombohedral perovskite is $LaCoO_3$. This was first described in terms of the space group $R\bar{3}m$ - D_{3d}^5 (Wold et al, 1957) but later established to have $R\bar{3}c$ - D_{3d}^6 symmetry (Raccah and Goodenough, 1967). On heating it transforms to another rhombohedral phase at 375°C with the space group $R\bar{3}$. In the low temperature phase all the Co ions are in the low spin state whereas in the high temperature phase there is ordering of the low spin and high spin Co ions in adjacent (111) planes. At 937°C $LaCoO_3$ undergoes a transition to another rhombohedral phase, the space group $R\bar{3}$ being retained, but the rhombohedral angle, α, changing from 60.4° to 60.0°. In this phase the geometry is apparently quite cubic but the symmetry is rhombohedral as the ions are shifted from their ideal positions. The transition at 937°C is described

according to a localized electron $\rightleftarrows$ collective electron model (Raccah and Goodenough, 1967).

30.2.5 Magnetic Properties

In the ideal cubic perovskite structure, each oxygen is shared by two B cations, forming a B-O-B angle of 180°. Such a configuration is generally highly favorable for superexchange interactions between magnetic B cations. This exchange is usually negative and therefore results in antiparallel coupling of nearest-neighbor magnetic moments. This may be viewed as a two-sublattice structure, one with spin-up and the other with spin-down moments, and a magnetic structure of this type is designated a G-type structure. Thus in a simple perovskite containing paramagnetic B ions, the sequence of moments from one (111) layer to the next can be represented as .... B(↑) B(↓) B(↑) B(↓) .... and the structure is antiferromagnetic. Goodenough (1963) and Kanamori (1959) have discussed the strength and sign of the 180° and 90° superexchange interactions.

When the ions on the two sublattices have different moments, as in $A_2BB'O_6$ perovskites, other spin arrangements are possible. If B' is a diamagnetic ion the B ions are usually aligned antiferromagnetically in the following sequence .... B(↑) B' B(↓) B' B(↑) B' B(↓).... (Blasse, 1965; Cox et al, 1967; Khattak et al, 1976). Here the most important exchange mechanism is believed to be a longer range superexchange interaction through two oxygens of the type B-O-B'-O-B or B-O-O-B. The B-B separation is now considerably more than the 4 Å, separation found in the ideal perovskites, and there are both 90° and 180° configurations. These interactions are by no means insignificant; for example, the Néel temperature of Sr_2NiMoO_6 is 71.5 K (Nomura and Nakagawa, 1966).

If both B and B' are paramagnetic ions, the linear B-O-B' interaction is expected to predominate once again, which for negative exchange results in the sequence ....B(↑) B'(↓) B(↑) B'(↓).... . An arrangement like this results in a

simple ferrimagnetic structure. However, if longer range interactions between B ions alone are of comparable strength, more complex structures can result, for example when B' is the Re^{6+} ion (Khattak et al, 1973, 1975).

The above discussion applies to cubic perovskites with non-magnetic A ions. In ABO_3 perovskites of this type the simplicity of the arrangement makes theoretical calculations more amenable. For ordered perovskites the longer range interactions complicate the situation somewhat. However, most of the rare earth perovskites have distorted variants of the cubic structure and, in some cases, the displacements from ideal positions may be very substantial. Under these circumstances such simple arguments are no longer valid. Furthermore, a distinction should be made according to the number and type of magnetic ions, viz. (i) magnetic ions on the A sites (for example, rare-earth aluminates), (ii) transition magnetic ions on B sites (for example, $LaMnO_3$, $YCrO_3$), and (iii) magnetic ions on both sites (for example, $HoFeO_3$, $ErCrO_3$). Even more complicated magnetic interactions occur when some of the A or B or both ions are replaced by others.

The rare-earth perovskites are usually treated in terms of a two-sublattice model with a rare-earth ion on the A site and a transition metal ion on the B site. Early neutron diffraction studies (Koehler et al, 1960) indicated that there was little interaction between the two sublattices. This is also suggested by the respective ordering temperatures: for example, in the orthoferrites the iron lattice orders around 700 K and the rare-earth lattice only at a few degrees kelvin. An advantage of the low ordering temperature of the rare-earth sublattice is that studies can be made well above T_N without much effect from the thermal vibrations of the lattice.

Magnetic structures have been derived as representations in the appropriate magnetic space group (analogous to the crystallographic space group which describes the crystal structure) by the introduction of an "antisymmetry" element. This new element may be thought of as a normal symmetry element combined with a time- (or current-) reversal operator. With the use of this operator the 32 crystalline classes are increased to 90 magnetic classes and the 230 space groups to 1651 'magnetic groups'. Reviews of this representation theory have been given by Belov et al (1957), Donnay et al (1958), Opechowski and Guccione (1965), Bertaut (1968), and Yamaguchi and Tsushima (1973).

Using this approach for the space group Pbnm eight possible magnetic groups are obtained. For each of the space groups, if one operates on the magnetic moment represented as a vector quantity a variety of magnetic modes can be derived as shown in Table 30.3. The notation for the positions of the moments is that of Cox (1972) as shown in Fig. 30.6. These simple structures can be combined to give a variety of noncollinear structures, and it is possible for reorientation of the magnetic moments to occur at intermediate temperatures. The magnetic structures of some of the rare-earth perovskites reported in the literature are given in Table 30.4.

In the series $RAlO_3$ the Al ion is a diamagnetic ion and the only magnetic contribution is from the rare-earth ion. Magnetic susceptibility data below 4 K for this series of compounds have been reported by Cashion et al (1968a; 1968b), and shows that the Gd, Tb and Dy compounds order whereas the Er and Ho compounds show no ordering down to 1.5 K. The phenomenon of metamagnetism, in which a ferromagnetic component is induced in an antiferromagnet by the application of a field, usually described as a "spin flip", has been observed in $TbAlO_3$ (Mareschal et al, 1968; Bertaut, 1972). Depending on the direction of the applied

field this can result in a single or a double ordering transition (Holmes et al, 1968).

The orthochromites are an example of a transition metal ion on the B site. The chromium sublattice in this series orders between 282 K (for $LaCrO_3$) and 112 K (for $LuCrO_3$), whereas the rare-earth sublattice ordering, if any, occurs below 17 K. Some very complex structures are observed, as for example in $TbCrO_3$, in which the Tb sublattice undergoes ordering at 4 K and transforms to a different structure at 3.05 K. The coupling between the two sublattices has been investigated by Pataud and Sivardiére (1970a, 1970b).

The rare-earth orthoferrites are one of the most widely studied series of compounds because of their possible application as technological magnetic materials (Koehler and Wollan, 1957; Treves, 1965; White, 1969; Moskvin and Sinitsyn, 1973a, 1973b; Yamaguchi, 1974). These compounds show a weak spontaneous moment which is attributed to a slight canting of the iron moments which are otherwise antiferromagnetically aligned in a G-type array (Treves, 1962). The iron moments align so that the direction of easy magnetization is along the a or c axis of the orthorhombic cell (Bozorth et al, 1958). The weak ferromagnetic moment of 0.03 - 0.07 μ_B/mole led to these materials being considered for bubble logic and memory devices (Van Uitert et al, 1970a; Antonov et al, 1973; Bobeck, 1975). The large anisotropy field and low saturation magnetic field results in flat, square magnetization curves for these compounds (Mikami et al, 1973). The strongest interaction in the orthoferrites is the antiferromagnetic coupling of the iron moments which is reflected in the high Néel temperatures of around 700 K. The weak ferromagnetic component is aligned along the c axis at high temperatures (Sherwood et al, 1959). On cooling the iron moments may undergo a reorientation to a preferred alignment along a axis. This transition has been the subject of

extensive study during recent years (Gyorgy et al, 1968; Gorodetsky et al, 1968; Pinto et al, 1971; Bidaux et al, 1974; Yamaguchi, 1974; Shapiro et al, 1974; Nikolaev and Rusakov, 1976). For some time there was uncertainty about whether this reorientation of moments was continuous or discontinuous. Recently torque measurements (Gyorgy et al, 1968) have indicated that the moments undergo orientation in a continuous manner. Finally, on cooling below 10 K the rare-earth ion sublattice orders ($TbFeO_3$, $DyFeO_3$, $HoFeO_3$, $ErFeO_3$).

The rare-earth manganites show very interesting magnetic properties. It is difficult to obtain the Mn ions as Mn^{3+} alone since there is usually some contamination by Mn^{4+}. When part of the rare-earth sites are substituted by a divalent ion a corresponding number of Mn^{4+} are created on Mn^{3+} sites to maintain stoichiometry. Compounds containing mostly Mn^{3+} or Mn^{4+} ions show antiferromagnetic behavior. However in the range of 25 - 35% Mn^{4+} content ferromagnetic behavior has been reported (Jonker and Van Santen, 1950; Jonker, 1956). These studies indicated that there was a weak magnetic interaction between Mn^{3+} ions, a negative interaction between Mn^{4+} ions and a strong positive interaction between Mn^{3+} and Mn^{4+} ions. Neutron diffraction studies (Wollan and Koehler, 1955; Koehler and Wollan, 1957) confirmed this, and additional support was provided by a model based on semicovalent exchange by Goodenough (1955). In previous studies it was assumed that the cations are ionically bound based on the overlap of the atomic orbitals of the cations and anions. The semicovalent exchange theory considers the overlap of the empty cation orbitals with the full orbitals of neighboring anions, thereby giving a covalent nature to the binding. The degree of covalency depends upon the relative stability of these orbitals. Similar behavior was found for the combination Co^{3+} and Co^{4+}, but the Cr and Fe compounds were found to be antiferromagnetic (Jonker and Van Santen, 1953).

Substitution of two kinds of transition elements in the B sites and the effect on magnetic properties has also been studied (Holmes et al, 1971; Rao et al, 1975).

Just as the presence of Mn^{4+} in (La, Sr)MnO_3 leads to deviations from simple behavior, the existence of low spin and high spin Co causes complicated behavior in the $RCoO_3$ compounds. The difference in energy of the trivalent diamagnetic (S = 0) low spin state, Co^{III}, and trivalent cobalt (S = 2) high spin state, Co^{3+}, is only 0.08eV (Reccah and Goodenough, 1967). Magnetic susceptibility data for $LaCoO_3$ showed three regions viz. a low temperature and a high temperature region in which $1/\chi$ vs T was linear but with different slopes, and an intermediate region where $1/\chi$ was essentially independent of temperature (Heikes et al, 1964; Bhide et al, 1972). This has been explained as due to the existence of the predominately low spin Co^{III} state at low temperatures, and a partial transformation to Co^{3+} up to about 200K. Above this temperature Co^{3+} and Co^{III} transform to Co^{II} and Co^{4+} pairs. The behavior of $LaCoO_3$ has been reported extensively in the literature (Jonker and Van Santen, 1953; Goodenough, 1958; Heikes et al, 1964; Goodenough and Raccah, 1965; Naiman et al, 1965; Jonker, 1966; Menyuk et al, 1967; Bhide et al, 1972; Bari, 1972).

Europium titanate, $EuTiO_3$, is an example of a rare-earth perovskite in which the Eu ion is in the divalent state. From magnetic measurements it was reported that $EuTiO_3$ is one of the few antiferromagnetic materials with a positive Curie-Weiss constant (McGuire et al, 1966). This was attributed to a 180° superexchange showing a positive value of the exchange integral for next nearest neighbors.

Table 30.3. Magnetic modes for 4(a) and 4(c) sites allowed by symmetry in the family of magnetic space groups derived from the crystallographic group Pbnm (see Fig. 30.6).

	A sites or 4(a) sites			B sites or 4(b) sites			
	x	y	z	x	y	z	
Pbnm	A	G	C	-	-	C'	Γ_{1g}
Pbn'm'	F	C	G	F'	C'	-	Γ_{2g}
Pb'nm'	C	F	A	C'	F'	-	Γ_{3g}
Pb'n'm	G	A	F	-	-	F'	Γ_{4g}
Pb'n'm'	-	-	-	G'	A'	-	Γ_{1u}
Pb'nm	-	-	-	-	-	A'	Γ_{2u}
Pbn'm	-	-	-	-	-	G'	Γ_{3u}
Pbnm'	-	-	-	A'	G'	-	Γ_{4u}

Table 30.4. Magnetic structures and transition temperatures[†] of some rare-earth perovskite oxides (see Fig. 30.6) The numbers enclosed in parentheses are for the rare-earth ion.

Compound	T_N(K)	Magnetic Str.	Moment(μ_B)	References
$SmAlO_3$	(1.3)			Combarieu et al. (1968)
$GdAlO_3$	(3.69)	G(Gd)		Cashion et al. (1968a)
$TbAlO_3$	(4)	G,A(Tb)	(8.25)	Mareschal et al. (1968)
$DyAlO_3$	(3.42)	F	(7.0)	Herpin and Meriel (1964)
	(3.525)	G,A(Dy)	(8.8)	Holmes et al. (1971b); Bidaux and Meriel (1968)
$LaCrO_3$	282	G(Cr)	2.45	Bertaut et al. (1966)
$PrCrO_3$	239	G(Cr)	2.46	Bertaut et al. (1966)
	(74.2)	F(Pr)	(0.5)	
$NdCrO_3$	224	G(Cr)	2.55	Bertaut et al. (1966)
	(10)	C(Nd)	(1.3)	Bertaut & Mareschal (1967)
$SmCrO_3$	192	G(Cr)		Bertaut et al. (1966)
$EuCrO_3$	181	G(Cr)		Bertaut et al. (1966)
$TbCrO_3$	158	G(Cr)	2.85	Bertaut et al. (1966);
	(4)	F,C(Tb)		Bertaut et al. (1967a);
	(3.05)	complex(Tb)	(8.6)	Mareschal et al. (1968)

[†]A compilation of the transition temperatures has been reported by Connolly and Copenhaver (1972).

Table 30.4 (Cont'd)

Compound	T_N(K)	Magnetic Str.	Moment(μ_B)	References
$DyCrO_3$	146 (2.16)	G(Cr) complex(Dy)	2.76 (9.6)	Bertaut & Mareschal (1968)
$HoCrO_3$	141 (12)	G(Cr) C,F(Ho)	2.94 (7.0)	Bertaut et al. (1966)
$ErCrO_3$	133 (16.8)	G(Cr) C(Er)	2.90 (5.2)	Bertaut et al. (1966); Bertaut & Mareschal (1967)
$TmCrO_3$	124 (>4)	G(Cr) F(Tm)	2.58 (0.8)	Bertaut et al. (1966)
$YbCrO_3$	118	G(Cr)	2.80	Bertaut et al. (1966)
$LuCrO_3$	112	G(Cr)	2.51	Bertaut et al. (1966)
$YCrO_3$	141	G(Cr)	2.96	Bertaut et al. (1966)
$LaFeO_3$	750	G(Fe)	4.6	Koehler & Wollan (1957)
$PrFeO_3$	711	G(Fe)		Treves (1965); Pinto and Shaked (1972)
$NdFeO_3$	760	G(Fe)	4.57	Koehler et al. (1960)
$TbFeO_3$	681 (8.4) (3.1)	G(Fe) C,F(Tb) A,G(Tb)	4.8 (8.6)	Bertaut et al. (1967b)
$DyFeO_3$	648 (3.7)	G(Fe) G,A(Dy)	(9.2)	Treves (1965); Gorodetsky et al. (1968) Berton & Sharon (1968)

Table 30.4 (Cont'd)

Compound	T_N(K)	Magnetic Str.	Moment(μ_B)	References
$HoFeO_3$	700 (6.5)	G(Fe) C,F(Ho)	4.60 (7.5)	Koehler et al. (1960)
$ErFeO_3$	620 (4.3)	G,F(Fe) C(Er)	4.62 (5.8)	Koehler et al. (1960) Gorodetsky et al. (1973) Vigneron (1976)
$TmFeO_3$	630	G(Fe)	-	Treves (1965); Leake et al. (1968)
$Sm_{1-x}Dy_xFeO_3$ ($0 \leq x \leq 1$)		G(Fe)		Pierce et al. (1969)
$LaMnO_3$	100	A(Mn)	3.9	Wollan and Koehler (1955); Koehler and Wollan (1957)
$PrMnO_3$	91	A(Mn)	1.8	Quezel-Ambrunaz (1968)
$NdMnO_3$	85	A(Mn)	1.7	Quezel-Ambrunaz (1968)
$LaErO_3$	(2.4)	complex(Er)	(6.3)	Moreau et al. (1968)
$BaTbO_3$	(37)	G(Tb)	(7.99)	Toefield et al. (1972)
$TbCoO_3$	(3.31)	A,G(Tb)	(8.0)	Mareschal et al. (1968)
$TbVO_3$		C,F(Tb)	(7.6)	Mareschal et al. (1968)
$EuTiO_3$	(5.3)	G(Eu)	(7)	McGuire et al. (1966)

Table 30.4 (Cont'd)

Compound	T_N(K)	Magnetic Str.	Moment(μ_B)	References
$La(Mn_{1-x}Cr_x)O_3$				
$0 \leq x < 0.15$		A		Bents (1957)
$0.15 \leq x < 0.60$		complex		
$0.60 \leq x \leq 1.00$		G		

30.2.6 Electrical Properties

Just as the magnetic properties of rare-earth perovskites exhibit very diverse behavior, the electrical conductivities also show wide variations. Some compounds have been utilized for their dielectric properties, others show metallic conductivity, but a majority are semiconductors. Large changes in conductivity have been observed as a result of ionic substitutions. The conductivity behavior is also influenced by structural or magnetic transformations.

The electrical behavior of a material is dependent on the outermost electrons, which may be localized at specific atomic sites or may be collective. Since localized electrons may carry a spontaneous moment, there is a strong correlation between the electrical and magnetic properties of perovskites. Rare earth perovskites with transition metal ions show widely differing electrical properties. For example, $LaNiO_3$, which contains Ni in the low spin state Ni^{III}, and $LaTiO_3$ exhibit collective d-electron behavior, showing a metallic conductivity and Pauli paramagnetism (Goodenough and Raccah, 1965; Ganguly and Rao, 1973).

The orthochromites have been studied by Ruiz et al (1967) and Subba Rao et al (1971). The former authors found $LaCrO_3$ to be a semiconductor with an activation energy of 0.6 eV, while the latter reported a value of 0.22 eV. It is possible that the 0.6 eV figure is related to impurities or native defects. For the heavier rare-earth chromites there seem to be two regions of conductivity. In the low temperature region the activation energy increases along the rare-earth series (from 0.27 ev for Dy to 0.37 eV for Yb) while the high temperature region is characterized by a value of about 0.23 eV. The mechanism of conduction is attributed to the presence of high mobility Cr^{4+} ions giving rise to p-type extrinsic conduction. The decrease of conductivity in the heavier rare-earth compounds may be related to a decrease in the covalency of the Cr-O bond and an

increased covalency of the R-O bond. This is similar to the arguments suggested by Goodenough (1966).

In the $RMnO_3$ series, the electrical behavior of $LaMnO_3$ has been studied in some detail (Jonker, 1966). He found an abrupt change in conductivity as well as in the magnetic susceptibility as a function of temperature near 450°C (Jonker, 1956). This electrical behavior is explained by Goodenough (1966) on the basis of arguments advanced for orthochromites, namely that the charge carriers are holes hopping amongst localized levels.

In the case of orthoferrites, although the magnetic properties have been studied extensively very little data on their transport properties exist (Jonker 1954; Subba'Rao et al, 1971). Here again, as for the $RCrO_3$ and $RMnO_3$ series, the conduction mechanism is p-type semiconduction associated with localized d-electrons.

Lanthanum cobaltite, $LaCoO_3$, has been reported to have very interesting electrical conductivity behavior (Heikes et al, 1964; Goodenough and Raccah, 1965; Raccah and Goodenough, 1967; Bhide et al, 1972). The material behaves like a semiconductor up to about 125°C. At higher temperatures, $125 < T < 650$°C, the conductivity increases much more rapidly and later $650 < T < 937$°C goes through a broad, flat maximum. Above 937°C it shows metallic behavior. At low temperatures the Co ions are essentially in the low spin Co^{III} state. As the temperature is increased there is coexistence of this and the high spin paramagnetic Co^{3+} state. As the temperature is increased further the Co^{3+} and Co^{III} ion pairs transform to Co^{2+} and Co^{IV} pairs. Thus with increasing temperature the fraction of Co^{3+} decreases and disappears around 937°C when only long range order is present, resulting in a first order transition. Along with the spin behavior the outer electrons also show a transition from localized to a collec-

tive behavior. $LaCoO_3$ is one of the few materials which shows a localized-collective electron transition.

The electrical properties of $LaVO_3$ have been studied by Rogers et al (1966), Dougier and Casalot (1970) and Sayer et al (1975). The material behaves as a semiconductor with an activation energy of 0.12 eV. The d-electrons are considered localized but the low activation energy indicates that the covalent mixing of the orbitals is close to inducing localized-collective electron behavior.

The rare-earth perovskites described above contain a trivalent transition metal ion, and the majority are semiconductors. Addition of suitable ions may force part of the transition ion into a higher oxidation state so as to maintain charge neutrality, thereby greatly modifying the conductivity behavior. One of the first such systems to be studied was $La_{1-x}M_xMnO_3$, where M is Ba, Ca or Sr (Van Santen and Jonker, 1950). The introduction of a divalent ion can be formulated as $La^{3+}_{1-x}M^{2+}_xMn^{3+}_{1-x}Mn^{4+}_xO_3$. For example, if M is Sr and $x = 0$, all the Mn ions are in the Mn^{3+} state and occupy equivalent sites, the spin moments are ordered antiferromagnetically below 150 K and the compound exhibits semiconducting properties. An increase in x results in the creation of Mn^{4+} holes, thereby increasing the conductivity. A change in activation energy is observed at the magnetic disorder temperature. For $0.2 < x < 0.4$ the system becomes ferromagnetic and shows a metal-semiconductor transformation (Parker, 1975). The cobaltites show similar behavior. In the case of $La_{1-x}Sr_xCoO_3$ and $Nd_{1-x}Sr_xCoO_3$ the conduction is metallic at room temperature for $x = 0.4$ and 0.23 respectively (Ohbayashi et al, 1974). As already discussed the activation energy for $LaVO_3$ is very low and following substitution of Sr corresponding to $x = 0.225$ on the La site, the material undergoes a semiconductor-metal transition (Dougier and

Hagenmuller, 1975). In the case of $La_{1-x}Sr_xCrO_3$ an increase in conductivity is also seen with increasing Sr content (Meadowcroft, 1969). In all the above examples an increase in conductivity is seen with the addition of Sr; however, for $La_{1-x}Sr_xNiO_3$ a decrease in conductivity is observed (Obayashi and Kudo, 1975). This is because in these compounds the charge neutrality is maintained by the creation of oxygen vacancies rather than Ni^{4+} ions.

Substitution in the B site by another transition metal cation has been studied by Rao et al (1975). For $LaNi_{1-x}Co_xO_3$ the behavior is metallic for $x = 0.50$, similar to that of $LaNiO_3$. This is attributed to the presence of low spin Co^{III}. When $x>0.50$ the compound is a semiconductor, with the behavior resembling that of $LaCoO_3$ for $x>0.90$. In the case of $LaNi_{1-x}Fe_xO_3$ a metallic-semiconductor transition occurs at $x = 0.2$.

The addition of rare-earths to dielectric materials has been studied for a long time. Rare-earth dopants in $BaTiO_3$ have been reported to lower the resistivity (Saburi, 1959), while La-doped $BaZrO_3$ showed an increase in resistivity by several orders of magnitude (Koenig and Jaffe, 1964). The former was attributed to the formation of Ti^{3+} ions whereas in the latter case the hole concentration was lowered.

30.2.7 Optical Properties

Although the optical absorption and fluoresence spectra of rare-earth compounds has been studied for a long time only recently has a correlation with the magnetic properties been studied. The rare-earth perovskites are of particular interest since the effect of magnetic ordering of the transition metal ion in the B site can be studied in addition to that of the rare-earth ion. Since the difference in ordering temperatures of the two types of ions is large there is little interaction. The absorption spectra either for the host ion or after introduction of a nominal 1% concentration "probe" into a diamagnetic lattice can be studied. In the former case of magnetically concentrated systems a broad spectrum is obtained (with linewidths typically 0.5 - 5 cm^{-1}), while in the latter a sharp spectrum is obtained (linewidths about 0.1 cm^{-1}). A study of the absorption spectra from a rare-earth ion is by no means trivial as a typical spectrum may contain at least 100 absorption lines with perhaps only as many as ten sharp enough to display structure related to magnetic effects.

Consider idealized behavior of single ion absorption spectra in a simple two sublattice antiferromagnet. At high temperatures a single absorption line is observed but on cooling below T_N the effective internal field produces a Zeeman splitting of both ground and excited doublet states. This means that as many as four lines are observed in the absorption spectrum below T_N. The appearance of these lines is related to the ordering of the moments. The existence of an external field below T_N may remove the sublattice degeneracy resulting in the appearance of additional splitting. When the external field is larger than that required for a spin-flip or spin-flop certain lines disappear, while others appear in the absorption spectrum (Leask, 1968).

In the rare-earth perovskite, RBO_3 type compounds the materials whose optical properties have been explored are those in which B is Al, Gd, Cr, or Fe.

Generally the bulk properties are determined by the B ion. When this is a transition metal ion the material tends to be opaque, otherwise transparent. This is associated with the localized 3d electrons of the transition metal ion (Allen 1975). The orthoaluminates and orthogallates are transparent throughout the visible region except for the areas where absorption lines due to the crystal field transitions of the rare-earth ion are present (Merker and Herrington, 1964). For example, a triplet structure associated with the Tb^{3+} transitions in $TbAlO_3$ has been reported by Hüefner et al (1968).

Amongst the RBO_3 compounds containing a transition metal B ion most of the optical work has been done on the orthoferrites. In typical examples of this type optical studies have been made on $ErFeO_3$ (Wood et al, 1969) and $TmFeO_3$ (Malozemoff, 1971). In addition to the absorption lines due to the rare-earth ions, broad bands related to the crystal field absorption of the Fe^{3+} ion are present. Another optical property studied for the orthoferrites is the polar Kerr effect (Wood and Remeika, 1967; Kahn et al, 1969). This is associated with the rotation of plane polarized light incident on a crystal due to the interaction with the magnetic moments present in the material.

The behavior of the orthochromites is similar to that of the orthoferrites but with additional spectra associated with Cr^{3+}. Recent optical data on orthochromites has been reported and discussed by Courths et al (1970), Tsushima et al (1970), Meltzer (1970) and Sugano et al (1971).

30.2.8 Catalytic Properties

The area of catalysis has recently received renewed attention because of possible applications in solving environmental problems. Precious metals have been found useful for the oxidation of CO to CO_2, but are not effective in the reduction of NO. The possibility of using perovskite type catalysts seems promising since it was reported that $LaCoO_3$, $LaMnO_3$ and their substituted derivatives have interesting catalytic properties in regard to application in fuel cell electrodes (Meadowcroft, 1970) and in the oxidation reduction reactions involved in the control of automotive exhaust emissions (Libby, 1971; Voorhoeve et al, 1972, 1973).

The catalytic properties of RBO_3 type compounds are related to the spin and valence state of the transition metal ion, B (Prakash et al, 1974). These authors have studied the oxidation of CO to CO_2 over rare-earth cobaltites and found that $NdCoO_3$ and $HoCoO_3$ showed the highest catalytic activity, which is related to the higher activation energy of these compounds ($\sim$0.3 eV) compared to others in the series ($\sim$ 0.1 eV). Sorenson et al (1974) have studied the reduction of NO over $LaCoO_3$ and attributed it to the creation of oxygen defects which leave the catalyst in a reduced state.

Since Prakash et al (1974) found a correlation between the fraction of high spin Co^{3+} present and the catalytic activity, attempts were made by Voorhoeve et al (1975a) to alter this ratio by substituting a divalent ion. It was found that partial substitution of La by a divalent ion in $LaCoO_3$ and $LaCrO_3$ reduced the activity of the compound. However, in the case of $LaMnO_3$ and $LaFeO_3$ the catalytic activity was enhanced. Thus efforts were concentrated on the system $La_{1-x}M_xMnO_3$ where M is Pb or Sr. Amongst these two series it was reported that the Sr containing compounds were more stable and catalytically more

active than the Pb containing compounds (Gallagher et al, 1974). This was attributed to migration of lead to the surface and deactivation of the catalytic action (Gallagher et al, 1975a). The perovskite systems $La_{1-x}M_xMnO_3$ where M is K, Na, Rb or Ce have also been studied (Voorhoeve et al 1975b; Johnson et al, 1976).

In order for the catalyst to be effective both in oxidation as well as reduction reactions it should equilibrate with the exhaust gases without being degraded or mechanically altered. A potential advantage of the oxide systems is the ability to form mixed valence states which are fairly stable under a given set of oxidising or reducing conditions. The compound can then adjust to these by minor changes in the stoichiometry and valency states of the cations. Another advantage is their resistance to poisoning. Platinum, the catalyst presently being used for automobile exhaust emission control, is deactivated or poisoned in the presence of lead (Dwyer, 1972). $La_{0.7}Pb_{0.3}MnO_3$ is also deactivated by the migration of lead to the surface when it is heated. However, $La_{0.7}Sr_{0.3}MnO_3$ does not have this problem, although it is poisoned by SO_2. An addition of as little as 200 ppm platinum imparted significant resistance to poisoning by SO_2 (Gallagher et al, 1975 b).

The only ordered perovskite which has been studied for catalytic activity is Ba_2COWO_6. This has been found to be comparable to the manganese based, rare-earth perovskite, but it is easily poisoned in the presence of SO_2 (Voorhoeve et al, 1974).

30.3.1 Crystal Structure

The determination of garnet structure was first made on natural garnet minerals nearly fifty years ago (Menzer, 1926). Structural refinements were carried out on synthetic YIG crystals (Geller and Gillco, 1957; Batt and Post, 1962; Euler and Bruce, 1965). The symmetry of the single crystal X-ray photograph is O_h-m3m. The following types of reflections are present:

(hkl), $h + k + l = 2n$

(hk0), $h = 2n$ and $k = 2n$

(hkl), $l = 2n$ and $2h + l = 4n$

Therefore, the most probable space group for garnets is established to be the cubic group O_h^{10}- Ia3d.

Garnets have the general chemical formula of $\{C_3\}[A_2](D_3)O_{12}$, where O denotes the oxygen atom or ion, and C, A, and D denote cations. There are eight formula molecules per unit cell. Therefore, there are 96 h-sites which are occupied by oxygens. The point symmetry of the h-site is $\bar{1}$. The cation sites in the garnet structure are classified into three types of sites. They are:

1. Tetrahedral sites: Each tetrahedral or d-site is surrounded by 4 h-sites to form a tetrahedron. There are 24 d-sites in each unit cell. Each d-site has the point symmetry group of $\bar{4}(S_4)$.
2. Octahedral sites: Each octahedral or a-site is surrounded by 6 h-sites to form an octahedron. There are 16 a-sites in each unit cell of garnet. Each a-site has the point group of $\bar{3}(S_6)$.
3. Dodecahedral sites: Each dodecahedral or c-site is surrounded by 8 h-sites to form a triangular dodecahedron. A triangular dodecahedron is a polyhedron which has 12 faces with each face a triangle. There

are 24 c-sites in each unit cell of garnet. Each c-site has the point group of $222(D_2)$.

Each d-site is surrounded by four d-sites, four a-sites, and six c-sites. Each a-site is surrounded by eight a-sites at the corners of a body-centered cube. It is also surrounded by six d-sites and six c-sites. Each c-site is surrounded by four c-sites, four a-sites, and six d-sites. Each c-site is translated one fourth of the lattice constant distance from its corresponding d-site.

The garnet structure has a high percentage of its polyhedra which share edges. Each tetrahedron shares two edges with triangular dodecahedra, and each octahedron shares six edges with triangular dodecahedra. The triangular dodecahedron has three types of shared polyhedral edges. Each triangular dodecahedron shares two edges with tetrahedra, four edges with octahedra, and four edges with other triangular dodecahedra. Tetrahedra share only corners, i.e., oxygens, with octahedra. A more detailed summary of the information on the crystal structure of garnet appeared elsewhere (Wang, 1973).

30.3.2 Crystal Chemistry

There exists a detailed review of the crystal chemistry of garnets (Geller, 1967). In the following, only a few general features relating to the rare earth ions in garnets will be discussed.

The primary consideration of the occupancy of polyhedral sites by cations is the ionic size. The ionic radius increases with the coordination number (C.N.). A table of effective ionic radii in sides was compiled (Shannon and Prewitt, 1969). In Table 30.5 are listed the known examples of rare earth ions occupying the c-sites, or the triangular dodecahedral sites in garnets. The examples refer to the site occupancy as a major constituent by the rare earth ions. In Table 30.6 are listed the examples of rare earth ions occupying the a-sites, or the ortahedral sites. Rare earth ions have not been found to exist in the d-site, or the tetrahedral site. It is apparent that the small size of the tetrahedral site precludes the large sized rare earth ions.

TABLE 30.5

Examples of rare earth ions at the c-sites (C.N.=8)

Ion	Ionic Radius (°A)	Example	Reference
Eu^{2+}	1.25	None reported	
La^{3+}	1.18	None reported	
Pr^{3+}	1.14	None reported	
Nd^{3+}	1.12	None reported	
Sm^{3+}	1.09	Fe-, Ga-garnets	
Eu^{3+}	1.07	Fe-, Ga-garnets	
Gd^{3+}	1.06	Al-, Fe-, Ga-garnets	
Tb^{3+}	1.04	Al-, Fe-, Ga-garnets	
Dy^{3+}	1.03	Al-, Fe-, Ga-garnets	
Ho^{3+}	1.02	Al-, Fe-, Ga-garnets	
Y^{3+}	1.015	Al-, Fe-, Ga-garnets	
Er^{3+}	1.00	Al-, Fe-, Ga-garnets	
Pr^{4+}	0.99	None reported	
Tm^{3+}	0.99	Al-, Fe-, Ga-garnets	
Yb^{3+}	0.98	Al-, Fe-, Ga-garnets	
Lu^{3+}	0.97	Al-, Fe-, Ga-garnets	
Sc^{3+}	0.87		

TABLE 30.6

Examples of rare earth ions at the a-sites (C.N.=6)

Ion	Ionic Radius (^{o}A)	Example	Reference
Pr^{3+}	1.013		
Nd^{3+}	0.995		
Sm^{3+}	0.964		
Tb^{3+}	0.923		
Dy^{3+}	0.912	Ge-garnets	(Mill', 1965a)
Ho^{3+}	0.901	Ge-garnets	(Mill', 1965a)
Y^{3+}	0.892	Ge-garnets	(Mill', 1965a)
Er^{3+}	0.890	Ge-garnets	(Mill', 1965a)
Tm^{3+}	0.869	Ge-garnets	(Mill', 1965a)
Yb^{3+}	0.858	Ge-garnets	(Mill', 1965a)
Lu^{3+}	0.848	Ge-garnets	(Mill', 1965a)
Pr^{4+}	0.78		
Tb^{4+}	0.76		
Sc^{3+}	0.730	Ge-garnets	(Tauber et al, 1961)

Garnets have the crystal structure: cubic (O_h^{10}-Ia3d). As a first approximation the cubic lattice constant of garnet, a, can be considered as the linear sum of contributions from the triangular dodecahedral (c)-sites, the octahedral (a-) sites, and the tetrahedral (d-) sites (Wang, 1973).

$$a = K_c\langle r_c\rangle + K_A\langle r_A\rangle + K_D\langle r_D\rangle \qquad (30.6)$$

where $\langle r_c\rangle$, $\langle r_A\rangle$, and $\langle r_D\rangle$ are the mean effective radius of c-site, a-site, and d-site cation, respectively, and K_c, K_A, and K_D are the least square parameters indicating the cation contributions to the lattice constant from the c-, a-, and d-sites, respectively. Effective radius values (Shannon and Prewitt, 1969) for the corresponding coordination number (C.N.) and lattice constants of various garnets (germanium garnets, aluminum garnets, iron garnets, gallium garnets: Geller, 1967; silicon garnets: Novak and Gibbs, 1971) were used to calculate the least squares parameters K_C, K_A, and K_D in Eq. (30.6) (Table 30.7). Values for silicate garnets are derived from the least square values given by Novak and Gibbs (1971). Values for the germanate garnets are also listed in several groups in Table 30.7.

TABLE 30.7

LEAST SQUARE PARAMETERS IN EQ. (11) FOR THE CATION CONTRIBUTIONS TO LATTICE CONSTANTS OF VARIOUS GARNETS (WANG, 1973)'.

Cations			Number of data	Parameter		
{C}	[A]	(D)		K_C	K_A	K_D
Ca	Cations exclusive of rare earth	Ge	13	1.89	1.81	22.60
Ca	Rare earths only	Ge	7	1.75	2.00	22.60
Ca	Cations including rare earths	Ge	20	1.85	1.87	22.60
Sr	Cations exclusive of rare earth	Ge	3	2.02	1.64	22.60
Sr	Rare earths only	Ge	7	1.83	1.95	22.60
Sr	Cations including rare earths	Ge	10	1.79	2.02	22.60
Cd	Cations exclusive of rare earth	Ge	9	1.99	1.70	22.60
Rare earths only	Al	Al	16	2.25	1.29	23.18
Rare earths only	Fe	Fe	35	2.06	1.94	18.45
Rare earths only	Ga	Ga	24	-0.32	5.75	19.23
Cations exclusive of rare earths	Cations exclusive of rare earths	Si	56	1.61	1.89	34.77

30.3.3 Phase Equilibria

Garnets have been synthesized in hundreds of varieties, but there are only a limited number of phase equilibria studies available in the systems which contain garnets. In the systems containing the iron garnets, the foremost example is the Y_2O_3-Fe_2O_3 system. The combined effects of oxygen partial pressure and the multivalencies of Fe convert this system into a ternary system of FeO-Fe_2O_3-$YFeO_3$ (VanHook, 1961, 1962a) Yttrium iron garnet (YIG) is an incongruent melting compound. Its incongruent melting point is related to the oxygen partial pressure (Van Hook, 1963b).

$$\log p_{O_2} \text{ (atm)} = -10^5 \ (1/T) \qquad (30.7)$$

TABLE 30.7

Melting Points of Rare Earth Garnets

Compound	Melting Points °C		Reference
$Y_3Fe_5O_{12}$ (YIG)	$1495^{\circ}\pm7^{\circ}$	in CO_2 (P_{O_2} =1.3 Torr)	(Van Hook,1962a)
(incongruent)	$1555^{\circ}\pm3^{\circ}$	in air	(Van Hook,1962a)
	$1582^{\circ}\pm5^{\circ}$	in O_2	(Van Hook, 1962a)
	$1350^{\circ}\pm50^{\circ}$	in CO_2	(Van Hook, 1962b)
$Gd_3Fe_5O_{12}$ (GdIG)	$1495^{\circ}\pm7^{\circ}$	in air	(Van Hook, 1962b)
(incongruent)	$1550^{\circ}\pm10^{\circ}$	in O_2	(Van Hook, 1962b)
$Y_3Al_5O_{12}$ (YAG)	1970°		(Warshaw & Roy, 1959)
(congruent)	1980°		(Van Hook, 1963a)
$Nd_3Ga_5O_{12}$ (NdGG)	1515°		(Brandle & Valentino, 1972)
$Sm_3Ga_5O_{12}$ (SmGG)	1620°		(Brandle & Valentino, 1972)
$Gd_3Ga_5O_{12}$ (GdGG)	1690°		(Brandle & Valentino, 1972)
$Tb_3Ga_5O_{12}$ (TbGG)	1715°		(Brandle & Valentino, 1972)
$Dy_3Ga_5O_{12}$ (DyGG)	1730°		(Brandle & Valentino, 1972)
$Ho_3Ga_5O_{12}$ (HoGG)	1750°		(Brandle & Valentino, 1972)
$Er_3Ga_5O_{12}$ (ErGG)	1760°		(Brandle & Valentino, 1972)

30.3.4 Preparation

A. Ceramic Synthesis

1. Oxide method: Polycrystalline garnets are prepared from the solid state reactions between the constituent oxides. This is the method most easily used and is applicable to all types of garnets. Reaction kinetics vary with the physical states and the impurity levels of the oxide raw materials.

2. Decomposition method: This method seeks an intimate mix of oxides by the thermal decomposition of mixed components. Preferably, these components are soluble in common liquid solvents, and they can be mixed in liquid form. For example, iron can be in the form of ferric ammonium sulfate $Fe(NH_4)(SO_4)_2 \cdot 12H_2O$, and aluminum can be in the form of aluminum ammonium sulfate $Al(NH_4)(SO_4)_2 \cdot 12H_2O$. Yttrium and rare earths can be in the form of chlorides or carbonates. Chlorides of yttrium or rare earths are readily available, but they are deliquescent. Carbonates are therefore to be preferred. This decomposition method is definitely an improvement over the oxide method. It works even in the case of some components which are not soluble. Thermal decomposition produces active sites in the decomposed products. These active sites promote the reactions of formation. The disadvantage lies, however, in the contamination of the reaction residues due to incomplete decomposition reactions.

3. Chemical Precipitation Method: In this method, the mixed cations are precipitated out of solution by suitable agents (usually, hydroxide); it produces very intimate mixing when conditions are perfect. The thermal decomposition process is then employed following the filtration of the precipitates. This method is limited in actual applicati

Disadvantages include the limits placed on the types of cations, the difficulty and inefficiency of the filtration process, and the expenses of extra reagents required. These last two points reduce the industrial importance of this method.

4. Conventional Sintering: The oxide mix, obtained by any of the above three methods, is pressed into sample shapes which are called green bodies. Green bodies are then sintered in air or in controlled atmospheres.

5. Pressure Sintering (Hot-Press): In this method, the oxide mix is simultaneously pressed and heated to an elevated temperature. For instance, Ga-doped GdIG powders of particle size 0.2 μm were cold-pressed at room temperature and 2000 kg/cm^2 to 50% theoretical density. The cold-pressed powder compacts were then transferred into alumina dies. Fine-sized alumina powder was used as the pressure transmitting medium. The die assembly was evacuated to about 0.1 Torr, and it was then hot-pressed at 900°-1300°C and 300-1000 kg/cm^2 for 1-20 hr (Coeure et al., 1969). At a hot-pressing operation of 3 hr at 1175°C and 1000 kg/cm^2, the GdIG samples had an average grain size of 3 μm. Hot-pressing shortens the total processing time and the time at elevated temperatures as compared with conventional sintering processes. The shortening of process time decreases the formation of second phase in the garnet, and it affords better control of grain size in the samples. Grain size can vary from 2 μm at 1050°C for 1 hr to 20 μm at higher temperatures (>1250°C) and longer times (>8 hr). An improved control of grain size can also be achieved by hot-pressing to 1 μm and by annealing at 1400°C to achieve the desired grain size of 10 μm

(Patton, 1970). Higher porosity is the result of hot-pressing plus annealing.

B. Single Crystal Methods:

Several recent books describe the growth methods of single crystals extensively (Brice, 1965; Laudise, 1970; Laudise et al, 1971). The methods which produced garnet crystals successfully include the following:

1. Flux Growth Method: Fluxes, such as PbO (Remeika, 1956), PbO-PbF_2 (Nielsen, 1960), PbO-B_2O_3 (Giess, 1962), BaO-B_2O_3 (Linares, 1962 b), PbO-PbF_2-B_2O_3 (VanUitert et al., 1965), and PbO-Bi_2O_3 (Esponoza and Geller, 1964), were used successfully. Gradient method (Laudise et al., 1962) was also employed to improve the crystal yield.
2. Czochralski Growth Method: Iron garnets, being incongruently melting compounds, cannot be grown by the Czochralski method. Aluminum and gallium garnets can be grown by this method readily.
3. Hydrothermal Growth Method: This method is possible to grow garnet crystals, but requires careful adjustment of growth conditions (Kolb and Laudise, 1971).

C. Epitaxial Garnet Films:

1. Sputtering Methods: Several sputtering methods can be used to grow garnet films (Sawatzky and Kay, 1968). One is the rf reactive sputtering. The other is the dc inert gas sputtering. The third method is the dc reactive sputtering. Currently, the sputtering technique cannot produce high quality epitaxial garnet films.
2. Chemical Vapor Deposition Method: The chemical vapor deposition (CVD) process can produce epitaxial garnet film of acceptable quality (Robinson et al., 1971). But a great deal of improvement in the process is still required.

3. Liquid Phase Epitaxy Methods: An extension of the flux grown method evolves into the liquid phase epitaxy (LPE) method. Currently, the LPE method produces the best quality garnet films. In this process, the liquid, which consists of flux and garnet, is made to be in contact with the substrate, and the epitaxial garnet film deposits onto the substrate. Most methods employed $PbO\text{-}B_2O_3$ as flux (Blank & Nilsen, 1972). Before insertion into the melt, the substrates, properly etched and cleaned, are held immediately above the melt surface to equilibriate in a region where the temperature is within $1^{o}C$ of the melt. The substrates are rotated in a horizontal place at 100-200 rpm during the epitaxial film growth which takes place with 5^{o} to $15^{o}C$ of supercooling (Gilss et al., 1972). To terminate growth, the substrates are withdrawn from the melt and held immediately above the melt surface rotating at 200-1000 rpm to remove flux adhering to the film. Finally, the wafers are withdrawn from the furnace at a maximum rate of 12 cm/min. to prevent thermal shock cracking (Hewitt, et al., 1973). Alternate to the horizontal rotation method, a vertical substrate dipping method produces epitaxial garnet film of good quality (Tolksdorf, 1975). The film quality is indicated by the effective lattice misfit, Δa. Below 0.02 A can be readily achieved by the above LPE method.

In epitaxy, there are three major causes of stress in the film. One is the lattice misfit. The other is the mismatch in the thermal expansions. The third cause is the concentration or impurity effect. The last effect is now reintroduced into the garnet film to achieve the increase in its magnetic uniaxial anisotropy. The ion implantation method is used to achieve this effect (Wolfe et al., 1973; Hu and Giess, 1975).

Direct measurement of stress and strain in epitaxial YIG films on YAG was made with an X-ray diffraction technique (Zeyfang, 1970; Klokholm et al., 1972). It employs the planes parallel to the film surface for diffraction. The strain perpendicular to the surface $\varepsilon^{\perp}$ is given by

$$\varepsilon^{\perp} = (\Delta d^{\perp})/d_o^{\perp} \tag{30.8}$$

where $d_o^{\perp}$ is the lattice spacing in the unstrained film, and $\Delta d^{\perp}$ is the difference between the lattice spacing in the strained and in the unstrained condition. It was found that $\varepsilon^{\perp}$ is -2.1×10^{-3}. The strain parallel to the film surface $\varepsilon^{||}$ is calculated to be 2.5×10^{-3}, using a Poisson's ratio of 0.29 (Spencer et al., 1963). Using a Young's modulus E of 2.0×10^{12} dyn/cm^2 for YIG, a tensile stress of about 6.5×10^{9} dyn/cm^2 parallel to the surface was found at room temperature in a film deposited at 1225^{o}C.

There are other methods of direct stress measurement for films, such as deflection measuring techniques with the traveling microscope (Weiss and Smith, 1962), and the electrobalance (Klokholm, 1969). These methods are limited to the measurement of a one-dimensional state of stress. The stress on a macroscopic scale was a priori assumed to be isotropic. A modified Ligtenberg reflective Moire method (Chiang et al., 1971) measures the two-dimensional state of stress in films. The method consists of projecting a grating onto the film surface which acts as a mirror. The distortion in the grating image due to the bending of the film plate is obtained through the Moire fringes which result from the superpositions of the distorted and reference gratings. The principal stresses can be obtained from the measured moments. This method enables a stress measurement on every point of

the film surface. It is a method which can be easily adopted to stress measurements in garnet films on garnet substrates.

30.3.5 Magnetic Properties

A. Magnetization:

There are extensive reviews of magnetic garnets (for example, Geller, 1966; Von Aulock, 1965). This article is limited to the magnetic properties of garnets as pertaining to their material properties. Magnetic garnets, such as YIG and RIG, were the first garnets found to be ferrimagnetic (Pauthenet, 1956, 57, 58). Neel theory of ferrimagnetism (Neel, 1948), as applied to the garnet structure, considers the sublattices of the a-site and the c-site cations to be ferromagnetically coupled. The d-site cation sublattice is considered to be antiferromagnetically coupled to the a-site sublattice. The net magnetic moment of the garnet is given by

$$\vec{M}(T) = \vec{M}_d(T) - \vec{M}_a(T) - \vec{M}_c(T) \qquad (30.8)$$

where $\vec{M}_d(T)$, $\vec{M}_a(T)$, and $\vec{M}_c(T)$ are the sublattice magnetizations of the d-site, a-site, and c-site, respectively. When a magnetic cation, such as Gd^{3+}, is used to substitute for the nonmagnetic Y^{3+} ions on the c-site, at a ratio greater than 0.4, there is a temperature at which $\vec{M}(T)=0$. This temperature is called the compensation temperature, $T_{comp.}$ Above $T_{comp,}$ the c-site sub-lattice contribution diminishes, and the $\vec{M}(T)$ curve tends to approach that of YIG. The T_{comp} value is a good indicator of the cation distribution in the garnet, dependent on the heat treatment, preparation condition, and chemical composition.

Magnetic properties of the garnets reveal a great deal about the rare earth ions. First there is a separation of grouping between the lighter rare earth ions, such as La, Pr Sm, and Eu (Geller et al., 1963e), and the other heavier rare earth ions. Second, some of the rare earth ions in the magnetic garnets have their magnetic spins

canted with respect to a preferred spin direction. In DyIG, ErIG, and YbIG, the rare earth spins were found to tilt away from the <111> easy axis in the {110} planes (Pickart et al., 1970). In HoIG, the Fe ions at the d-site have their moments along the <111> axis, and the Fe ions at the a-site have their moments along the <$\bar{1}\bar{1}\bar{1}$> axis. The Ho ions at the c-site have a double conical arrangement about this axis, and their resultant moment is along the <$\bar{1}\bar{1}\bar{1}$> direction (Herpin et al., 1960; Allain et al., 1966). The spin canting of rare earth ions adds to the complexity, for the spin canting angle can change with temperature and composition. Third, the mixed rare earth garnets, in which more than one kind of rare earth ions exist, show that rare earth ions behaved differently in the presence of other rare earth ions. For example, one finds a magnetic moment of 1.6 and 1.8 Bohr magnetons per Pr^{3+} and Nd^{3+} substituted in LuIG, as compared with 0.8 and 1.0 Bohr magnetons per Pr^{3+} and Nd^{3+} substituted in YIG (Perel and Schieber, 1962).

B. Molecular Field Theory

The Neel theory of antiferromagnetism (a molecular field treatment for three sublattices of the garnet structure), as applied to ferrimagnetism (Neel, 1948), shows that the fields acting at a-, d-, and c-sites, respectively, are

$$\begin{aligned} \vec{H_a} &= \vec{H} - N_{aa}\vec{M_a} - N_{ad}\vec{M_d} - N_{ac}\vec{M_c} \\ \vec{H_d} &= \vec{H} - N_{da}\vec{M_a} - N_{dd}\vec{M_d} - N_{dc}\vec{M_c} \\ \vec{H_c} &= \vec{H} - N_{ca}\vec{M_a} - N_{cd}\vec{M_d} - N_{cc}\vec{M_c} \end{aligned} \tag{30.9}$$

where the molecular field coefficients $N_{ad} = N_{da}$, $N_{ac} = N_{ca}$, $N_{cd} = N_{dc}$, and the applied magnetic field is $\vec{H}$. The moduli of the sublattice

magnetizations are given by

$$|\vec{M_a}| = N_a g\mu_B J_a B(x_a)$$
$$|\vec{M_d}| = N_d g\mu_B J_d B(x_d) \qquad (30.10)$$
$$|\vec{M_c}| = N_c g\mu_B J_c B(x_c)$$

where

$$x_i = J_i g\mu_B |\vec{H_i}|/kT, \qquad i = a,d, \text{ or } c \qquad (30.11)$$

and where N_a, N_d, and N_c are the numbers of atoms per unit volume for a-, d-, and c-sites, respectively, J_a, J_d, and J_c are the intrasublattice exchange constants, g is the splitting factor, μ_B is the Bohr magneton, and B(x) is the Brillouin function (Morrish, 1965). The canting of the rare earth ion can be included in this treatment by considering all magnetic moments in vectors. Magnetism equations (30.9) - (30.11) are implicit functions of $\vec{M}$; namely, $\vec{M}$ exists on both sides of the same equation. The simultaneous sets of three equations for three sublattices make them infinitely more difficult to solve, even with computers. Therefore, there is no thought of further subdividing each crystallographic site into sublattices of Bravais lattices.

In YIG where the c-site ions are nonmagnetic, the picture is simplified into two sublattices, namely, the d- and a-sublattices. A spin wave study of YIG produces exchange constants $J_{ad} = J_{da} = 4.8\text{x}10^{-15}$ erg, $J_{aa} = 1.1\text{x}10^{-15}$ erg, and $J_{dd} = 2.1\text{x}10^{-15}$ erg (Douglas, 1960).

In $\{Y_3\}$ $[R_xFe_{2-x}]$ $(Q_yRe_{3-y})O_{12}$, where R and Q are nonmagnetic ions, such as In, Ga, and Al, the molecular field coefficients were found to be (Dionne, 1970)

$$N_{dd} = -30.4(1-0.43x)$$
$$N_{aa} = -65.0(1-0.42y) \qquad (30.12)$$
$$N_{ad} = 97.0(1-0.125x-0.127y) \text{ mole/cm}^3$$

for $x \leq 0.70$ and $y \leq 1.95$. The values x and y are related to k_a and k_d, which represent the fraction of nonmagnetic ions in the respective sublattice. Thus, the molecular field coefficients are linearly related to k_a and k_d. For substitutions in one sublattice, the coefficient of the opposite sublattice is reduced in magnitude while its own coefficient remains unchanged. For substitutions in either sublattice, the intersublattice coefficient N_{ad} is reduced. Geller (Geller et al., 1964b) found that the concept of canting (Yafet and Kittel, 1952) can be used to interpret the magnetizations of substituted YIG. When substitutions are made in one sublattice, random canting takes place in the opposite one. The amount of canting in a given sublattice appears to be directly related to a change in its molecular field coefficient. Since $|N_{dd}| < |N_{aa}|$ initially, canting would be expected to occur earlier in the d-site in accord with experiment. An extension of this approach (Brnadle and Blank, 1976) produced the list of molecular field coefficients for rare-earth iron garnets, as shown in Table 30.8. The multiplying factor f is given by the equation.

$$M(T) = f\, M_{YIG}(T) \qquad (30.13)$$

This is due to great similarity between the saturation magnetization of the rare earth iron garnet, M(T) and the saturation magnetization of YIG, $M_{YIG}(T)$. Only in the case of Eu, the multiplying factor of needs to be a function of temperature. This approach (Dionne, 1970) relies on the best fit of experimental magnetization data, and it has some

inherent disadvantages. It depends on a large amount of experimental data and consistencies among the data. It has a degree of arbitrariness which lacks suitable explanation. The results of this approach, however, relate the magnetic data directly to the cation distribution in the garnet.

Another approach (Gilleo, 1960) uses the statistics of interactions to relate the magnetic data with the cation distributions. For the garnet $\{R_3\}[M_yFe_{2-y}](M_2Fe_{3-z})O_{12}$ where R is magnetic and M is nonmagnetic, the total magnetic moment can be estimated to be, in Bohr magnetons

$$\begin{aligned} |n| &= |n_c - n_d + n_a| \\ &= \{3M_c[1-E_c(k_d)]\} \\ &\quad - \{3M_d(1-k_d)[1-E_d(k_a)] - 2M_a(1-k_a)[1-E_a(k_d)]\} \end{aligned} \tag{30.14}$$

where E_i is the probability of an ion at i-site to be linked with at most one of the magnetic ions.

$$\begin{aligned} E_c &= 4k_d^3 - 3k_d^4 \\ E_a &= 6k_d^5 - 5k_d^6 \\ E_d &= 4k_a^3 - 3k_a^4 \end{aligned} \tag{30.15}$$

This approach does not take into account spin canting. It also fails to include the temperature dependence, but it allows a simple check between the magnetic moment and the cation distribution. Therefore, with either of these two approaches, one can obtain a picture of cation distribution in the garnets from their magnetication data. Magnetization data can be readily obtained in comparison to either X-ray or neutron diffractions, which are usually employed to gain cation distribution information. Because many cations can enter into the garnet structure, and many garnets are magnetic, this approach is a very useful one.

TABLE 30.8

Molecular Field Coefficients for Rare-Earth Iron Garnets
(Brandle and Blank, 1976)

	g	N_{ac}	N_{dc}	N_{cc}	Mult.	J
Sm	0.000	0.00	0.00	0.00	0.94	0.0
Eu	0.000	0.00	0.00	0.00	0.518	0.0
Gd	2.000	-3.44	6.00	0.00	1.000	3.5
Tb	1.500	-1.80	3.40	0.00	1.000	6.0
Dy	1.333	-3.35	3.95	0.10	1.000	7.5
Ho	1.25	-0.75	1.50	0.25	1.000	8.0
Er	1.20	-0.75	1.25	0.00	1.000	7.5
Tm	1.17	-1.00	8.00	0.00	0.760	6.0
Yb	1.144	-1.70	2.00	0.00	0.967	3.5
Lu	0.000	0.00	0.00	0.00	0.862	0.0
Y	0.000	0.00	0.00	0.00	1.000	0.0

*Mult. = 0.000645T + 0.4538, for $T \geq 100^{o}K$.

C. Magnetocrystalline Anisotropy

The magnetization $\vec{M}$ in a ferrimagnetic material is always bound to a certain preferred crystallographic direction, which is the easy axis. Anisotropy energy F_k is required to turn $\vec{M}$ from the easy axis direction to any other direction. Phenomenologically, this magnetocrystalline anisotropy can be described, to a second approximation, for cubic crystals as

$$F_k = F_o + K_1 (\alpha_1^2\alpha_2^2\alpha_2^2\alpha_3^2+\alpha_3^2\alpha_1^2) + K_2\alpha_1^2\alpha_2^2\alpha_3^2+ \qquad (30.1b)$$

The coordinate axis coincide with the crystal axes, and α_1, α_2, and α_3 are the direction cosines of $\vec{M}$ with respect to the crystal axes. The constants K_1 and K_2 are the first-order and the second-order magnetocrystalline anisotropy cosntants, respectively. For the purpose of energy minimization, the F_o term can be neglected. The constants K_1 and K_2 are used to represent the magnetocrystalline anisotropy in the crystal.

The magnetocrystalline anisotropy is a direct measure of the contributions from individual cations in the lattice. The success of the single ion model of the anisotropy theory (Yoshida and Tachiki, 1957; Wolf, 1957), as applied to the ferrites and garnets, makes the anisotropy constants very useful.

A list of magnetocrystalline anisotropy constants of several garnets is shown in Table 30.9. There are several general features about them. First, the rare earth ions make a huge contribution to the magnetocrystalline anisotropy constants. Tb ion has the most significant effect, and TbIG has the largest anisotropy constants. Second, K_1 and K_2 are phenomenological constants. Consequently, the neglect of K_2, or its inclusion, makes a significant difference in the

TABLE 30.9
Magnetocrystalline Anisotropy Constants of Garnets

Formula	(°K)	$K_1 \times 10^{-3}$ (ergs/cm^3)	K_2	Reference
YIG	4	-24.8	-	
	100	-20.2	-	
	200	-11.0	-	
	300	-5	-	(von Aulork, 1965)
	78	-22.4	-	(Iida, 1967)
$Y_3Sc_{0.4}Fe_{4.6}O_{12}$	4	-14.5	-	
	100	-12.0	-	
	200	-6.0	-	
	300	-1.8	-	(Pearson, 1962)
$Y_3Sc_{0.9}Fe_{4.1}O_{12}$	4	-6.0	-	
	100	-4.0	-	
	200	-1.5	-	
	300	-0.3	-	(Pearson, 1962)
SmIG	100	-8.0×10^{1}	-	
	200	-8.0	-	
	300	-2.0	-	(Pearson, 1962)
	78	-12×10^{2}	-	(Iida, 1967)
EuIG	170	-1.95×10^{1}	0.9×10^{4}	
	190	-1.6×10^{1}	0.48×10^{4}	
	210	-0.9×10^{1}	0.23×10^{4}	
	230	-0.7×10^{1}	0	(Miyadai, 1960)
GdIG	4	-26.8	-	
	100	-21.0	-	
	200	-13.2	-	
	300	-6.0	-	(Rodrigue et al., 1960)
	78	-30	-	(Iida, 1967)
TbIG	80	-760.0	-7.6×10^{6}	
	100	-295 0	-	
	200	--20.0	-	
	300	--5.0	-	(Pearson, 1962)
	78	≥1000	-	(Iida, 1967
DyIG	80	-970.0	$+214\times10^{3}$	
	100	-400.0	-	
	200	--20.0	-	
	300	--5.0	-	(Pearson, 1962)
DyIG	78	-980	-	(Iida, 1967)
HoIG	4	$--12\times10^{3}$	-	
	80	-800.0	-270×10^{3}	
	100	-250.0	-	
	200	--5.0	-	
	300	--5.0	-	(Pearson, 1962)
	78	-800	-	(Iida, 1967)
ErIG	100	-2.1×10^{1}	-	
	200	-1.05×10^{1}	-	
	300	-5.5	-	(Pearson, 1962)
	78	-22	-	(Iida, 1967)
TmIG	77	-2.1×10^{2}	10^{5}	
	100	-1.3×10^{2}	-	
	200	-0.3×10^{2}	-	
	300	-1.1×10^{1}	~0	(Miyadai, 1960)
YbIG	100	-3×10^{1}	-	
	200	-1.4×10^{1}	-	
	300	-7	-	
	4	-62×10^{2}	68×10^{2}	
	30	-45×10^{1}	20×10^{1}	(Pearson, 1962)
	78	-38	-	(Iida, 1967)

values of K_1 and K_2. Third, the temperature dependence of K_1 or K_2 is generally a monotonic varying function. Si^{4+} -doped YIG shows a maximum in the temperature dependence of K_1 which has been attributed to the onset of a relaxation process (VanGroenou et al., 1967).

D. Growth - Induced Noncubic Anisotropy

Whenever multiple types of cations occupy the same crystallographic sites in the garnets, noncubic uniaxial magnetic anisotropy was found to exist. Although the presence of rare earth ions is not the necessary condition (Akselrad and Callen, 1971), the existence of such a noncubic anisotropy with the magnetic garnets containing mixed rare earth ions is most interesting. For it demonstrates most dramatically that rare earth ions, notwithstanding with their many similarities, are distinctly different from each other.

There are six inequivalent c-sites in the garnet structure. The site notation in terms of the orientation of local axes of the c-site is listed in Table 30.10, following that used by Rosencwaig et al (1971b). When the magnetic rare earth iron garnets are grown from the melt, either by the flux method or by the liquid phase epitaxy method, the rare earth ions apparently show different crystallographic site preferences according to the substrate crystal orientation and the different rare earth ions.

There are six types of facet cuts which yield useful uniaxial garnet platelets (Bobeck et al, 1971). Type I cut is perpendicular to the <111> axis which is nearly normal to the {211} facets. This <111> direction is the easy axis emergent from the junction of, and $19^{o}28'$ off of, the normal to the three {211} facets. Type II cut is perpendicular to the <111> axis contained in a {211} facet. The

TABLE 30.10

Orientation of Local Axes of the Dodecahedra, or c-, Sites (D^2 Symmetry) (Rosencwaig et al, 1971b)

Site	Axes a	b	c	Site Equivalence {110} facet	{211} facet
X_1	$01\bar{1}$	011	100	X	X_1
X_2	011	$0\bar{1}1$	100	X	X_2
Y_1	$\bar{1}01$	101	010	X	X_1
Y_2	101	$10\bar{1}$	010	X	X_2
Z_1	$1\bar{1}0$	110	001	Z_1	Z_1
Z_2	110	$\bar{1}10$	001	Z_2	Z_2

easy axis of the type II cut is also the <111> axis. Type III cut is perpendicular to the easy axis <100> in the {110} facet. Types IV, V, VI cuts have their easy axis directions in <110>. Type VI cut is for the {211} faceted crystal, and Type IV and V cuts are for {110} facet crystals.

Representative noncubic anisotropy results can be shown in the case of the garnet

$$\{(Y_{0.62}\ Eu_{0.06}\ Gd_{0.17}\ Tb_{0.15})_3\}\ [Fe_2]\ (Al_{0.6}\ Fe_{2.4})O_{12}$$

where the measured cubic anisotropy K, of the type III cut of the garnet was found to be -3300 erg/cm^3 (Rosencwaig et al, 1971a). The type III cut has the easy axis in <100>, the medium axis in $\langle 110\rangle_{\perp}$, and the hard axis in $\langle 110\rangle_{11}$ (LeCraw et al, 1971). Its average noncubic, uniaxial, growth-induced, anisotropy was found to be 0 in the easy axis, 7100 erg/cm^3 in the medium axis, and 9200 erg/cm^3 in the hard axis. A different cut from the {211} facet of the same crystal has an easy axis in the $(\bar{1}10)$ plane containing the $\langle 11\bar{1}\rangle$ and <112> axes, and at an angle of 52° from $\langle 11\bar{1}\rangle$ toward the <112> axis. The hard axis lies in this plane, normal to the easy axis. The intermediate axis is the $\langle \bar{1}10\rangle$ direction. The cubic anisotropy was found to be -3100 erg/cm^3 for this cut. Its noncubic anisotropy was 0 in the easy axis, 1200 erg/cm^3 in the medium axis, and 8000 erg/cm^3 in the hard axis. The noncubic anisotropy can be eliminated by annealing at temperatures above 1200°C. It was found that the cubic anisotropies are nery nearly the same for all samples and in good agreement with the total anisotropy measured in the same samples after elimination of the noncubic anisotropy by annealing. The magnitude of noncubic anisotropy varies from sample to sample. This variation is significantly greater than can be attributed to experimental uncertainty. It suggests that the growth conditions may be the deciding factor in this variance.

The origin of the uniaxial anisotropy is uncertain, but there are many theoreies about it. Early explanations of the strains induced during growth are found wanting (Lefever et al., 1965). The current theories include the growth-induced pair-ordering model, the site-!reference model, the dipolar mechanism, and the local symmetry distortion model.

The growth-induced pair ordering model (Rosencwaig and Tabor, 1971) proposes that the noncubic anisotropy arises from the presence of a small amount of growth-induced short-range pair ordering which occurs during crystallization. This pair ordering is a result of preferential cation pair-bond directions with respect to the crystal growth facets. There are two mechanisms for this model. One involves the c-site rare earth ions and the d-site iron ions. The other involves the c-site rare earth ions and the d-site iron ions. In applying this model to $\{Eu_2Er_1\}[Fe_2](Fe_{2.4}Ga_{0.6})O_{12}$ (Rosencwaig and Tabor, 1971), less than 1% preferential pair ordering, i.e., <100> in the first mechanism and <210> in the second mechanism, can account for the observed noncubic anisotropy.

The site preference model (Callen, 1971a,b) explains the noncubic anisotropy in terms of the preferential occupation, by one of the multiple types of rare earth ions, of particular c-sites. There are two nearest-neighbor tetrahedral sites for each c-site. The next closest neighbors are the octahedral sites. The second-nearest tetrahedral neighbors are sources of the observed noncubic anisotropy, according to Callen (1971a). A combination of pair ordering and site preference is another form of the site preference model (Rosencwaig et al., 1971b). In this version, the nearest tetrahedral and the nearest octahedral

neighbors lead to a uniaxial anisotropy under both growth facets. Inclusion of the next-nearest tetrahedral neighbors results in the observed orthorhombic anisotropies. The site selectivity for rare earth ions in garnets was confirmed by the spin resonance spectra. They demonstrated facet-related site selectivity for Nd^{3+} and Yb^{3+} ions in flux-gown YAG (Wolfe et al., 1971). In Table 30.11, the average populations of X_1, X_2, Y_1, and Y_2 sites are taken as unity, and the populations of Z_1 and Z_2 sites are presented relative to this average. Under a {211} facet, a Z_1 site is 2.3 times as likely and a Z_2 site is 3.5 times as likely as any X or Y site are to be occupied by Nd ions. Equal population of the Z_1 and Z_2 sites would imply uniaxial anisotropy. The orthorhombic anisotropy implies that the Z_1-Z_2 population difference is as important as the Z-(X,Y) difference. The site population ratios vary approximately exponentially with Δr, where Δr is the excess of the ionic radius of the rare earth ion over Y^{3+}.

The dipolar mechanism (Sturge, 1972), applied to a garnet containing only Gd^{3+} anf Fe^{3+} as magnetic ions, together with the site selectivity on the c-site sublattice, accounts well for the uniaxial term in the growth-induced anisotropy of $\{Y_2Gd\}[Fe_{2.2}Al_{0.8})O_{12}$. This model requires the calculation of the dipolar and crystal field contributions to the noncubic anistropy. The rhombic term in the anisotropy cannot be attributed solely to the dipolar mechanism and is attributed to a contribution from the Fe^{3+} sublattices.

The local symmetry distortion model (Akselrad and Callen, 1971) is based on the distortion of the local symmetry around the tetrahedral d-site, caused by referential ordering among their tetrahedral (or other)

TABLE 30.11

Relative Populations of Impurity Ions in Dodecahedral Sites of YAG (Wolfe et al., 1971)

Impurity (Approx. at. %)	Facet	Relative population ([X]≈[Y]≈1)		Accuracy (%)
		$[Z_1]$	$[Z_2]$	
3% Nd	{110}	0.65	0.60	10
3% Nd	{211}	2.30	3.50	10
1% Yb	{110}	1.18	1.12	5
1% Yb	{211}	0.93	0.91	7
3% Nd (annealed)	{211}	1.15	1.30	15

neighbors. This model is especially useful when the rare earth-based mechanism cannot be operative. In mixed rare earth garnets, a distortion of tetrahedral symmetry can be caused by ordering of dodecahedral site ions. This local symmetry distortion is the cause of noncubic anisotropy.

E. Magnetostriction

The interaction between magnetization and strain produces a lattice deformation in a magnetized body. When the specimen is magnetized to saturation, the saturation magnetostrictions laong the <100> and <111> directions are denoted by $\lambda_{<100>}$ and $\lambda_{<111>}$, respectively. These linear magnetostrictions arise from the strain-dependence of the magnetic anisotropy. The magnetoelastic energy tensor B_{ijkl} is given by (White and Phillips, 1968)

$$H_{ME} = \sum_{ijkl} B_{ijkl}\alpha_i\alpha_j\epsilon_{kl} \tag{30.17}$$

where α_i's are the direction cosines of the magnetization (considered to lie along an external magnetic field) with respect to the crystal axes, and the ϵ_{kl} are the strain components in Love's notation. Keeping terms up to second degree in spin operators, the magnetic Hamiltonian can be written as

$$H_M = \beta\vec{H}\cdot\overleftrightarrow{g}\cdot\vec{S} + \vec{S}\cdot\overleftrightarrow{D}\cdot\vec{S} + H_{elast} \tag{30.18}$$

where $\overleftrightarrow{g}$ and $\overleftrightarrow{D}$ are the g-tensor and the crystal-field tensor of the ion, respectively, $\vec{H}$ is the applied external magnetic field in the case of a paramagnet or the molecular field in the case of the magnetically ordered crystal, and $\vec{S}$ is the spin of the ion. The magnetoelastic energy linear in the strains is

$$\begin{aligned} H_{ME} &= \sum_{kl} (\partial H_M/\partial\epsilon_{kl})\epsilon_l \\ &= \sum_{\sigma}\sum_{ijkl} \beta(\partial g^{\sigma}_{ij}/\partial\epsilon_{kl})_o H_i {}^oS_j\epsilon_{kl} \\ &+ \sum_{\sigma}\sum_{ijkl} (\partial D^{\sigma}_{ij}/\partial\epsilon_{kl})_o S_iS_j\epsilon_{kl} \end{aligned} \tag{30.19}$$

where the derivatives evaluated at equilibrium are the magnetoelastic constants and the summation is over all σ sites. For a cubic crystal, Eq. (30.17) can be written as

$$H_{ME} = B_1 [\alpha_1^2 - 1/3)\epsilon_{xx} + (\alpha_2^2 - 1/3)\epsilon_{yy} + (\alpha_3^2 - 1/3)\epsilon_{zz}] \quad (30.20)$$
$$+ B_2[\alpha_1\alpha_2\epsilon_{xy} + \alpha_2\alpha_3\epsilon_{yz} + \alpha_3\alpha_1\epsilon_{zx}]$$

The magnetoelastic energy tensor B_{ijkl} is reduced to two independent magnetoelastic constants B_1 (= $B_{11} - B_{12}$) and B_2 (= $2B_{44}$), which are related to the saturation magnetostriction constants $\lambda_{<100>}$ and $\lambda_{<111>}$ by

$$B_1 = -(3/2)\ \lambda_{<100>}(c_{11}-c_{12})$$
$$B_2 = -3\lambda_{<111>}\ c_{44} \quad (30.21)$$

If the directional cosines of the linear dilation are β_1, β_2, and β_3 with respect to the crystal axes, the dilation is related to magnetostriction constants by

$$\delta l/l = \lambda_o(T,H) + (3/2)\lambda_{<100>}(T,H)\ [\alpha_1^2\beta_1^2 + \alpha_2^2\beta_2^2$$
$$+ \alpha_3^2\beta_3^2 - 1/3] \quad (30.22)$$
$$+ 3\lambda_{<111>}(T,H)[\alpha_1\alpha_2\beta_1\beta_2 + \alpha_2\alpha_3\beta_2\beta_3 + \alpha_3\alpha_1\beta_3\beta_1] + \ldots$$

The origins of the magnetoelastic constants have been discussed in several reviews (Kanamori, 1963; Comstock, 1965; Jones, 1966; Callen, 1968). Fundamentally, they are the indicators of the changes in crystal field due to strains. Experimentally, they are determined with certain degrees of arbitrariness. Consequently, they have significant variances in values determined by either the strain gauge method or the parallel pump method of the resonance technique. This does not take into account the reduction of symmetry by the presence of the magnetization or strain

vector, which adds to the complexities. Phenomenologically, the magnetoelastic constants, or the linear magnetostriction constants as shown in Table 30.12, are algebraically additive over all sublattices of the garnet structure. The similarity between them and the sublattice magnetization is very real, and there is also a compensation temperature from the competition of sublattice magnetostrictions. The additive property of magnetostriction is exemplified by the linear dependence of magnetostriction or rare earth iron garnets on the rare earth concentration (Clark et al., 1968). The difference between the magnetostrictions of YIG and ReIG denotes the rare-earth contribution to magnetostriction, which is related to the rare earth magnetization. For GdIG, the results showed

$$\frac{\lambda_{<100>}(\text{GdIG},\ 77^{\circ}) - \lambda_{<100>}(\text{YIG},\ 77^{\circ})}{\lambda_{<100>}(\text{GdIG},4.2^{\circ}) - \lambda_{<100>}(\text{YIG},4.2^{\circ})} = 0.63$$

$$\frac{M(\text{GdIG},77^{\circ}) - M(\text{YIG},77^{\circ})}{M(\text{GdIG},4.2^{\circ}) - M(\text{YIG},4.2^{\circ})} = 0.60$$

$$\frac{\lambda_{<100>}(\text{GdIG},296^{\circ}) - \lambda_{<100>}(\text{YIG},296^{\circ})}{\lambda_{<100>}(\text{GdIg},4.2^{\circ}) - \lambda_{<100>}(\text{YIG},4.2^{\circ})} = 0.19$$

$$\frac{M(\text{GdIG},296^{\circ}) - M(\text{YIG},296^{\circ})}{M(\text{GdIG},4.2^{\circ}) - M(\text{YIG},4.2^{\circ})} = 0.18$$

Also, as shown in Table 30.13, the doping of 1.8% Mn in YIG changed the $\lambda_{<100>}$ from -1.4×10^{-6} erg/cm^3 for YIG to $+9.0 \times 10^{-6}$ erg/cm^3 at 300°K. The λ values are therefore very sensitive to the impurity ions. Present quantum mechanical theory (Callen and Callen, 1963, 1965) fits experimental results in the garnet systems very well. The magnetostriction allows a better understanding of the strain dependence of the crystal field surrounding a single ion. Moreover, garnets have useful technical acoustic properties. Magnetoacoustic, or magnetoelastic, interactions

in the magnetic garnets require a knowledge of their magnetostrictions. Therefore, it is an important property which needs to be investigated more thoroughly.

TABLE 30.12

Magnetoelastic Constants of Garnets

Garnet		B_1	B_2		Reference
YIG	0°K	+6	+29	(cm^{-1}/molecule)	(Andres & Luthi, 1963)
	4.2°K	7.2	41	(erg/cm^3 x 10^{-6})	(Nilsen et al, 1965)
	20.4°K	5.2	23	(erg/cm^3 x 10^{-6})	(Nilsen et al, 1965)
	78°K	2.3	8.2	(erg/cm^3 x 10^{-6})	(Nilsen et al, 1965)
	293°K	3.5	6.9	(erg/cm^3 x 10^{-6})	(Bartel, 1969)
	300°K	+11	+20	(cm^{-1}/molecule)	(Andres & Luthi, 1963)
EuIG	4°K	-650	-110	(cm^{-1}/molecule)	(Nilsen et al, 1965)
	4.2°K	272	45	(erg/cm^3 x 10^{-6})	(Nilsen et al, 1965)
	77°K	-500	-53	(cm^{-1}/molecule)	(Iida, 1963)
	78°K	227	22	(erg/cm^3 x 10^{-6})	(Nilsen et al, 1965)
	300°K	-120	-10	(cm^{-1}/molecule)	(Iida, 1963)
GdIG	4.2°K	-39	+22	(cm^{-1}/molecule)	(Philips and White, 1966)
	77°K	-23	+29	(cm^{-1}/molecule)	(Jones, 1966)
	300°K	~0	+17	(cm^{-1}/molecule)	(Jones, 1966)
TbIG	77°K	-3200	-360	(cm^{-1}/molecule)	(Iida, 1963)
	300°K	-69	+18	(cm^{-1}/molecule)	(Iida, 1963)
$Yb_{0.1}Y_{0.9}IG$	4°K	-41	+34	(cm^{-1}/molecule)	(Jones, 1966)
	77°K	-6	+24	(cm^{-1}/molecule)	(Jones, 1966)
DyIG		B^{12}(cm^{-1})	$B^{,2}$(cm^{-1})		(Clark et al, 1966)
	0°K	2900	1090		
HoIG	0°K	1930	430		
ErIG	0°K	-870	590		

TABLE 30.13

Linear Magnetostriction Constants of Garnets

		1.5°K	4°K	4.2°K	77°K	78°K	100°K	200°K	300°K	375°K
YIG	$\lambda_{100} \times 10^6$	-1.1[e]				-1.0[a]	—	-1.1[a]	-1.4[a]	—
	$\lambda_{111} \times 10^6$	-5.4[e]				-3.6[a]	—	-3.9[a]	-2.4[a]	—
SmIG	$\lambda_{100} \times 10^6$					—	159[a]	49[a]	21[a]	—
	$\lambda_{111} \times 10^6$					—	183[a]	-28.1[a]	-8.5[a]	—
EuIG	$\lambda_{100} \times 10^6$		110[e]			86[a]	—	51[a]	21[a]	11[a]
	$\lambda_{111} \times 10^6$		20[e]			9.7[a]	—	5.3[a]	1.8[a]	—
GdIG	$\lambda_{100} \times 10^6$			7.1[e]		4.0[a]	—	1.7[a]	0[a]	—
	$\lambda_{111} \times 10^6$			-3.9[e]		-5.1[a]	—	-4.5[a]	-3.1[a]	—
TbIG	$\lambda_{100} \times 10^6$					560[a]	—	65[a]	12[a]	—
	$\lambda_{111} \times 10^6$					67[a]	—	-10.3[a]	-3.3[a]	—
DyIG	$\lambda_{100} \times 10^6$					-16.9[a]	—	-46.6[a]	-12.5[a]	—
	$\lambda_{111} \times 10^6$					-145[a]	—	-21.5[a]	-5.9[a]	—
HoIG	$\lambda_{100} \times 10^6$					-82.2[a]	—	-10.6[a]	-4.0[a]	—
	$\lambda_{111} \times 10^6$					-56.3[a]	—	-7.4[a]	-3.4[a]	—
ErIG	$\lambda_{100} \times 10^6$		420[b]			10.7[a]	—	4.1[a]	2.0[a]	—
	$\lambda_{111} \times 10^6$		-300[b]			-19.4[a]	—	-8.8[a]	-4.9[a]	—
TmIG	$\lambda_{100} \times 10^6$					25[a]	—	4.9[a]	1.4[a]	—
	$\lambda_{111} \times 10^6$					-31.2[a]	—	-11.3[a]	-5.2[a]	—
YbIG	$\lambda_{100} \times 10^6$		49[b]			18.3[a]	—	5.0[a]	1.4[a]	—
	$\lambda_{111} \times 10^6$		-27[b]			-14.4[a]	—	-7.1[a]	-4.5[a]	—
YIG:Mn 1.8%	$\lambda_{100} \times 10^6$		—			—	—	—	9.0[c]	—
	$\lambda_{111} \times 10^6$		—			—	—	—	0.4[c]	—
YIG:Mn 2.3%	$\lambda_{100} \times 10^6$		—		43[c]	—	—	—	11.5[c]	—
	$\lambda_{111} \times 10^6$		—		-11.8[c]	—	—	—	0.4[c]	—
					(H along $[1\bar{1}1]$ axis)				0.99[d]	—
					(H along [100] and $[0\bar{1}1]$ axes)				1.00[d]	—
$Yb_{0.1}Y_{0.9}IG$	$\lambda_{100} \times 10^6$		7[e]		1[e]	—	—	—	—	—
	$\lambda_{111} \times 10^6$		-6[e]		-4[e]	—	—	—	—	—

[a]Iida, 1967.
[b]Phillips and White, 1967.
[c]Gyorgy et al, 1967.
[d]Dionne, 1970.
[e]Jones, 1966.

30.3.6 Optical Properties

Synthetic garnets have excellent optical properties. Aluminum garnets are excellent crystal hosts and they are useful as solid state laser materials. Iron garnets have interesting infrared properties. The magnetic optical effects in iron garnets are not only useful in devices, but also provide fundamental information about the materials themselves. Finally, silicon-doped iron garnets have photoinduced effects which increase the potentiality of these materials in solid state devices.

A. Crystal Field Effect

The garnet structure, as discussed extensively in Section 3.1, can accommodate a great variety of cations. It is, therefore, an excellent crystal host which can be employed to study the crystal field effects on various cations. The crystal field analysis provides much detailed information about the electronic structure of the cation, and it enables the determination of crystal field parameters for the garnet crystals. The parameters are usually fitted to experimental optical or magnetic data or both. There are still large overall errors in these parameters but they enable us to understand the magnetic anisotropy and optical spectroscopy of the garnet crystals. In recent years, there have been many crystal field studies in rare earth garnets, and they were reviewed and compared in a paper by Wolf (1964), where the principal results are summarized. There are a number of general conclusions, stated by Wolf, which are listed here.

1. Crystal fields are generally large ($\approx 500\ cm^{-1}$): about an order of magnitude larger than the iron-rare earth exchange.

2. The local symmetry is far from cubic.

3. The effect of neighbors other than the eight nearest O^{2-} ions on the crystal field is appreciable.

4. The second degree terms are extremely sensitive to small changes or uncertainties in structure. This rules out the possibility of extrapolating these parameters from one compound to another (e.g., from a gallium garnet to an iron garnet).

5. The sixth degree terms in the crystal field are not negligible.

The magnetic anisotropy in the rare earth garnets can be understood by the g-factor values. The agreement between experiments and theoretical calculations is very good, as shown in Table 30.14. As discussed, there are six nonequivalent c-sites in the garnet structure. The g-factor axes, as oriented relative to the cubic crystal axes, follow the convention that the g_z direction is along the c axis, as listed in Table 30.10. The g_x direction can be either the a axis or the b axis, and the selection is arbitrary. The g-factor values, as shown in Table 30.14, are very anisotropic, and the g_x and g_z values are negative in sign.

TABLE 30.14

The g-Factors of Garnets

		$\|g_x\|$	$\|g_y\|$	$\|g_z\|$	g_x	g_y	g_z
	(calc.)	0.9	0.5	17.5[a]			
Y(Dy)AG							
	(expt.)	0.7	0.4	17.7[b]			
	(calc.)	11.3	1.9	7.4[a]			
Y(Dy)GAG							
	(expt.)	10.8	1.2	7.0[c]			
	(calc.)	5.1	3.9	10.8[d]	-5.1	+3.9	-10.8[d]
ErGAG		4.0	10.6	4.0[e]	-4.0	+10.6	-4.0[e]
	(expt.)	4.3 ± 0.3	4.3 ± 0.3	11.3 ± 0.3[d]			
	(calc.)				-8.2	+3.4	-7.2[d]
ErAG							
	(expt.)	8.29	3.47	7.27[d]			

[a]Grünberg et al, 1969.
[b]Ball et al, 1963.
[c]Wolf et al., 1962.
[d]Orlich and Hüfner, 1969.
[e]Crosswhite and Moos, 1967.

B. Magneto-Optical Effects

Magneto-optical effects are useful in unraveling the electronic structure of atomic, molecular, and solid state systems. There are many types of magneto-optical effects, which have been discussed in several reviews (Pershan, 1967; Freiser, 1968; Dillon, 1968; Suits, 1972). Iron garnets were found to exhibit much Faraday rotation (Dillon, 1958). The present discussion is confined to the Faraday rotation effect. In the near infrared, there are at least two contributions to the Faraday effect in the iron garnets (Krinshick and Chetkin, 1962). The first part is nondispersive and due to ferrimagnetic resonance. It is given for ReIG by the formula

$$\underset{\text{(nondispersive)}}{\alpha_F} = \left[\frac{2\pi\langle n\rangle}{c}\right] [\gamma_{Fe}(M_{Fe(d)} - M_{Fe(a)}) - \gamma_{Re}M_{Re}] \qquad (30.23)$$

where $M_{Fe(d)}$, $M_{Fe(a)}$ and M_{Re} are the algebraic sublattice magnetizations; (d) and (a) in the subscripts of M_{Fe} denote the d-site and the a-site, respectively; γ_{Fe} and γ_{Rc} are gyromagnetic ratios; $\langle n\rangle$ is the average refractive index; and c is the free-space velocity of light. The second part is a dispersive contribution associated with the allowed electric dipole transitions of Fe^{3+}, which give rise to strong absorption in the visible region. It is given by the expression for the ReIG

$$\underset{\text{(dispersive)}}{\alpha_F} = - A(\omega)M_{Fe(a)} + B(\omega)M_{Fe(d)} - C(\omega)M_{Rc} \qquad (30.24)$$

where the A, B, and C are the frequency-dependent coefficients for the electric-dipole rotation. The coefficients for YIG, GdIG, and TbIG are listed in Table 30.15 (Cooper et al., 1968; Crossley et al., 1969). All the electric-dipole (dispersive) parameters are negative, implying positive rotations from an ion whose moment is antiparallel to the light direction.

The octahedral Fe^{3+} gives a much larger contribution than the tetrahedral Fe^{3+} in YIG and GdIG leading to the resultant positive rotations.

Faraday rotation does not depend on frequency for $\lambda > 6$ μm. In TbIG, α changes sign at the compensation point. At T = 110°K, α undergoes a second change in sign and increases with further decrease in temperature (Chetkin and Shalygin, 1968). This second change in the sign of α was also observed in $Y_{0.5}Dy_{0.5}IG$ in the region of 50°K. At a wavelength greater than 4 μm, the α of $Bi_{0.24}Ca_{2.76}Fe_{3.62}V_{1.38}O_{12}$ (Chetkin and Shalygin, 1968) is positive and independent of λ. The α is 16°/cm. In the visible region, the α value is negative.

There are various mechanisms operating in different parts of the spectrum (Dillon, 1968). The magneto-optical effects can arise from:

1. Spin orbit splitting of Fe^{3+} ion allowed transitions in the visible or above. These may be charge transfer transitions or allowed single-ion transitions.
2. Exchange splitting of rare earth sharp-line transitions.
3. Exchange or spin orbit splittings of rare earth allowed transitions.
4. Ferromagnetic resonance and exchange resonances correspond to the response of whole sublattices to external magnetic fields.

Faraday rotations were studied in $\{Bi_{3-2x}Ca_{2x}\}$ $[Fe_2]$ $(Fe_{3-x}V_x)O_{12}$ where the V substitutes for tetrahedral Fe leading to a magnetically compensated ferrimagnetic composition at x = 1.0 (Buhrer, 1969). Ultraviolet measurements of the complex polar-Kerr effect (rotation and ellipticity) were reported between 1.7 and 5.64 eV for YIG, EuIG, ErIG, and Ga-substituted EuIG (Kahn et al., 1969a,b). Charge transfer transitions at about 4 and 5 eV, associated with Fe(a) and Fe(d), respectively, are found to be responsible for the principal ultraviolet magneto-optical spectra.

TABLE 30.15

Coefficients for Nondispersive and Dispersive Contributions[a] to the Faraday Rotations of YIG, GdIG, and TbIG at 1.15 μm

Nondispersive		Fe^{3+}	Gd^{3+}	Tb^{3+}
	$(2\pi\langle n\rangle/c)\gamma$	9.15	9.15	6.86
Dispersive		A	B	C
	YIG	-40.3 ± 1.7	-21.4 ± 1.2	—
	GdIG	-42.4 ± 1.8	-27.1 ± 1.3	-1.0 ± 0.2
	TbIG	-9.0 ± 15.0	-10.0 ± 11.0	-84.4 ± 2.5

[a]From Cooper et al., 1968, and Crossley et al., 1969.

C. Photomagnetic Effect

The photomagnetic effect induces a change in magnetic properties through the influence of photons, whereas the magneto-optic effects, such as Faraday rotation, etc., cause the light propagation to be influenced by the magnetization distribution. The photomagnetic effect was first observed in Si-substituted YIG (Teale and Temple, 1967). Changes in crystalline anisotropy were found in YIG:Si, and they depend on the angle between the light polarization and the crystal axes (R. F. Pearson et al., 1968). At 77°K, a single crystal picture frame $YIG:Si_{0.05}$ had its initial permeability of 6 changed to 4 after the light irradiation, and a polycrystalline toroid $YIG:Si_{0.005}$ had its initial permeability of 120 changed to 20 after exposure to the light at an intensity of about 10^{-2} W/cm^2 (Enz et al., 1969). The light also influences the switching behavior of Si-doped YIG. After irradiation with light, YIG:Si has an extremely square hysteresis loop. When a step field is applied there is a certain period of time during which no flux is switched irreversibly. The level of this delay depends on the amplitude of the applied step field. After this delay, the YIG:Si switches in the normal way. At 4.2° and 77°K these changes are permanent; at 200°K the effects disappear after the termination of light (Holtwijk et al., 1970).

A saturating field was applied along [100] of a [001] polished plate of $YIG:Si_{0.03}$. Since [100] is a symmetry direction of the cubic crystal, the anisotropy contributes no torque. After 50 sec of illumination with intense white light, linearly polarized with $\tilde{E}$ along [100], the axis of polarization is rotated to $[1\bar{1}0]$. A torque appears and increases rapidly to a value of 1.2×10^4 dyn-cm/cm^3. After 150 sec, the polarization axis rotates to [110]. Over the next 100 sec the torque decreases to

a large negative value. This type of photoinduced anisotropy implies that there is an anisotropy in the absorption of light by a single set of crystallographic sites. This is a photoinduced dichroism (Dillon et al., 1970). For a crystal plate thickness of 0.011 cm, the dichroism was found to be at 1.5°K

$$\frac{2\Delta I_{<111>}}{I} = 0.035 \quad \text{and} \quad \frac{2\Delta I_{<100>}}{I} = 0.007$$

where I is the light transmitted.

The above photoinduced effects at relatively high levels of Si are reversible. The photoinduced effect at low Si content, i.e., 0.01 to 0.017 Si per YIG formula, is irreversible and does not depend on the polarization of light. A [110] plate of YIG:$Si_{0.017}$ at 4.2°K shows a change in its cubic magneto-crystalline anisotropy after irradiation of light. The contribution of the Fe^{2+} ions to the crystal anisotropy is large, is of opposite sign to K_{YIG}, and increases rapidly with decreasing temperatures. Light irradiation decreases the absolute value of $K_{Fe^{2+}}$ at 77°K and increases the value at 4.2°K. The percent at 77°K decreases with Si content. Samples doped with Ca instead of Si, and so containing Fe^{4+}, showed no changes under the same condition. It appears that there are near and far sites for Fe^{2+} in YIG:Si and their relative proportion is influenced by irradiation. At each temperature, the experiment detects only those sites whose relaxation is of the order of ω^{-1}. Consequently, the Fe^{2+} detected at 77°K must be in a substantially different local environment than that observed at 4.2°K (Flanders et al., 1971). Each site has its own easy axis (one of the four <111> cubic directions) and when the population balance among sites is upset, a uniaxial anisotropy appears. Polarized light can create an imbalance because its coupling

to the pancake-like Fe^{2+} wave function is different for differently oriented sites. Using a crystal field theory, it was found that a 5-10% population imbalance between different oriented sites is expected for light polarized along the <110> direction (Allen et al., 1971). Irreversible photoinduced changes in optical absorption of YIG:Si^{4+} and YIG:Ca^{2+} were found in the near infrared region (Gyorgy et al., 1971).

D. Infrared Spectra

Ferrimagnetic garnets, namely the iron garnets, are transparent within the infrared region. The infrared spectra of RIG for various rare earth cations are listed in Table 30.16 (McDevitt, 1969). Similarly, the infrared spectra of RAG and RGaG are listed in Tables 30.17 and 30.18, respectively. The total irreducible representations of the transverse optical modes are

$$\Gamma = 3A_{1g} + 5A_{2g} + 8E_g + 14F_{1g} + 14F_{2g} + 5A_{1u} + 5A_{2u} + 10E_u + 18F_{1u} + 16F_{2u} \qquad (30.25)$$

The factor-group analysis predicts a total of 98 lattice-vibration modes; however, the character table for the point group O_h shows that the translation operations are of symmetry species F_{1u} only. One acoustic mode will also be found in this species and will be infrared-inactive. Therefore, this analysis predicts seventeen infrared-active lattice modes. In Table 30.16, ten frequencies were listed for the RIG series. Twelve frequencies were listed for the RGaG series (Table 30.18), and fifteen frequencies were listed for the RAG series (Table 30.17). They suggest that the powder-transmission method does not yield all of the infrared-active modes.

All of the rare-earth garnets have a set of three bands in the 800-600 cm^{-1} region. These bands are isolated by a high-transmission

maximum from other spectral features. One other general characteristic shows a strong absorption band in the region 470-370 cm^{-1}.

TABLE 30.16

Infrared Lattice Frequencies of $R_3Fe_5O_{12}$ Garnets[a]

R =	Sm	Eu	Gd	Dy	Ho	Y	Er	Tm	Yb	Lu
	630 cm^{-1}	635 cm^{-1}	638 cm^{-1}	647 cm^{-1}	655 cm^{-1}	655 cm^{-1}	656 cm^{-1}	658 cm^{-1}	658 cm^{-1}	655 cm^{-1}
	580*	588*	590*	597*	600*	605*	606*	607*	612*	616*
	550	553	555	562	565	566	567	568	568	570
	426	427	435	—	—	—	—	—	—	—
	373	373	379	380	—	381	—	—	—	—
	352	358	361	365	386	369	370	371	374	383
	326	326	326	330	330	338	328	329	331	333
	311	309	307	309	308	318	305	303	305	306
	252	252	254	255	255	269	254	251	253	254
	214	214	213	215	213	227	212	208	211	211
	—	—	—	—	—	144	—	—	—	—
	115	115	112	111	107	110	110	108	108	106
	110	109	107	108	(108)	—	(107)	(106)	(106)	—

[a]After McDevitt, 1969.

TABLE 30.17

Infrared Lattice Frequencies of $R_3Al_5O_{12}$ Garnets[a]

R =	Dy	Ho	Y	Er	Tm	Yb
	785 cm^{-1}	788 cm^{-1}	789 cm^{-1}	795 cm^{-1}	800 cm^{-1}	805 cm^{-1}
	723*	727*	726*	733*	737*	742*
	690	695	698	698	700	709
	560	563	569	566	570	569
	510	511	512	515	518	516
	455	468	465	460	463	468
	432	438	436	436	440	439
	388	395	398	397	397	397
	—	389	390	388	—	—
	370	371	378	370	371	372
	323	324	332	323	323	322
	280	282	292	279	279	278
	208	206	220	206	201	202
	—	—	178	—	—	—
	168	169	166	168	167	165
	128	126	122	127	126	125
	94	93	—	93	92	92

[a]After McDevitt, 1969

TABLE 30.18

Infrared Lattice Frequencies of $R_3Ga_5O_{12}$ Garnets[a]

R =	Sm	Eu	Gd	Dy	Ho	Y	Er	Tm	Yb	Lu
	665 cm^{-1}	609 cm^{-1}	673 cm^{-1}	681 cm^{-1}	684 cm^{-1}	688 cm^{-1}	691 cm^{-1}	697 cm^{-1}	700 cm^{-1}	704 cm^{-1}
	604	608*	612*	620*	623*	627*	630*	636*	639*	640*
	573	575	578	587	589	590	592	596	595	600
	461	464	469	476	474	476	480	485	483	490
	384	384	388	388	390	393	385	392	387	392
	324	324	322	322	323	340	322	323	320	322
	246	246	246	249	251	257	249	251	251	251
	222	222	222	220	221	234	222	220	219	221
	145	145	145	145	144	147	144	144	143	141
	119	119	118	117	116	114	116	115	113	113
	113	111	111	111	111	—	110	108	108	107
	(88)	(88)	(88)	(88)	(86)	—	(86)	(84)	(84)	(84)

[a]After McDevitt, 1969.

The yttrium garnets have a number of distinctive features that set them apart from the rest of the rare-earth garnets in each series. The frequencies for YAG at 378, 332, 292, 220 cm^{-1} are higher than the other frequencies in the RAG series (Table 30.17). In the low frequency region the 93 cm^{-1} band is missing from the YAG spectrum. Similarly, the frequencies for YGaG at 393, 340, 257, 234 cm^{-1} are higher than others in the series (Table 30.18). In the low frequency region, the 110 and 86 cm^{-1} bands are missing. In the case of YIG, the 338, 318, 259, 227 cm^{-1} are higher than others, the 144 cm^{-1} band is nonexistent in others, and the 107 cm^{-1} band is missing in the YIG spectrum (Table 30.16). From the optical spectra, the energy levels of the ground state multiplets of trivalent rare-earth ions in garnets can be determined and are listed in Table 30.19 (Oliver et al., 1969a).

TABLE 30.19

Energy Levels of the Ground State Multiplet of Trivalent Rare Earth Ions in Garnets[a]

Ion	Host crystal	Multiplet	No. of levels	Wave number (cm^{-1})	Ref.
Gd^{3+}	GdAG	$^8S_0$	1	0	(b)
Gd^{3+}	GdGaG	$^8S_0$	1	0	(b)
Tb^{3+}	TbAG	$^7F_6$	13	0; 4	(c)
Tb^{3+}	YAG	$^7F_6$	13	0; 5; 61; 70; 116; 207; 270; 432; 443	(d)
Tb^{3+}	TbGaG	$^7F_6$	13	unknown	—
Tb^{3+}	YGaG	$^7F_6$	13	unknown	—
Tb^{3+}	YIG	$^7F_6$	13	0; 6; 38; 40; 55; 55	(e)
Dy^{3+}	DAG	$^6H_{15/2}$	8	0; 70; 116; 197; 256	(f)
Dy^{3+}	YAG	$^6H_{15/2}$	8	0; 59; 101; 175; 233; (474); (517); 860	(g,h)
Dy^{3+}	DyGaG	$^6H_{15/2}$	8	0; 20; 71	(g,h)
Dy^{3+}	YGaG	$^6H_{15/2}$	8	0; 20; 71; 118; 149; (466); 527; 579	(g)
Ho^{3+}	HoAG	$^5I_8$	17	0; 36; 42; 54; 63	(i)
Ho^{3+}	YAG	$^5I_8$	17	unknown	—
Ho^{3+}	HoGaG	$^5I_8$	17	0; 5; 27; 30; 39; 44	(j, k)
Ho^{3+}	YGag	$^5I_8$	17	unknown	—
Er^{3+}	ErAG	$^4I_{15/2}$	8	0; 27; 58; 79; 423; 436; 530; 574	(l)
Er^{3+}	ErGaG	$^4I_{15/2}$	8	0; 46; 56; 76	(m)
Er^{3+}	YGag	$^4I_{15/2}$	8	0; 44; 49; 76; 422; 430; 490; 527	(n)
Tm^{3+}	TmAG	$^3H_6$	13	0; 35	(i, o)

Tm^{3+}	YAG	$^3H_6$	13	0; 28; 43; 270; 490	(p, q)
Tm^{3+}	TmGaG	$^3H_6$	13	0; 63; 85; 113; 123; 184	(o, q)
Tm^{3+}	YGaG	$^3H_6$	13	0; 64; 87; 99; 188	(q, r)
Yb^{3+}	YbAG	$^2F_{7/2}$	4	0; 618; 701; 766	(s)
Yb^{3+}	YbGaG	$^2F_{7/2}$	4	0; 546; 599; 624	(s)

[a]Oliver et al., 1969a.
[b]Dieke and Crosswhite, 1963.
[c]Cooke et al., 1967.
[d]Koningstein, 1964.
[e]Knight and Huber, 1968.
[f]Koningstein and Ng, 1969.
[g]Grunberg et al., 1967.
[h]Veyssie and Dreyfus, 1967.
[i]Milward, 1967.
[j]Sievers and Tinkham, 1963.
[k]Onn et al., 1967a.
[l]Hellwege et al., 1966.
[m]Dreyfus et al., 1965.
[n]Crosswhite and Moos, 1967.
[o]Bierig and Rimai, 1965.
[p]Koningstein, 1966.
[q]J. J. Pearson et al., 1968.
[r]Buchanan et al., 1969.
[s]Buchanan et al., 1967.

E. Optical Absorption

The optical absorption coefficient α can be determined by the equation

$$I = I_o(1-R)^2 \exp(-\alpha t) \qquad (30.26)$$

where I is the transmitted light intensity, I_o the incident light intensity, R the single-surface reflection loss at normal incidence, and t is the thickness in centimeters. The α values are useful technical quantities and are also excellent monitors of the purity of samples. For example, in an undoped YIG, the α values are about 0.03 cm^{-1} in the infrared region between 2250 and 8350 cm^{-1}. With a 0.13 at.% Si addition, the α value changes to 6 cm^{-1} in the region between 5800 and 9100 cm^{-1} (LeCraw et al., 1965).

The optical absorption of YAG was studied in the region from 10 to 55,000 cm^{-1} (Slack et al., 1969). No lattice absorption peaks were observed in YAG for wave number less than 80 cm^{-1} (Milward, 1967). The wave number $\bar{\nu}$ region between 0 and 860 cm^{-1} is labeled as the one-phonon region where the absorption of one photon generates one phonon. The α values in this region are all fairly high and then decrease rapidly for $\bar{\nu} > 860$ cm^{-1} (Slack et al., 1969).

The absorption peaks at $\bar{\nu} = 700, 729, 792$ cm^{-1} are components of the $\bar{\nu}_3$ vibration of the AlO_4 molecular group. These $\bar{\nu}_3$ peaks shift to about 600 cm^{-1} in YGaG and YIG, caused by GaO_4 and FeO_4 groups and the larger sizes and masses of Ga and Fe.

The very lowest wave number mode is at $\bar{\nu} = 123$ cm^{-1} in YAG. In DyAG, HoAG, and ErAG where the rare earth ion substitutes for Y, this mode shifts to 95 cm^{-1}. It further shifts to 85 cm^{-1} for ErGaG and YbGaG. This lowest mode in YAG is probably an external mode of the whole lattice, involving the Y and Al ions.

The region between 860 and 2400 cm^{-1} is believed to be caused by multi-phonon processes in which one photon generates two or more phonons. The α values for the two-phonon processes are about 10^{-2} times as large as the one-phonon processes, and the three-phonon processes give α values about 10^{-4} times as large.

The two phonon processes produce an absorption peak in YAG at 1450 cm^{-1} which is just about $2\tilde{\nu}_3$. The three-phonon processes produce the peak at 2120 cm^{-1}, which is nearly equal to $3\tilde{\nu}_3$ of the AlO_4 vibration, and it is an intrinsic feature of YAG and is not caused by trace impurities. The $2\tilde{\nu}_3$ and $3\tilde{\nu}_3$ peaks of FeO_4 groups in YIG occur at 1200 and ~1700 cm^{-1} (Cockayne, 1966; Wood and Remeika, 1967).

The range between 30,000 and 52,000 cm^{-1} appears to depend on the purity or the growing conditions of the crystal or both. The α values vary from sample to sample. They do not depend on the stoichiometry of the melt.

The far-infrared lattice absorption bands in garnets at ~4°K are listed in Table 30.20 (Oliver et al., 1969b). Three types of excitations occur in ReIG. The first is the splitting of the ground Kramers doublet by the exchange field; the second is a transition to a higher crystal field level as split by the exchange field; and the third is a collective mode in which the entire Fe and rare earth sublattices undergo a mutual precession (Tinkham, 1962). The far-infrared magnetic resonance results for YbIG, as extrapolated to 0°K, show a ferrimagnetic resonance at 3.00 $\pm$ 0.05 cm^{-1} with a linewidth of <0.2 cm^{-1}; an exchange resonance at 13.65 $\pm$ 0.05 cm^{-1} with a linewidth of <0.38 cm^{-1}; two single Yb ion resonances at 23.2 $\pm$ 0.1 cm^{-1} with a linewidth of 0.5 cm^{-1} and at 27.0 $\pm$ 0.1 cm^{-1} with a linewidth of 0.5 cm^{-1}; and a Yb-Yb combination resonance at 26.3 $\pm$ 0.1 cm^{-1} with a linewidth of 0.5 cm^{-1} (Richards, 1963).

TABLE 30.20

Far-Infrared Lattice Absorption Bands[a] in Garnets at ~4°K

Garnet	$\bar{\nu}_1$ (cm^{-1})	$\bar{\nu}_2$ (cm^{-1})	Ref.
$Y_3Al_5O_{12}$ (YAG)	12.30	148	(b)
$Dy_3Al_5O_{12}$ (DAG)	94.2 ± 0.4	—	(c)
$Ho_3Al_5O_{12}$ (HoAG)	94.5 ± 0.4	—	(c)
$Er_3Al_5O_{12}$ (ErAG)	96.0 ± 2.0	109 ± 3.0	(d)
$Tm_3Al_5O_{12}$ (TmAG)	87.0	—	(c)
$Yb_3Al_5O_{12}$ (YbAG)	90.0 ± 0.8	—	(e)
$Lu_3Al_5O_{12}$ (LuAG)	88.0 ± 1.0	106.5 ± 0.5	(e)
$Ho_3Ga_6O_{12}$ (HoGaG)	86.0 ± 1.0	111 ± 2.0	(d)
$Er_3Ga_5O_{12}$ (ErGaG)	86.0 ± 1.0	114 ± 3.0	(d)
$Yb_3Ga_5O_{12}$ (YbGaG)	85.0 ± 1.0	111 ± 3.0	(d)
$Sm_3Fe_5O_{12}$ (SmIG)	83.0 ± 2.0	—	(d)
$Ho_3Fe_5O_{12}$ (HoIG)	81.6 ± 0.9	98 ± 2.0	(d)

[a] From Oliver et al., 1969b.
[b] Slack et al., 1969.
[c] Milward, 1967.
[d] Sievers and Tinkham, 1963.
[e] Oliver et al., 1969b.

The optical absorption bands of Cr^{3+}, Fe^{3+}, OH^-, impurities in garnets are listed in Table 30.21 (Oliver et al., 1969a). Impurities are dependent on crystal growing conditions. Hydrothermal YIG contain an appreciable concentration of the OH group which absorbs radiation in a line spectrum extending from 2500 to 3700 cm^{-1} in the infrared. YIG crystals grown from D_2O solution have the OD isotope stretching frequency from 2200 to 2700 cm^{-1} with one-to-one correspondance with the OH lines at $\bar{\nu}_{OH} = 1.3\ \bar{\nu}_{OD}$. The very broad line at 2930 cm^{-1} is associated with a site containing the Na^+ ion.

A Ga-doped YIG crystal contains two lines at 3442 and 3419 cm^{-1}. In undoped YIG, two lines at 3578 and 3568 cm^{-1} disappear with Ga substitution. They may be due to OH groups in the vicinity of a vacancy in the tetrahedral site.

The OH absorption spectrum is different for different seed orientations, with some individual lines present in crystals of (100) seeds, and missing from crystals of (111) or (211) seeds. The absolute intensity of the strongest OH lines is the least for growth on (111) while the growth on (100), (110), and (211) shows increasing amounts in that order (Wood et al., 1968).

The refractive index of single crystal YIG over the wavelength range 1-6 μm was measured by the minimum deviation method (Johnson and Walton, 1965). The mean refractive indices of YIG as a function of wavelength are listed in Table 30.22. The dispersion curve agrees with the mean index results for YIG to within 0.2% by a set of constants $f_1 = 3.739$, $\lambda_1 = 0.28$ μm, $f_2 = 0.79$, $\lambda_2 = 10.0$ μm as applied to a dispersion curve equation of the form

$$n^2 = 1 + \sum_{i=1,2} \frac{fi\lambda^2}{\lambda^2 - \lambda_i^2} \qquad (30.27)$$

TABLE 30.21

Optical Absorption Bands of Cr, Fe, OH Impurities in Garnets[a]

Impurity	Garnet	Wave Number of absorption band maximum (cm^{-1})	Ref.
Cr^{3+}	YAG	17,000; 23,000	(b)
Cr^{3+}	YGaG	17,000; 22,500	(b)
Fe^{3+} (a-site)	YIG	10,200; 11,100; 14,280	(c)
Fe^{3+} (d site)	YIG	16,400	(c)
Fe^{3+} (a-site)	YGaG	23,000; 23,870; 24,270	(c)
Fe^{3+} (d-site)	YGaG	20,410; 21,050; 26,300; 26,670	(c)
OH^-	YIG	3571	(d)

[a]From Oliver et al., 1969a.
[b]Wood et al., 1963.
[c]Wood and Remeika, 1967.
[d]Kolb et al., 1967.

TABLE 30.22

Mean Infrared Refractive Index of YIG[a]

λ (μm)	n
1.4	2.209
1.6	2.200
1.8	2.194
2.0	2.188
2.5	2.177
3.0	2.168
3.5	2.158
4.0	2.148
4.5	2.134
5.0	2.118
5.5	2.103

[a]Johnson and Walton, 1965.

30.3.7 Thermal Properties

A. Thermal Conductivity

The thermal conductivities of garnet crystals, as a group, have been extensively investigated. Studies were made on YIG (Luthi, 1962; Friedberg and Harris, 1963; Douglass, 1963; Oliver and Slack, 1966; Rives et al., 1966), on YAG (Oliver and Slack, 1966; Klein and Croft, 1967), on YGaG (Holland, 1968), and on DAG (Landau and Dixon, 1970). Theoretical studies were also made on YIG (Bhandari and Verma, 1966; Joshi and Sinha, 1966). These garnet crystals have a thermal conductivity κ of about 0.07 to 0.10 W/cm^{o}K at 300^{o}K and reach a κ maximum of 1 to 5 W/cm^{o}K near 20^{o}K. The similarity in κ among the garnets, both synthetic and natural, provides a study case of the effect of crystal structure on κ. In the rare earth doped garnet crystals, the κ data can reveal the phonon scattering by the rare earth ions. A detailed discussion of the thermal conductivity of garnets has been presented in an extensive article (Slack and Oliver, 1971), which readers are advised to consult for κ data of garnet crystals.

Briefly, the κ results of garnets can be summarized as follows. All garnets are nonmetallic. They have no free electrons to carry heat, and thus heat transport is predominantly via the phonons. From the Debye temperature, θ_D, obtained in other studies, the κ vs. T experimental curve can be extrapolated to give an experimental value of κ_0 at $T = \theta_D$. This value can be calculated by the equation

$$\kappa_0' = 1.43 \times 10^{-8} \langle M \rangle (\langle V_o \rangle)^{1/3} \theta_D^{\,2} \text{ W/cm}^{o}\text{K} \qquad (30.28)$$

where $\langle M \rangle$ is the average atomic mass of an atom in the garnet crystal in grams, and $\langle V_o \rangle$ is the average volume in cubic angstroms, occupied by one atom of the solid. The ratio κ_0/κ_0' is called the crystal complexity

factor G (Oliver and Slack, 1966). The values of κ_0, κ_0', and G, for several garnets are listed in Table 30.23 (Slack and Oliver, 1971). The crystal complexity factor G varies from 0.080 to 0.114 for these garnets, with an average value of 0.09 ± 0.01. The factor G for the natural garnet, i.e., grossulanite [essentially $(Mg, Fe, Mn)_3Al_2Si_3O_{12}$] agrees with other synthetic garnets. The ferrimagnetic YIG agrees with other nonmagnetic garnets in their G factors.

TABLE 30.23

Thermal Conductivity Values at θ_D for Garnet Crystals[a]

Crystal	Debye temperature θ (^oK)	Thermal conductivity (W/cm^oK)		G
		κ_0	κ_0'	
Grossularite	770	0.043	0.418	0.103
YAG	750	0.042	0.527	0.080
GdAlG	640	0.045	0.521	0.086
LuAlG	620	0.043	0.515	0.083
YGaG	585	0.046	0.447	0.103
GdGaG	520	0.051	0.446	0.114
YbGaG	520	0.039	0.464	0.084
YIG	565	0.038	0.384	0.099

[a]From Slack and Oliver, 1971.

Therefore, the crystal complexity factor G can be considered as a characteristic feature of the garnet structure, with an average value of 0.09 ± 0.01.

The theory of the effect of crystal structure on κ is still in a very rudimentary state. It is generally observed that the larger the number of optical branches in the phonon spectrum, the lower the thermal conductivity. In garnets, there are 80 atoms in the primitive unit cells, and there are 97 optical modes at the zone center (Hurrell et al., 1968). The combination of infrared and Raman studies has at most found 42 of the 97 optical unknowns. A phonon of energy $k_B T$ at $T = 300^{\circ}K$ has an energy in wave number of 209 cm^{-1}, it is an optical phonon in YAG, and it has a very small or nearly zero propagation velocity. It contributes very little to the thermal conduction in the crystal.

The presence of the low-lying optical modes in YAG and their absences in Al_2O_3 caused the absence and presence of the Umklapp processes in κ data. The characteristic of Umklapp processes in the exponential rise in κ with decreasing temperature. Umklapp processes require that the wave vectors of the three interacting acoustic phonons combine to equal a wave vector of the reciprocal lattice. The wave vectors of the reciprocal lattice are very small in garnets because of the large size of its unit cell. The phonons of relatively low wave vector and low energy can undergo Umklapp processes in garnet. The critical phonon energy is that of the acoustic phonons at the zone boundary. The κ of YAG rises with decreasing temperature with a dependence of $\exp(\theta/bT)$, where b is about 2 and 0 is $177^{\circ}K$. This dependence agrees with the observed data.

If the only mechanism which limits the mean free path of the phonon

is the boundary scattering, then κ should be proportional to the sample size (Thacher, 1967). At $3^{o}K$, the experimental ratio of κ to the sample diameter d of YAG had a temperature dependence of $T^{2.5}$ (Slack and Oliver, 1971).

Phonon scattering produced by the low-lying electronic levels of the rare-earth ions in garnets reduces the κ below that of the corresponding non-magnetic garnet. The data on DAG show no anomaly in and through it Neel point T_N of $2.54^{o}K$. If there is a magnon contribution to κ near T_N of DAG, it is less than 10% of the lattice κ, and may be zero (Slack and Oliver, 1971). This is in disagreement with the report of a minimum in κ at T_N (Landau and Dixon, 1970). The κ of some magnetic garnets, such as those of Tb, Dy, Ho, Er, and Tm, is suppressed by a one-phonon resonance scattering process for those phonons whose energies are equal to the energy difference between two electronic levels. The effectiveness of this magnetic scattering is largest for Dy and decreases in the series, Dy, Tb, Tm, Er, and Ho. Its temperature dependence is closely related to the thermally determined population differences between the two levels involved in the transition (Slack and Oliver, 1971).

B. Specific Heat

Specific heat in garnets has been analyzed theoretically (Harris and Meyer, 1962). It can be expressed by

$$C_V = C_L + C_M + C_N \qquad (30.29)$$

where C_L, C_M, and C_N refer to the contribution to the total specific heat, C_V, from the lattice, from the interactions between unpaired electrons of the ions (magnetic), and from the electron-nuclear spin interactions (nuclear), respectively. The lattice specific heat, C_L, follows the well-known T^3 law at low temperatures where the ratio Θ/T may be taken to be

infinite for all practical purposes, and 0 is the Debye temperature.

$$C_L = RA_L T^3 \tag{30.30}$$

where R is the gas constant. An interpolation scheme to calculate the C_L of ReIG from the C_L of EuIG is found to be more successful in the case of the scaling factor being the 3/2 power of the ratio of masses of rare earth ion to Eu ion than in the case of the scaling factor being the ratio of the molecular weights of the two garnets. The former case is given by

$$C_L(\text{RIG}) = (W_{RE}/W_{EU})^{3/2} C_L(\text{EuIG}) \tag{30.31}$$

where W_{RE} and W_{EU} are the masses of the rare earth ion and Eu ion, respectively (Henderson et al., 1969). A list of the lattice specific heat temperature coefficients, A_L, for several RIG and YIG is given in Table 30.24.

The nuclear specific heat, C_N, has a T^{-2} dependence given by

$$\begin{aligned} C_N &= RA_N T^{-2} \\ &= RT^{-2} 6 \sum_i (1/3) I_i (I_i+1) (\Delta_i/k_B)^2 \end{aligned} \tag{30.32}$$

for $\Delta_i < k_B T$, where the summation is over the different isotopes and where

$$\Delta_i = g_{N,i} \beta_N H_{N,i} \tag{30.33}$$

is the separation between successive nuclear levels. I_i is the nuclear spin, $g_{N,i}$ is the nuclear splitting factor, β_N is the nuclear magnetron, and $H_{N,i}$ is the field at the nucleus. The C_N of Fe^{57} above 0.4^oK is negligible because of the small splitting $\Delta(Fe^{57})/k_B \simeq 3 \times 10^{-3o}K$, and because of the low abundance of this isotope, 2.5%. Therefore, only the C_N of the rare earth ions needs to be considered in RIG. A list of nuclear specific heat temperature coefficients, A_N, for several RIG is also given in Table 30.24.

For the magnetic iron garnets, there is a magnetic contribution, C_M, to the specific heats. The magnetic specific heat of YIG, EuIG, and

TmIG can be attributed entirely to the acoustical spin-wave modes, since their optical modes have too high an energy to be populated at low temperatures (Harris, 1963). For YbIG and SmIG, the C_M is dominated by the contributions from the twelve low-lying optical modes with energy $E_j(k)$ corresponding to the 12 inequivalent c-sites in the unit cell.

TABLE 30.24

Specific Heat Temperature Coefficients for Several ReIG

	Temperature coefficients[a]	
	Lattice A_L	Nuclear A_N
YIG	0.53×10^{-4}	
SmIG	0.75×10^{-4}	$2.6 \pm 0.4 \times 10^{-3}$
EuIG	0.75×10^{-4}	$9.07 \pm 0.1 \times 10^{-3}$
GdIG	0.75×10^{-4}	
TmIG	0.93×10^{-4}	$0.78 \pm 0.04 \times 10^{-3}$
YbIG	0.96×10^{-4}	$1.6 \pm 0.3 \times 10^{-3}$
LuIG	0.98×10^{-4}	0.82×10^{-3}

[a]Henderson et al., 1969.

For the acoustic spin-wave modes, the temperature dependence of C_M follows mainly the $T^{3/2}$ relationship coupled with a moderating function G(T).

$$C_M = (0.113/4)R(k_BT/D)^{3/2}G(T) \tag{30.34}$$

where D is the dispersion constant which is a linear combination of the exchange integrals in the garnet. The moderating function G(T) can be either calculated or experimentally curve-fitted. One calculated expression of G(T) is (Harris, 1963)

$$G(T) = [1 + 1.17(k_BT/D)[(5E + F)/D]\}$$
$$x\ [k_BT-1.6g\beta M][k_BT-g\beta H_A][k_BT]^{-2} \tag{30.35}$$

where H_A is the anisotropy field. For YIG, the C_M data, calculated from Eqs. (30.34) and (30.35), using the values E = 5 cm^{-1}, F = 0, and D = 30 cm^{-1}, and the C_L data, calculated from Eq. (30.36) with $A_L = 0.557 \times 10^{-4}$ can be subtracted from the total specific heat, C_V. The remaining part can be empirically fitted by a linear expression (Onn et al., 1967b)

$$C_r = (C_V-C_L-C_M) = R \times 10^{-4} \times 1.11T \tag{30.36}$$

An alternate expression for G(T) is (Henderson et al., 1969)

$$G(T) = \exp(-0.45x) \tag{30.37}$$

where

$$x = g\beta H_i/k_BT \tag{30.38}$$

for YIG, the residual part of C_V after the subtraction of C_L and C_M where C_M is calculated from Eqs. (30.34), (30.37), and (30.38), is, within the error limit, a linear function of temperature. The linear temperature coefficient ε was found to be $(6.4\pm1.5) \times 10^{-5}$ R at H = 0 and $(9.0\pm2) \times 10^{-5}$ R for H > 4kOe. At 1^oK and at 4^oK, this linear residual part accounts for ~35% and ~6%, respectively, of the total specific heat (Henderson et al., 1969).

In EuIG, the nuclear specific heat, C_N, must be included. The linear residual part had a temperature coefficient of $(0.23 \pm 0.03) \times 10^{-3} R$, and it is ~15% of C_V above 2^oK, but becomes negligible below 1.2^oK (Henderson et al., 1969). The C_V data of TmIG behave approximately the same as for EuIG and YIG. Their analysis is hampered by the uncertainty on the value of D for TmIG. No evidence of a Tm^{3+} optical level becoming populated at temperatures below 4.5^oK was found in the C_V data.

In SmIG, where the optical spin-wave modes dominate, the C_M data can be fitted by the expression

$$C_M = (R/6)(E/k_BT)^2 \exp(-E/k_BT) \qquad (30.39)$$

with $E = 38^o \pm 3^oK$ (Henderson et al., 1969). The same situation obtains for YbIG, but here agreement between data and calculation is not very good (Henderson et al., 1969).

Specific heat measurement is an effective method of obtaining the Debye temperature, θ_D, but it is affected by impurities in the samples. In the case of YIG where many samples were used by different workers, the θ_D, as obtained from the C_V data, varies from 572^o to 538^oK. A list of the Debye temperatures of several garnets is given in Table 30.25, with some of the θ_D values obtained from elastic constant measurements (Oliver et al., 1969a).

TABLE 30.25

Debye Temperatures of Garnets[a,b]

Crystal	<M> (gm)	θ (^{o}K)	Method	Ref.
YAG	29.68	750	C_{ij}	(c,d)
$Fe_3Al_2Si_3O_{12}$ (Almandite)	23.80	745	C_{ij}	(e)
TbAG	40.22	670	C_{ij}	(f)
TmAG	41.76	620	C_{ij}	(f)
YGaG	40.37	585	C_{ij}	(c)
YIG	36.90	572	C_p	(g)
YIG	36.90	565	C_{ij}	(h)
EuIG	43.36	495	C_{ij}	(h)
LuIG	49.81	458	C_v	(g)
NdGaG	48.67	380	C_v	(i)
YbGaG	52.99	380	C_v	(i)

[a]The terms used:

M	average mass of an atom of the crystal
θ	Debye temperature
C_{ij}	denotes the determination of θ from room temperature elastic constants
C_p, C_v	denotes the determination of θ from specific heat measurement at low temperatures.

[b]From Oliver et al., 1969a.
[c]Spencer et al., 1963.
[d]Alton and Barlow, 1967.
[e]Soga, 1967.
[f]Oliver et al., 1969a.
[g]Harris and Meyer, 1962.
[h]Bateman, 1966.
[i]Onn et al., 1967b.

Dysprosium aluminum garnet (DAG) is an interesting compound which resembles closely a two-lattice Ising antiferromagnet (Ball et al., 1964). The Dy^{3+} ions have an extremely anisotropic g factor with $g_z \simeq 18$ and $g_x \simeq g_y \simeq 0$. DAG is a highly anisotropic antiferromagnet with moments $S' = \frac{1}{2}$ which point along the $\pm$ x, $\pm$ y, and $\pm$ z axes. In a magnetic field along a <111> axis, the x, y, and z sublattices become equivalent. Below 1.66°K, the specific heat of DAG undergoes a first-order transition in applied fields, and above 1.66°K, the transition has a continuous, but finite derivative, in the observed thermodynamic functions (Keen et al., 1966). Close to T_N (2.53°K), the phase boundary between the antiferromagnetic and the paramagnetic phases can be accurately fitted to the data by the expression:

$$H^c_{int} = A[1-(T/T_N)]^n \qquad (30.40)$$

with $n = 0.50 \pm 0.02$ as predicted by theory (Fisher, 1960), $A = 6.52$ kOe, and $T_N = 2.53 \pm 0.01$°K.

The specific heat results of DAG can best be fitted by the equation

$$C = A'(T-T_N)^{-\alpha} + B' \qquad (30.41)$$

with $\alpha = 0.31 \pm 0.02$ (Keen et al., 1967).

The lambda transition of DAG can also be indicated by the thermal expansion data. For $|1-(T/T_N)| < 0.1$., the thermal expansion data are consistent with a logarithmic singularity when $T < T_N$ and with a power law behavior for $T > T_N$ (Philip et al., 1969).

C. Thermal Expansion

Lattice constants of YAG, YGaG, GdGaG, GdIG, and YIG were measured in the temperature range 296°-1400°K (Geller et al., 1969). The data were fitted to the expression

$$(\Delta a)/a_o = I + bT + (c/2)T^2 + dT^{-1} \qquad (30.42)$$

where a_o was the lattice constant at 296°K. The polynomial parameters I, b, c, and d for these garnets are listed in Table 30.26. Below the Curie temperature of both YIG and GdIG, there is a slight concavity of $(\Delta a/a_o)$ vs. T, while above T_c, $(\Delta a/a_o)$ vs. T is straight for both garnets. The parameters listed in Table 30.26 are very sensitive to the observed α values. They are simply empirical parameters used to fix the data.

Dilatometry studies of YAG crystals (Gupta and Valentich, 1971) show good agreement with lattice parameter measurements of YAG powders (Croft, 1965; Geller et al., 1969). Dilatometric data on a polycrystalline YAG sample with about 5% porosity show lowering of thermal expansion. From room temperature to 1673°K, the linear thermal expansion coefficients are $8.9 \times 10^{-6}/°K$ and $8.0 \times 10^{-6}/°K$ for single crystal and polycrystalline YAG, respectively. Change in density, from 4.38 gm/cm^3 to 4.35 gm/cm^3, of the polycrystalline sample showed no differences in its expansion.

TABLE 30.26

Polynomial Parameters for the Mean Thermal Expansion Coefficients of Several Garnets (Gelber et al., 1969)

	I ($\times 10^{-3}$)	b ($\times 10^{-6}$)	c ($\times 10^{-9}$)	d ($\times 10^{-1}$)	a_o at 296°K (Å)	Temperature range (°K)
YAG	-2.968	8.192	0.994	1.535	12.008	296-1401
YGaG	-0.747	4.692	4.519	-2.545	12.274	296-1309
GdGaG	-2.201	7.084	2.457	-0.034	12.375	296-1402
GdIG	-8.580	21.335	-14.422	8.564	12.471	296-553
	-3.012	10.177	—	—	12.471	553-1273
YIG	-11.258	25.661	-17.810	13.155	12.376	296-553
	-3.117	10.496	—	—	12.375	553-1398

30.3.8 Elastic Properties

A. Elastic Constants

The elastic constants of EuIG, YIG, GdIG, GeGaG, YGaG, and YAG are tabulated in Table 30.27. Two natural silicate garnets are also included in Table 30.27. They are designated Si-garnet 1,

$$3(Mn_{55}Fe_{43.5}Mg_{0.2}Ca_{1.3})O_{100}.Al_2O_3.3SiO_2,$$

and Si-garnet 2, $3(Fe_{81}Mg_{14}Mn_1Ca_4)O_{100}.Al_2O_3.3SiO_2$ (Varma, 1960). The elastic constants increase in the order of EuIG, YIG, GdIG, GdGaG, YGaG, Si-garnets 1 and 2, and YAG. Elastic anisotropy is defined for the garnet structure as

$$A = 2C_{44}/(C_{11}-C_{12}) \qquad (30.43)$$

From the A values listed in Table 30.27, GdIG with an A of 1.0007 has the lowest anisotropy, YGaG with an A of 1.10 has the highest anisotropy. Most of the listed A values in Table 30.27 lie within ± 5% of isotropy.

The longitudinal and shear velocities of several garnets are listed in Table 30.28. Longitudinal velocities fall within the range 6.3-8.6 x 10^5 cm/sec, and shear velocities fall within the range 3.3-5.0 x 10^5 cm/sec.

The temperature dependences of the elastic constants of YAG are found to be negative (Alton and Barlow, 1967). Based on the elastic constants at 25°C C_{11} for YAG is 1.0127 times greater than at 150°K, C_{44} is 1.010 times greater, and C_{12} is 1.007 times greater at 150°K. The isotropy factor A is found to decrease from 1.033 at 300°K to 1.027 at 150°K. As a comparison, the temperature dependences of elastic compliances of natural silicate garnets are found to be positive for s_{11} and s_{44}, and negative for s_{12} (Reddy and Bhimasenacha, 1964). The s_{11} value is 3.84 x 10^{13} cm^2/dyn at 93°K, 3.95 x 10^{13} at 323°K, and 4.17 x 10^{13} at 573°K.

The s_{12} value is -1.17 x 10^{13} cm^2/dyn at 93°K, -1.14 x 10^{13} at 323°K, and -1.09 x 10^{13} at 573°C. The s_{44} value is 2.45 x 10^{13}, 2.42 x 10^{13}, and 2.62 x 10^{13} cm^2/dyn for 93°, 323°, and 573°K, respectively. The temperature gradient of s_{11} varies from 0.00025 at 93°K to 0.0006 at 323°K, and to 0.0012 at 573°K. The $(\Delta s_{12}/\Delta T)$ varies from -0.000125 at 93°K to -0.0002 at 323°K, and to -0.0004 at 573°K. The $(\Delta s_{44}/\Delta T)$ varies from 0.00075 at 93°K to 0.0018 at 323°K, and to 0.0016 at 573°K.

Microhardness values of YIG, YGaG, and YAG are listed in Table 30.29 (Gendelev and Shcherbak, 1966). The values are more refined than the previously reported 1500 kg/mm^2 for YIG (Courtel et al., 1962). On {110} faces, the microhardness is maximum in <100> and minimum in <111>. On the (110) face of YIG, M.H. <100> = 1340 kg/mm^2, M.H. <111> = 1210 kg/mm^2, and M.H. <100> > M.H. <110> > M.H. <111> (Gendelev and Shcherbak, 1966). On {211} faces the maximum M.H. direction is <110>; the M.H. values fall in the directions <311> and <210>. On the (211) face of YIG, M.H. <110> = 1320 kg/mm^2, and M.H. <111> = 1230 kg/mm^2. Replacement of Fe by Ga, and especially by Al, increases microhardness in all directions of the (110) plane. In YAG, {110} faces predominate markedly over {211}, and also prove to be harder. YIG and YGaG {211} faces are harder than {110} faces.

TABLE 30.27

Elastic Constants of Several Garnets

	C_{11}	C_{12}	C_{44}	Elastic anisotropy $A = \frac{2C_{44}}{C_{11}-C_{12}}$	Density (gm/cm^3)	Ref.[a]
	x 10^{-11} dyn/cm^2					
EuIG	25.10	10.70	7.62	1.051	6.28	1
YIG	26.80	11.06	7.66	0.973	5.17	1
	26.90	10.77	7.64	0.947	5.17	2
GdIG	27.31	12.50	7.41	1.0007		3
GdGaG						
[001]	28.57	11.49	9.02	1.0562	7.085	4
[110]	28.59	10.53	9.03	1.0574	7.085	4
[$\bar{1}$10]	28.51	10.47	9.02	1.0574	7.085	4
YGaG	29.03	11.73	9.547	1.10	5.79	5
YAG	33.32	11.07	11.50	1.03	4.55	5
Si-garnet 1	30.73	10.97	9.52		4.247	6
Si-garnet 2	30.48	11.23	9.44		4.183	6

[a]Key to reference numbers: 1. Bateman, 1966; 2. Clark and Strakna, 1961; 3. Comstock et al., 1966; 4. Graham and Chang, 1970; 5. Spencer et al., 1963; 6. Varma, 1960.

TABLE 30.28

Longitudinal and Shear Velocities of Several Garnets

	Longitudinal velocity v_l (x 10^{-5} cm/sec)			Shear velocity v_s			Ref.[a]
EuIG	W[110],	P[110]	6.375	W[110],	P[1$\bar{1}$0]	3.385	
				W[110],	P[001]	3.484	1
YIG	W[110],	P[110]	7.172	W[110],	P[1$\bar{1}$0]	3.902	
	W[100]		7.209				
	W[110]		7.153	W[110]		3.843	2
GdIG			6.50			3.39	3
GdGaG	W[001]		6.399	W[001]		3.469	
	W[110]		6.402	W[110]		3.470	
	W[$\bar{1}$10]		6.394	W[$\bar{1}$10]		3.467	4
YGaG	W[001]		7.080	W[001]		4.0601	
	W[110]		7.1914	W[110],	P[001]	4.0614	
				W[110],	P[1$\bar{1}$0]	3.8655	5
YAG	W[001]		8.5630	W[001]		5.0293	
	W[110]		8.6016	W[110],	P[001]	5.0274	
				W[110],	P[1$\bar{1}$0]	4.9438	5
Si-garnet 1[b]	W[100],	P[100]	8.51	W[100],	P[100]	4.74	
	W[100],	P[110]	8.47				6
Si-garnet 2[b]	W[100],	P[100]	8.54	W[100],	P[100]	4.75	
	W[100],	P[110]	8.51				6

[a]The key to the reference numbers is given in Table 30.27.

[b]The chemical formulas are Si-garnet 1:3$(Mn_{55}Fe_{43.5}Mg_{0.2}Ca_{1.3})O_{100}.Al_2O_3.3SiO_2$; Si-garnet 2:3$(Fe_{81}Mg_{14}Mn_1Ca_4)O_{100}.Al_2O_3.3SiO_2$.

TABLE 30.29

Microhardness of YIG, YGaG, and YAG

(Gendelev and Shcherbak, 1966)

	Mean microhardness of faces (kg/mm^2)		Error in measuring microhardness of faces (kg/mm^2)		Mean microhardness of crystal H_m	Class of Hardness H_o
	(110)	(211)	(110)	(211)		
YIG	1210	1240	35	50	1230	7.5
YGaG	1450	1520	45	75	1490	8.0
YAG	1900	1650	50	85	1730	8.4

B. Ultrasonic Attenuation

The observed sound attenuations at room temperature were theoretically related with the measured thermal properties of several insulating crystals (Woodruff and Ehrenreich, 1961). The theory applies for the limit of $\omega\tau \ll 1$, where ω is the angular frequency of the sound wave, and τ is the relaxation time of thermal phonons. The sound attenuation Γ in decibels per centimeter is given by

$$\Gamma = 8.68(\langle\gamma\rangle^2\Omega^2\kappa T/\rho\langle v\rangle^5) \tag{30.44}$$

where $\langle\gamma\rangle$ is the average Gruneisen constant, which depends on the mode and polarization of the sound wave, κ is the thermal conductivity, ρ is the density, Ω is the angular frequency of the sound wave, and $\langle v\rangle$ is the average velocity of sound in the Debye approximation. From the work of Oliver and Slack (1966), a figure of merit R can be obtained from Eq. (30.44):

$$R = (\kappa_0/\kappa_0')(300/_0)^2(V_o)^{-1/3} \tag{30.45}$$

The sound attenuation Γ in decibels per centimeter can be expressed in terms of Γ_T in decibels per micron second by the equation (Oliver et al., 1969a)

$$\Gamma_T = \Gamma \times v \times 10^{-5} \tag{30.46}$$

The sound attenuations, sound velocities, Debye temperatures, and figures of merit for several garnets are listed in Table 30.30 (Oliver et al., 1969a). The data for other crystals are also included in Table 30.30 for comparison.

TABLE 30.30

Sound Attenuations, Sound Velocities, Debye Temperatures and Acoustic Figures of Merit of Garnets[a]

	Sound attenuation		Sound velocity	Debye Temp.	Acoustic figure of merit
	Γ_θ (dD/cm)	Γ_T (dD/μsec)	v (10^5 cm/sec)	θ (°K)	R_θ (1/Å)
Ge	30(l)	14.7	4.96	395	0.22
	9(s)	3.2	3.56		
Si	10(l)	8.5	8.47	674	0.086
	3(s)	1.6	5.42		
SiO_2	3(l)	2.2	7.2	469	0.06
	2.1(s)	1.2	5.75		
MgO	0.44(s)	0.3	6.50	949	0.013
Diamond			17.5(l)	1900	0.013
			12.8(s)		
TiO_2	0.6(l)	0.6	10.6	758	0.0068
	0.37(s)	0.2	5.38		
Al_2O_3	0.2(l)	0.2	11.03	950	0.0073
	0.5(s)	0.34	6.78		
$LiNbO_3$	0.4(l)	0.29	7.2	785	0.004
$Bi_{12}GeO_{20}$	1.5(s)	0.3	1.65	240	0.05
$MgAl_2O_4$	0.4(l)	0.34	8.71	900	0.0083
	0.1(s)	0.07	6.63		
YAG	0.3(l)	0.26	8.56	750	0.006
	0.15(s)	0.075	5.03		
YGaG	0.37(l)	0.26	7.08	585	0.016
	0.2(s)	0.08	4.06		

YIG	0.34(s)	0.165	4.14	540	0.013
TbAlG			7.31(1) 4.15(s)	620	0.004
TmAlG			4.14(s)	620	0.004

[a]From Oliver et al., 1969a.

30.4. Acknowledgments

It is a pleasure to thank Dr. David E. Cox for helpful discussions and cooperation throughout the course of this work.

30.5. References

Akaba, R., 1974, J. Crystal Growth 24/25, 537.

Akselrad, A. and H. B. Callen, 1971, Appl. Phys. Lett. 19, 464.

Allain, Y., M. Bichara and A. Herpin, 1966, J. Appl. Phys. 37, 1316.

Allen, J. W., 1975, Optical Properties of Magnetic Oxides, in: Craik, D. J., ed., Magnetic Oxides, Part 1 (John Wiley and Sons, New York) p. 349.

Allen, R., J. F. Dillon, Jr., E. M. Gyorgy and J. P. Remeika, 1971, J. Appl. Phys. 42, 1447.

Alton, W. J. and A. J. Barlow, 1967, J. Appl. Phys. 38, 3023.

Andres, K. and B. Luthi, 1963, J. Phys. Chem. Solids, 24, 584.

Antonov, A. V., A. M. Balbashov, V. A. Baltinskii and A. Ya. Chervonenkis, 1973, Soviet Phys. - Solid State 14, 1649.

Awasthi, S. K., D. M. Chackraburtty and V. K. Tondon, 1967, J. Inorg. Nucl. Chem. 29, 1225.

Bari, R. A., 1972, AIP Conf. Proc. No. 5, 290.

Ball, M., M. T. Hutchins, M. J. M. Leask and W. P. Wolf, 1963, Proc. Conf. Low Temp Phys., 8th, 1962 (Butterworth, London) p. 248.

Bartel, L. C., 1969, J. Appl. Phys. 40, 661.

Bateman, T. B., 1966, J. Appl. Phys. 37, 2194.

Batt, A. and B. Post, 1962, Acta Crystallogr. 15, 1268.

Bents, U. H., 1957, Phys. Rev. 106, 225.

Belov, N. V., N. N. Neronova and T. S. Smirnova, 1957, Soviet Phys.-Crystallogr. 2, 311.

Berndt, U., D. Maier and C. Keller, 1975, J. Solid State Chem. 13, 131.

Berndt, U., R. Tanamas and C. Keller, 1976, J. Solid State Chem. 17, 113.

Bertaut, E. F., 1968, Acta Crystallogr. A24, 217.

Bertaut, E. F., 1972, Ann. Phys. (Paris) 7, 203.

Bertaut, E. F. and F. Forrat, 1956, J. Phys. Radium 17, 129.

Bertaut, E. F., F. Forrat and P. Fang, 1963, C. R. Acad. Sci., Paris 256, 1958.

Bertaut, E. F., G. Bassi, G. Buisson, P. Burlet, J. Chappert, A. Delapalme, J. Mareschal, G. Rault, R. Aleonard, R. Pauthenet and J. P. Rebouillat, 1966, J. Appl. Phys. 37, 1038.

Bertaut, E. F. and J. Mareschal, 1967, Solid State Commun. 5, 93.

Bertaut, E. F., J. Mareschal and G. F. DeVries, 1967a, J. Phys. Chem. Solids 28, 2143.

Bertaut, E. F., J. Chappert, J. Mareschal, J. P. Rebouillat and J. Sivardière, 1967b, Solid State Commun. 5, 293.

Bertaut, E. F. and J. Mareschal, 1968, J. Phys. (Paris) 29, 67.

Berton, A. and B. Sharon, 1968, J. Appl. Phys. 39, 1367.

Bhandari, C. M. and G. S. Verma, 1966, Phys. Rev. 152, 731.

Bhide, V. G., D. S. Rajoria, G. Rama Rao and C. N. R. Rao, 1972, Phys. Rev. B6, 1021.

Bhide, V. G., D. S. Rajoria, C. N. R. Rao, G. Rama Rao and V. G. Jadhao, 1975, Phys. Rev. B12, 2832.

Bidaux, R. and P. Mériel, 1968, J. Phys. (Paris) 29, 220.

Bidaux, R., J. E. Bouree and J. Hammann, 1974, J. Phys. Chem. Solids 35, 1645.

Bierig, R. W. and L. Rimai, 1965, J. Appl. Phys. 36, 1199.

Birgeneau, R. J., J. K. Kjems, G. Shirane and L. G. Van Uitert, 1974, Phys. Rev. B10, 2512.

Blank, S. L. and J. W. Nielsen, 1972, J. Crystal Growth 17, 302.

Blasse, G., 1965a, Philips Research Report 20, 327.

Blasse, G., 1965b, J. Inorg. Nucl. Chem. 27, 993.

Bobeck, A. M., 1975, Magnetic Bubbles, in: Craik, D. J., ed., Magnetic Oxides, Part 2 (John Wiley and Sons, New York) p. 743.

Bobeck, A. H., D. H. Smith, E. G. Spencer, L. G. Van Uitert and E. M. Walters, 1971, IEEE Trans. Magn. 7, 461.

Bozorth, R. M., V. Kramer and J. P. Remeika, 1958, Phys. Rev. Lett. 1, 3.

Brandle, C. D. and A. J. Valentino, 1972, J. Crystal Growth 12, 3.

Brandle, C. D. and S. L. Blank, 1976, IEEE Trans. Magn. 12, 14.

Brixner, L. H., 1974, Mater. Res. Bull. 9, 1041.

Brous, J., I. Fankuchen and E. Banks, 1953, Acta Crystallogr. 6, 67.

Buchanan, R. A., K. A. Wickersheim, J. J. Pearson and G. F. Herrmann, 1967, Phys. Rev. 159, 245.

Buchanan, R. A., J. J. Pearson and G. F. Herrmann, 1969, Solid State Commun. 7, 195.

Buhrer, C. F., 1969, J. Appl. Phys. 40, 4500.

Burbank, R. D., 1970, J. Appl. Crystallogr. 3, 112.

Callen, E. R., 1968, J. Appl. Phys. 39, 519.

Callen, E. R. and H. B. Callen, 1963, Phys. Rev. 129, 578.

Callen, E. R. and H. B. Callen, 1965, Phys. Rev. 139, A455.

Callen, H. B., 1971a, Appl. Phys. Lett. 18, 311.

Callen, H. B., 1971b, Mater. Res. Bull. 7, 931.

Cashion, J. D., A. H. Cooke, J. F. B. Hawkes, M. J. M. Leaske, T. L. Thorp and M. R. Wells, 1968a, J. Appl. Phys. 39, 1360.

Cashion, J. D., A. H. Cooke, M. J. M. Leaske, T. L. Thorp and M. R. Wells, 1968b, J. Mater. Sci. 3, 402.

Chetkin, M. V. and A. N. Shalygin, 1968, J. Appl. Phys. 39, 561.

Chiang, F. P., C. S. Faber and F. F. Y. Wang, 1971, J. Appl. Phys. 42, 1422.

Clark, A. E. and R. E. Strakna, 1961, J. Appl. Phys. 32, 1172.

Clark, A. E., B. F. DeSavage, N. Tsuya and S. Kawakami, 1966, J. Appl. Phys. 37, 1324.

Clark, A. E., J. J. Rhyne and E. R. Callen, 1968, J. Appl. Phys. 39, 573.

Cockayne, B., 1966, J. Amer. Ceram. Soc. 49, 204.

Coeuré, P., F. Forrat and J.-C. Gay, 1969, IEEE Trans. Magn. 5, 898.

Cohen, E., L. A. Risberg, W. A. Nordland, R. D. Burbank, R. C. Sherwood and L. G. Van Uitert, 1969, Phys. Rev. 186, 476.

Cohen, E., M. D. Sturge, R. J. Birgeneau, E. I. Blount, L. G. Van Uitert and J. K. Kjems, 1974, Phys. Rev. Lett. 32, 232.

Combarieu, A., J. Mareschal, J. Michel, J. Peyrard and J. Sivardière, 1968, C. R. Acad. Sci., Paris 267, 1169.

Comstock, R. L., 1965, Proc. IEEE 53, 1508.

Comstock, R. L., J. J. Raymond, W. G. Nilsen and J. P. Remeika, 1966, Appl. Phys. Lett. 9, 274.

Connolly, T. F. and E. D. Copenhaver, 1972, Bibliography of Magnetic Materials and Tabulation of Magnetic Transition Temperatures, Solid State Literature Guides, Vol. 5 (IFI/Plenum Press, New York).

Cooke, A. H., T. L. Thorp and M. R. Wells, 1967, Proc. Phys. Soc., London 92, 400.

Cooper, R. W., W. A. Crossley, J. L. Page and R. F. Pearson, 1968, J. Appl. Phys. 39, 565.

Coppens, P. and M. Eibschütz, 1965, Acta Crystallogr. 19, 524.

Courths, R., S. Hüefner and J. Pelzl, 1970, Solid State Commun. 8, 1163.

Coutures, J. and M. Foex, 1974, J. Solid State Chem. 11, 294.

Cox, D. E., 1972, IEEE Trans. Magn. 8, 161.

Cox, D. E., G. Shirane and B. C. Frazer, 1967, J. Appl. Phys. 38, 1459.

Croft, W. J., 1965, Amer. Mineral. 50, 1634.

Crossley, W. A., R. W. Cooper, J. L. Page and R. P. Van Stapele, 1969, J. Appl. Phys. 40, 1497.

Crosswhite, H. M. and H. W. Moos, 1967, Optical Properties of Ions in Crystals (Wiley-Interscience, New York) p. 3.

Dalziel, J. A. W., 1959, J. Chem. Soc., London 1959, 1993.

Damen, J. P. M. and J. M. Robertson, 1972, J. Crystal Growth 16, 50.

Demazeau, G., M. Pouchard and P. Hagenmuller, 1974, J. Solid State Chem. 9, 202.

Derighetti, B., J. E. Drumheller, F. Laves, K. A. Müller and F. Waldner, 1965, Acta Crystallogr. 18, 557.

Dernier, P. D. and R. G. Maines, 1971, Mater. Res. Bull. 6, 433.

Dieke, G. H. and H. M. Crosswhite, 1963, Appl. Opt. 2, 675.

Dillon, J. F., Jr., 1958, J. Appl. Phys. 29, 539.

Dillon, J. F., Jr., 1968, J. Appl. Phys. 39, 922.

Dionne, G. F., 1970, J. Appl. Phys. 41, 2264.

Donnay, G., L. M. Corliss, J. D. H. Donnay, N. Elliott and J. M. Hastings, 1958, Phys. Rev. 112, 1917.

Dougier, P. and A. Casalot, 1970, J. Solid State Chem. 2, 396.

Dougier, P. and P. Hagenmuller, 1975, J. Solid State Chem. 15, 158.

Douglass, R. L., 1960, Phys. Rev. 120, 1612.

Douglass, R. L., 1963, Phys. Rev. 129, 1132.

Dreyfus, B., J. Verdone and M. Veyssie, 1965, J. Phys. Chem. Solids 26, 107.

Drofenik, M., D. Kolar and L. Golic, 1973, J. Crystal Growth 20, 75.

Dwyer, F. G., 1972, Catalysis Rev. 6, 261.

Eibschütz, M., 1965, Acta Crystallogr. 19, 337.

Elwell, D. and H. J. Scheel, 1975, Crystal Growth from High Temperature Solutions (Academic Press, New York).

Enz, U., W. Lems, R. Metselaar, P. J. Rignierse and R. W. Teale, 1969, IEEE Trans. Magn. 5, 467.

Espinosa, G. P. and S. Geller, 1964, J. Appl. Phys. 35, 2551.

Euler, F. and J. A. Bruce, 1965, Acta Crystallogr. 19, 971.

Faucher, M. and P. Caro, 1975, Mater. Res. Bull. 10, 1.

Fayolle, J., F. Studer, G. Desgardin and B. Raveau, 1975, J. Solid State Chem. 13, 57.

Fesenko, E. G. and G. A. Geguzina, 1973, Soviet Phys.-Crystallogr. 18, 336.

Fisher, M. E., 1960, Proc. Roy. Soc., Ser. A 254, 66.

Flanders, P. J., C. D. Graham, Jr., J. F. Dillon, Jr., E. M. Gyorgy and J. P. Remeika, 1971, J. Appl. Phys. 42, 1443.

Flicstein, J. and M. Schieber, 1973, J. Crystal Growth 18, 265.

Freiser, M. J., 1968, IEEE Trans. Magn. 5, 152.

Friedberg, S. A. and E. D. Harris, 1963, Proc. Int. Conf. Low Temp. Phys., 8th, 1962, p. 302.

Fukanaga, O. and T. Fujita, 1973, J. Solid State Chem. 8, 331.

Gai, P. L. and C. N. R. Rao, 1975, Mater. Res. Bull. 10, 787.

Galasso, F. S., 1969, Structure, Properties and Preparation of Perovskite-type Compounds (Pergamon Press, Hungary).

Galasso, F. S., L. Katz and R. Ward, 1959, J. Amer. Chem. Soc. 81, 820.

Galasso, F. S. and W. Darby, 1963, J. Phys. Chem. 66, 131.

Galasso, F. S., G. K. Layden and D. E. Flinchbaugh, 1966, J. Chem. Phys. 44, 2703.

Gallagher, P. K., D. W. Johnson, Jr. and F. Schrey, 1974, Mater. Res. Bull. 9, 1345.

Gallagher, P. K., D. W. Johnson, Jr., J. P. Remeika, F. Schrey, L. E. Trimble, E. M. Vogel and R. J. H. Voorhoeve, 1975a, Mater. Res. Bull. 10, 529.

Gallagher, P. K., D. W. Johnson, Jr., E. M. Vogel and F. Schrey, 1975b, Mater. Res. Bull. 10, 623.

Ganguly, P. and C. N. R. Rao, 1973, Mater. Res. Bull. 8, 405.

Garton, G. and B. M. Wanklyn, 1967, J. Crystal Growth 1, 164.

Garton, G., B. F. Hann, B. M. Wanklyn and S. H. Smith, 1972, J. Crystal Growth 12, 66.

Geller, S., 1956, J. Chem. Phys. 24, 1236.

Geller, S., 1957a, Acta Crystallogr. 10, 243.

Geller, S., 1957b, Acta Crystallogr. 10, 248.

Geller, S., 1966, J. Appl. Phys. 37, 1408.

Geller, S., 1967, Z. Kristallogr., Kristagggeomtrie, Kristallphys., Kristallchem. 125, 1.

Geller, S. and V. B. Bala, 1956, Acta Crystallogr. 9, 1019.

Geller, S. and E. A. Wood, 1956, Acta Crystallogr. 9, 563.

Geller, S. and M. A. Gilleo, 1957, J. Phys. Chem. Solids 3, 30.

Geller, S., H. J. Williams, R. C. Sherwood, J. P. Remeika and G. P. Espinosa, 1963, Phys. Rev. 131, 1080.

Geller, S., H. J. Williams, G. P. Espinosa and R. C. Sherwood, 1964, Bell Syst. Tech. J. 43, 565.

Geller, S., G. P. Espinosa and P. B. Crandall, 1969, J. Appl. Crystallogr. 2, 86.

Geller, S., P. J. Curlander and G. F. Ruse, 1974, Mater. Res. Bull. 9, 637.

Gendelev, S. S. and N. G. Shcherbak, 1966, Soviet Phys.-Crystallogr. 10, 592.

Gendelev, S. S. and A. G. Titova, 1971, Bull. Acad. Sci., USSR, Phys. Ser. 6, 1131.

Giess, E. A., 1962, J. Amer. Ceram. Soc. 45, 53.

Giess, E. A., D. C. Cronemeyer, L. L. Rosier and J. D. Kuptsis, 1970, Mater. Res. Bull. 5, 495.

Giess, E. A., J. D. Kuptsis and E. A. D. White, 1972, J. Crystal Growth 16, 36.

Gilleo, M. A., 1956, J. Chem. Phys. 24, 1239.

Gilleo, M. A., 1957, Acta Crystallogr. 10, 161.

Gilleo, M. A., 1960, J. Phys. Chem. Solids 13, 33.

Glazer, A. M., 1972, Acta Crystallogr. B28, 3384.

Glazer, A. M., 1975, Acta Crystallogr. A31, 756.

Goldschmidt, V. M., 1926, Skrifter Norske Videnskaps-Akad. Oslo, I. Mat.-Naturv. Kl., No. 8.

Goodenough, J. B., 1955, Phys. Rev. 100, 564.

Goodenough, J. B., 1958, J. Phys. Chem. Solids 6, 287.

Goodenough, J. B., 1966, J. Appl. Phys. 37, 1415.

Goodenough, J. B., 1968, Magnetism and the Chemical Bond (John Wiley and Sons, New York) pp. 165-184.

Goodenough, J. B. and P. M. Raccah, 1965, J. Appl. Phys. 36, 1031.

Goodenough, J. B. and J. M. Longo, 1970, in Magnetic and Other Properties of Oxides and Related Compounds, Hellwege, K. H., ed., Landolt-Bornstein, Vol. 4 (Springer-Verlag, New York) p. 126.

Goodenough, J. B., J. A. Kafalas and J. M. Longo, 1972, High Pressure Synthesis, in: Hagenmuller, P., ed., Preparative Methods in Solid State Chemistry (Academic Press, New York) p. 2.

Gorodetsky, G., B. Sharon and S. Shtrikman, 1968, J. Appl. Phys. 39, 1371.

Gorodetsky, G., R. M. Hoenreich, I. Yaeger, H. Pinto, G. Shachar and H. Shaked, 1973, Phys. Rev. B8, 3398.

Graham, L. J. and R. Chang, 1970, J. Appl. Phys. 41, 2247.

Granicher, H., K. Hubner and K. A. Müller, 1957, Helv. Phys. Acta 30, 480.

Greedan, J. E., G. J. McCarthy and C. Sipe, 1975, Inorg. Chem. 14, 775.

Grünberg, P., K. H. Hellwege and S. Hüfner, 1967, Phys. Kondens. Mater. 6, 95.

Grünberg, P., S. Hüfner, E. Orlich and J. Schmitt, 1969, J. Appl. Phys. 40, 1501.

Gupta, T. K. and J. Valentich, 1971, J. Amer. Ceram. Soc. 54, 355.

Gyorgy, E. M., J. T. Krause, R. C. LeCraw, L. R. Testardi and L. G. Van Uitert, 1967, J. Appl. Phys. 38, 1226.

Gyorgy, E. M., J. P. Remeika and F. B. Hagedorn, 1968, J. Appl. Phys. 39, 1369.

Gyorgy, E. M., J. F. Dillon, Jr. and J. P. Remeika, 1971, J. Appl. Phys. 42, 1454.

Harley, R. T., W. Hayes, A. M. Perry and S. R. P. Smith, 1973, J. Phys. C: Solid State 6, 2382.

Harris, A. B., 1963, Phys. Rev. 132, 2398.

Harris, A. B. and H. Meyer, 1962, Phys. Rev. 127, 101.

Heikes, R. R., R. C. Miller and R. Mazelsky, 1964, Physica 30, 1600.

Hellwege, K. H., S. Hüfner, M. Schinkman and H. Schmidt, 1966, Phys. Kondens. Mater. 4, 396.

Henderson, A. J., Jr., D. G. Onn, H. Meyer and J. P. Remeika, 1969, Phys. Rev. 185, 1218.

Herpin, A., W. C. Koehler and P. Meriel, 1960, C. R. Acad. Sci. Paris 251, 1359.

Herpin, A. and P. Meriel, 1964, C. R. Acad. Sci. Paris 259, 2416.

Hewitt, B. S., R. D. Pierce, S. L. Blank and S. Knight, 1973, IEEE Trans. Magn. 9, 366.

Holland, M. G., 1968, IEEE Trans. Sonics Ultrason. 15, 18.

Holmes, L., R. Sherwood and L. G. Van Uitert, 1968, J. Appl. Phys. 39, 1373.

Holmes, L., L. G. Van Uitert and R. Hecker, 1971a, J. Appl. Phys. 42, 657.

Holmes, L., L. G. Von Uitert and G. W. Hull, 1971b, Solid State Commun. 9, 1373.

Holtwijk, T., W. Lems, A. G. H. Verhulst and U. Enz, 1970, IEEE Trans. Magn. 6, 853.

Hu, H. L. and E. A. Geiss, 1975, IEEE Trans. Magn. 11, 1085.

Hüefner, S., L. Holmes, F. Varsanyi and L. G. Van Uitert, 1968, Phys. Rev. 171, 507.

Hurrell, J. P., S. P. S. Porto, I. F. Chang, S. S. Mitra and R. P. Bauman, 1968, Phys. Rev. 173, 851.

Iida, S., 1963, Phys. Lett. 6, 165.

Iida, S., 1967, J. Phys. Soc. Japan 22, 1201.

Iwahashi, K. and S. Iida, 1965, J. Phys. Soc. Japan 20, 1526.

Jacobson, A. J., B. C. Toefield and B. E. F. Fender, 1972, Acta Crystallogr. B28, 956.

Janes, D. L. and R. E. Bodnar, 1971, J. Appl. Phys. 42, 1500.

Johnson, B. and A. K. Walton, 1965, Brit. J. Appl. Phys. 16, 475.

Johnson, D. W., Jr., P. K. Gallagher, F. Schrey and W. W. Rhodes, 1976, Amer. Ceram. Soc. Bull. 55, 520.

Jones, R. V., 1966, IEEE Trans. Sonics Ultrason. 13, 86.

Jonker, G. H., 1954, Physica 20, 1118.

Jonker, G. H., 1956, Physica 22, 707.

Jonker, G. H., 1966, J. Appl. Phys. 37, 1424.

Jonker, G. H. and J. H. Van Santen, 1950, Physica 16, 337.

Jonker, G. H. and J. H. Van Santen, 1953, Physica 19, 120.

Joshi, A. W. and K. P. Sinha, 1966, Proc. Phys. Soc., London 88, 685.

Kahn, F. J., P. S. Pershan and J. P. Remeika, 1969a, J. Appl. Phys. 40, 1508.

Kahn, F. J., P. S. Pershan and J. P. Remeika, 1969b, Phys. Rev. 186, 891.

Kanamori, J., 1959, J. Phys. Chem. Solids 10, 87.

Kanamori, J., 1963, Anisotropy and Magnetostriction of Ferromagnetic and Antiferromagnetic Materials, Rado, G. T. and H. Suhl, eds., Magnetism, Vol. 1 (Academic Press, New York) p. 217.

Keen, B. E., D. P. Landau, B. Schneider and W. P. Wolf, 1966, J. Appl. Phys. 37, 1120.

Keith, M. L. and R. Roy, 1954, Amer. Mineral. 39, 1.

Keller, C., 1965, J. Inorg. Nucl. Chem. 27, 321.

Khattak, C. P., D. E. Cox and F. F. Y. Wang, 1973, AIP Conf. Proc. No. 10, 674.

Khattak, C. P., 1974, unpublished research.

Khattak, C. P., D. E. Cox and F. F. Y. Wang, 1975, J. Solid State Chem. 13, 77.

Khattak, C. P., D. E. Cox and F. F. Y. Wang, 1976, J. Solid State Chem. 17, 323.

Kim, Y. S., 1968, Acta Crystallogr. B24, 295.

Kiro, D., W. Low and A. Zusman, 1963, in: Low, W., ed., Paramagnetic Resonance, Vol. 1 (Academic Press, New York) p. 44.

Kjems, J. K., G. Shirane, K. A. Müller and H. J. Scheel, 1973a, Phys. Rev. B8, 1119.

Kjems, J. K., G. Shirane, R. J. Birgeneau and L. G. Van Uitert, 1973b, Phys. Rev. Lett. 31, 1300.

Klein, P. H. and W. J. Croft, 1967, J. Appl. Phys. 38, 1603.

Klokhohm, E., 1969, Rev. Sci. Instrum. 40, 1054.

Klokhohm, E., J. W. Matthews, A. F. Mayadas and J. Angilello. 1972, AIP Conf. Proc. No. 5, Part 1, 105.

Knight, W. D. and D. L. Huber, 1968, J. Appl. Phys. 39, 1069.

Koehler, W. C. and E. O. Wollan, 1957, J. Phys. Chem. Solids 2, 100.

Koehler, W. C., E. O. Wollan and M. K. Wilkinson, 1960, Phys. Rev. 118, 58.

Koenig, J. and B. Jaffe, 1964, J. Amer. Ceram. Soc. 47, 87.

Kolb, E. D. and R. A. Laudise, 1971, J. Appl. Phys. 42, 1552.

Kolb, E. D., D. L. Wood, E. G. Spencer and R. A. Laudise, 1967, J. Appl. Phys. 38, 1027.

Kolb, E. D., D. L. Wood and R. A. Laudise, 1968, J. Appl. Phys. 39, 1362.

Koningstein, J. A., 1964, Phys. Rev. 136A, 717.

Koningstein, J. A., 1966, Theor. Chim. Acta 5, 327.

Koningstein, J. A. and T. Ng, 1969, Solid State Commun. 1, 351.

Krinchik, G. S. and N. V. Chetkin, 1962, Soviet Phys.-JETP 14, 485.

Landau, D. P. and G. S. Dixon, 1970, Bull. Amer. Phys. Soc. [2] 15, 1381.

Laudise, R. A., 1970, The Growth of Single Crystals (Prentice Hall, New Jersey).

Laudise, R. A., R. C. Linares and E. F. Dearborn, 1962, J. Appl. Phys. 33, 1362.

Laudise, R. A., J. R. Carruthers and K. A. Jackson, 1971. In Annual Review of Materials Science, Huggins, R. A., R. H. Bube and R. W. Robers, eds., (Annual Review, California) Vol. 1, p. 253.

Leake, J. A., G. Shirane and J. P. Remeika, 1968, Solid State Commun. 6, 15.

Leask, M. J. M., 1968, J. Appl. Phys. 39, 908.

LeCraw, R. C., D. L. Wood, J. F. Dillon, Jr. and J. P. Remeika, 1965, Appl. Phys. Lett. 7, 27.

LeCraw, R. C., R. Wolfe, A. H. Bobeck, R. D. Pierce and L. G. Van Uitert, 1971, J. Appl. Phys. 42, 1641.

Lefever, R. A., K. A. Wickersheim and A. B. Chase, 1965, J. Phys. Chem. Solids 26, 1529.

Libby, W. F., 1971, Science 171, 499.

Linares, R. C., 1962a, J. Appl. Phys. 33, 1747.

Linares, R. C., 1962b, J. Amer. Ceram. Soc. 45, 307.

Lüthi, B., 1962, J. Phys. Chem. Solids 23, 35.

Lyubutin, I. S. and Yu. S. Vishnyakov, 1973, Soviet Phys.-Crystallogr. 17, 847.

Malozemoff, A. P., 1971, J. Phys. Chem. Solids 32, 1669.

Mareschal, J., J. Sivardière and G. F. DeVries, 1968, J. Appl. Phys. 39, 1364.

Marezio, M., J. P. Remeika and P. D. Dernier, 1966, Mater. Res. Bull. 1, 247.

Marezio, M., J. P. Remeika and P. D. Dernier, 1968, Inorg. Chem. 7, 1337.

Marezio, M., J. P. Remeika and P. D. Dernier, 1970, Acta Crystallogr. B26, 2008.

McCarthy, G. J. and J. E. Greedan, 1975, Inorg. Chem. 14, 772.

McCarthy, G. J., W. B. White and R. Roy, 1969, Mater. Res. Bull. 4, 251.

McCarthy, G. J., P. V. Gallagher and C. Sipe, 1973, Mater. Res. Bull. 8, 1277.

McCarthy, G. J., C. A. Sipe and K. E. McIlvried, 1974, Mater. Res. Bull. 9, 1279.

McDevitt, N. T., 1969, J. Opt. Soc. Amer. 59, 1240.

McGuire, T. R., M. W. Shafer and R. J. Joenk, 1966, J. Appl. Phys. 37, 981.

Meadowcroft, D. B., 1968, Energy Conversion 8, 185.

Meadowcroft, D. B., 1969, Brit. J. Appl. Phys. (J. Phys. D) Ser. 2, 2, 1225.

Meadowcroft, D. B., 1970, Nature 226, 847.

Megaw, H. D., 1946, Proc. Phys. Soc. 58, 133, 326.

Megaw, H. D., 1968a, Acta Crystallogr. A24, 583.

Megaw, H. D., 1968b, Acta Crystallogr. A24, 589.

Megaw, H. D., 1968c, Acta Crystallogr. B24, 149.

Megaw, H. D., 1972, J. Phys., Paris 33, Suppl. C2, 1.

Megaw, H. D. and C. N. W. Darlington, 1975, Acta Crystallogr. A31, 161.

Meltzer, R. S., 1970, Phys. Rev. B2, 2398.

Menyuk, N., K. Dwight and P. M. Raccah, 1967, J. Phys. Chem. Solids 28, 549.

Merker, L. and K. D. Herrington, 1964, Appl. Opt. 3, 1311.

Mikami, I., 1973, J. Phys. Soc. Japan 34, 338.

Mikami, I., M. Hirano and G. Kamoshita, 1973, Jap. J. Appl. Phys. 12, 557.

Mill', B. V., 1965, Dokl. Akad. Nauk SSSR 165, 555.

Milward, R. C., 1967, Phys. Lett. A25, 19.

Miyadai, T., 1960, J. Phys. Soc. Japan 15, 2205.

Moreau, J. M., J. Mareschal and E. F. Bertaut, 1968, Solid State Commun. 6, 751.

Morrish, A. H., 1965, The Physical Principles of Magnetism (John Wiley and Sons, New York) p. 500.

Morrish, A. H., B. J. Evans, J. A. Eaton and L. K. Leung, 1969, Can. J. Phys. 47, 2691.

Moskvin, A. S. and E. V. Sinitsyn, 1973a, Soviet Phys.-Solid State 14, 2198.

Moskvin, A. S. and E. V. Sinitsyn, 1973b, Soviet Phys.-Solid State 14, 2363.

Müller, O. and R. Roy, 1974, in: Crystal Chemistry of Non-metallic Materials, R. Roy ed., No. 4 (Spring-Verlag, New York) p. 153.

Muller, K. A., W. Berlinger and F. Waldner, 1968, Phys. Rev. Lett. 21, 814.

Muller-Buschbaum, H. K. and C. Teske, 1968, J. Inorg. Nucl. Chem. Lett. 4, 151.

Naiman, C. S., B. DiBartolo, A. Linz and R. Santoro, 1965, J. Appl. Phys. 36, 879.

Nakada, I., R. Akaba and T. Yanase, 1972, Jap. J. Appl. Phys. 11, 1583.

Néel, L., 1948, Ann. Phys. (Paris) 3, 137.

Nielsen, J. W., 1960, J. Appl. Phys, 31, 51S.

Nikolaev, V. I. and V. S. Rusakov, 1976, Soviet Phys.-Crystallogr. 20, 519.

Nilsen, W. G., R. L. Comstock and L. R. Walker, 1965, Phys. Rev. 139, A472.

Nomura, S. and T. Nakagawa, 1966, J. Phys. Soc. Jap. 21, 1068.

Novak, G. A. and G. V. Gibbs, 1971, Amer. Mineral. 56, 791.

Obayashi, H. and T. Kudo, 1975, Jap. J. Appl. Phys. 14, 330.

Obayashi, H., Y. Sakurai and T. Gejo, 1976, J. Solid State Chem. 17, 299.

Ohbayashi, H., T. Kudo and T. Gejo, 1974, Jap. J. Appl. Phys. 13, 1.

Oliver, D. W. and G. A. Slack, 1966, J. Appl. Phys. 37, 1542.

Oliver, D. W., G. A. Slack and J. D. Young, 1969a, 1st Semiannual Report, Air Force Mater. Lab. Contract No. F33615-69-C-1286, Proj. No. 7371, June 1969, S-69-1103, General Electric R. & D. Center.

Oliver, D. W., G. A. Slack and J. D. Young, 1969b, 2nd Semiannual Report, Air Force Mater. Lab. Contract No. F33615-69-C-1286, Proj. No. 7371, December 1969, S-69-1176, General Electric R. & D. Center.

Onn, D. G., J. P. Remeika, H. Meyer and A. J. Henderson, Jr., 1967, J. Appl. Phys. 38, 1023.

Opechowski, W. and R. Guccione, 1965, Magnetic Symmetry, in Rado, G. T. and H. Shull eds., Magnetism, Vol. II A (Academic Press, New York) p. 105.

Orlich, E. and S. Hüfner, 1969, J. Appl. Phys. 40, 1503.

Parker, R., 1975, Electrical Transport Properties, in: Craik, D. J. ed., Magnetic Oxides, Part 1 (John Wiley and Sons, New York) p. 421.

Pataud, P. and J. Sivardière, 1970a, J. Phys., Paris 31, 803.

Pataud, P. and J. Sivardière, 1970b, J. Phys., Paris 31, 1017.

Patton, C. E., 1970, J. Appl. Phys. 41, 1637.

Pierce, R. D., R. Wolfe and L. G. Van Uitert, 1969, J. Appl. Phys. 40, 1241.

Pauthenet, R., 1956, C. R. Acad. Sci., Paris 242, 1859.

Pauthenet, R., 1957, Thesis, Grenoble, France.

Pauthenet, R., 1958, J. Appl. Phys. 29, 253.

Pearson, J. J., G. F. Herrmann and R. A. Buchanan, 1968, J. Appl. Phys. 39, 980.

Pearson, R. F., 1962, J. Appl. Phys. 33, 1236.

Pearson, R. F., A. D. Annis and P. Kompfner, 1968, Phys. Rev. Lett. 21, 1805.

Perel, J. and M. Schieber, 1962, Jap. J. Appl. Phys. 1, 243.

Pershan, P. S., 1967, J. Appl. Phys. 38, 1482.

Philp, J. W., R. Gonono and E. D. Adams, 1969, J. Appl. Phys. 40, 1275.

Phillips, T. G. and R. L. White, 1966, Phys. Rev. Lett. 16, 650.

Phillips, T. G. and R. L. White, 1967, Phys. Rev. 160, 316.

Pickart, S. J., H. A. Alperin and A. E. Clark, 1970, J. Appl. Phys. 41, 1192.

Pinto, H. and H. Shaked, 1972, Solid State Commun. 10, 663.

Pinto, H., G. Shachar, H. Shaked and S. Shtrikman, 1971, Phys. Rev. B3, 3861.

Prakash, O., P. Ganguly, G. Rama Rao, C. N. R. Rao, D. S. Rajoria and V. G. Bhide, 1974, Mater. Res. Bull. 9, 1173.

Quezel-Ambrunaz, S., 1968, Bull. Soc. France Mineral. Crystallogr. 91, 339.

Quezel-Ambrunaz, S. and M. Mareschal, 1963, Bull. Soc. France Mineral. Crystallogr. 86, 204.

Quon, H. H., A. Potvin and S. D. Entwistle, 1971, Mater. Res. Bull. 6, 1175.

Raccah, P. M. and J. B. Goodenough, 1967, Phys. Rev. 155, 932.

Rango, C., G. Tsoucaris and C. Zelwer, 1966, Acta Crystallogr. 20, 590.

Rao, C. N. R., O. Prakash and G. Ganguly, 1975, J. Solid State Chem. 15, 186.

Reddy, P. J. and J. Bhimasenacha, 1964, Acta Crystallogr. 17, 31.

Remeika, J. P., 1956, J. Amer. Ceram. Soc. 78, 4259.

Remeika, J. P. and T. Y. Kometani, 1968, Mater. Res. Bull. 3, 895.

Remeika, J. P., E. M. Gyorgy and D. L. Wood, 1969, Mater. Res. Bull. 4, 51.

Richards, P. L., 1963, J. Appl. Phys. 34, 1237.

Rives, J. E., G. S. Dixon and D. Walton, 1966, J. Appl. Phys. 40, 1555.

Robbins, M. G. K. Wertheim, A. Menth and R. C. Sherwood, 1969, J. Phys. Chem. Solids 30, 1823.

Robinson, M., A. H. Bobeck and J. W. Nielsen, 1971, IEEE Trans. Magn. 7, 464.

Rodrigue, G. P., H. Meyer and R. V. Jones, 1960, J. Appl. Phys. 31, 376S.

Rogers, D. B., A. Ferretti, D. H. Ridgley, R. J. Arnott and J. B. Goodenough, 1966, J. Appl. Phys. 37, 1431.

Roth, R. S., 1957, J. Res., Natl. Bur. Stds. 58, 75.

Rosencwaig, A. and W. J. Tabor, 1971, J. Appl. Phys. 42, 1643.

Rosencwaig, A., W. J. Tabor and R. D. Pierce, 1971, Phys. Rev. Lett. 36, 775.

Roy, R., 1954, J. Amer. Ceram. Soc. 37, 581.

Ruggiero, A. and R. Ferro, 1955, Gazz. Chim. Ital. 85, 892.

Ruiz, J. S., A. M. Anthony and M. Foëx, 1967, C. R. Acad. Sci., Paris 264, 1271.

Saburi, O., 1959, J. Phys. Soc. Japan 14, 1159.

Sakhnenko, V. P., E. F. Fesenko, A. T. Shuvaev, E. T. Shuvaeva and G. A. Geguzina, 1972, Soviet Phys.-Crystallogr. 17, 268.

Sato, K., G. Adachi and J. Shiokawa, 1975, Mater. Res. Bull 10, 113.

Sawatzky, E. and E. Kay, 1968, J. Appl. Phys. 39, 4700.

Sayer, M., R. Chen, R. Fletcher and A. Mansingh, 1975, J. Phys. C: Solid State Phys. 8, 2059.

Scheel, H. J., 1972, J. Crystal Growth 13/14, 560.

Scheel, H. J. and E. O. Schulz-Dubois, 1971, J. Crystal Growth 8, 304.

Schieber, M., 1964, J. Amer. Ceram. Soc. 47, 537.

Schneider, S. J. and R. S. Roth, 1960, J. Amer. Ceram. Soc. 43, 115.

Schneider, S. J., R. S. Roth and J. L. Waring, 1961, J. Res. Natl. Bur. Stds. 65A, 345.

Shafer, M. W., 1965, J. Appl. Phys. 36, 1145.

Shannon, R. D., 1967, Inorg. Chem. 6, 1474.

Shannon, R. D., 1970, Acta Crystallogr. B26, 447.

Shannon, R. D. and C. T. Prewitt, 1969, Acta Crystallogr. B25, 925.

Shapiro, S. M., J. D. Axe and J. P. Remeika, 1974, Phys. Rev. B10, 2014.

Sherwood, R. C., J. P. Remeika and H. J. Williams, 1959, J. Appl. Phys. 30, 217.

Shick, L. K. and J. W. Nielsen, 1971, J. Appl. Phys. 42, 1554.

Shin-ike, T., T. Sakai, G. Adachi and J. Shiokawa, 1976, Mater. Res. Bull. 11, 249.

Sievers, A. J. and M. Tinkham, 1963, Phys. Rev. 189, 1995.

Sis, L. B., G. P. Wirtz and S. C. Sorenson, 1973, J. Appl. Phys. 44, 5553.

Slack, G. A. and D. W. Oliver, 1971, Phys. Rev. B4, 592.

Slack, G. A., D. W. Oliver, R. M. Chrenko and S. Roberts, 1969, Phys. Rev. 177, 1308.

Soga, N., 1967, J. Geophys. Res. 72, 4227.

Solov'eva, A. E. and A. M. Gavrish, 1974, Inorg. Mater. 10, 1336.

Sorenson, S. C., J. A. Wronkiewicz, L. B. Sis and G. P. Wirtz, 1974, Amer. Ceram. Soc. Bull. 53, 446.

Spencer, E. G., R. T. Denton, T. B. Bateman, W. B. Snow and L. G. Van Uitert, 1963, J. Appl. Phys. 34, 3059.

Steward, E. G. and H. P. Rooksby, 1951, Acta Crystallogr. 4, 503.

Sturge, M. D., 1972, AIP Conf. Proc. No. 5, Part 1, 205.

Sugano, S., K. Aoyagi and K. Tsushima, 1971, J. Phys. Soc. Japan 31, 706.

Suits, J. C., 1972, IEEE Trans. Magn. 8, 95.

Tauber, A., C. G. Whinfrey and E. Banks, 1961, J. Phys. Chem. Solids 21, 25.

Teale, R. W. and D. W. Temple, 1967, Phys. Rev. Lett. 19, 904.

Thacher, P. D., 1967, Phys. Rev. 156, 975.

Tinkham, M., 1962, J. Appl. Phys. 33, 1248.

Toefield, B. C., A. J. Jacobson and B. E. F. Fender, 1972, J. Phys. C : Solid State Phys. 5, 2887.

Tolksdorf, W., 1975, IEEE Trans. Magn. 11, 1074.

Traverse, J., J. Coutures and M. Foëx, 1968, C. R. Acad. Sci., Paris 267, 391.

Treves, D., 1962, Phys. Rev. 125, 1843.

Treves, D., 1965, J. Appl. Phys. 36, 1033.

Tsushima, K., 1966, J. Appl. Phys. 37, 443.

Tsushima, K., K. Aoyagi and S. Sugano, 1970, J. Appl. Phys. 41, 1238.

Van Groenou, A. B., J. L. Page and R. F. Pearson, 1967, J. Phys. Chem. Solids 28, 1017.

Van Hook, H. J., 1961, J. Amer. Ceram. Soc. 44, 208.

Van Hook, H. J., 1962a, J. Amer. Ceram. Soc. 45, 162.

Van Hook, H. J., 1962b, J. Amer. Ceram. Soc. 45, 369.

Van Hook, H. J., 1963a, J. Amer. Ceram. Soc. 46, 121.

Van Hook, H. J., 1963b, J. Amer. Ceram. Soc. 46, 248.

Van Santen, J. H. and G. H. Jonker, 1950, Physica 16, 599.

Van Uitert, L. G., W. H. Grodkiewicz and E. F. Dearborn, 1965, J. Amer. Ceram. Soc. 48, 105.

Van Uitert, L. G., R. C. Sherwood, E. M. Gyorgy and W. H. Grodkiewicz, 1970a, Appl. Phys. Lett. 16, 84.

Van Uitert, L. G., R. C. Sherwood, W. A. Bonner, W. H. Grodkiewicz, L. Pictroski and G. Zydzik, 1970b, Mater. Res. Bull. 5, 153.

Varma, R. K., 1960, J. Geophys. Res. 65, 757.

Veyssie, M. and B. Dreyfus, 1967, J. Phys. Chem. Solids 28, 499.

Vigneron, F., 1976, J. Phys., Paris 37, 103.

Viskov, A. S., Yu. N. Venevtsev, G. S. Zhdanov and L. D. Onikienko, 1966, Soviet Phys.-Crystallogr. 10, 720.

Vogel, E. M. and J. W. Fleming, 1975, J. Crystal Growth 29, 234.

von Aulock, W. H. ed., 1965, Handbook of Microwave Ferrite Materials (Academic Press, New York).

Voorhoeve, R. J. H., J. P. Remeika, P. E. Freeland and B. T. Matthais, 1972, Science 177, 353.

Voorhoeve, R. J. H., J. P. Remeika and D. W. Johnson, Jr., 1973, Science 180, 62.

Voorhoeve, R. J. H., L. E. Trimble and C. P. Khattak, 1974, Mater. Res. Bull. 9, 655.

Voorhoeve, R. J. H., J. P. Remeika and L. E. Trimble, 1975a, Talk presented at Academy of Sciences, New York, to be published in Ann. of New York Acad. Sci. (in press).

Voorhoeve, R. J. H., J. P. Remeika, L. E. Trimble, A. S. Cooper, F. D. DiSalvo and P. K. Gallagher, 1975b, J. Solid State Chem. 14, 395.

Waintal, A. and J. Chenavas, 1967, Mater. Res. Bull. 2, 819.

Waintal, A., J. J. Capponi and E. F. Bertaut, 1966, Solid State Commun. 4, 125.

Wang, F. F. Y., 1973, Physical and Chemical Properties of Garnets in: Herman, H., ed., Treatise on Materials Science and Technology, Vol. 2 (Academic Press, New York) p. 279.

Wanklyn, B. M., 1969, J. Crystal Growth 5, 323.

Wanklyn, B. M., 1972, J. Mater. Sci. 7, 813.

Wanklyn, B. M., D. Midgley and B. K. Tanner, 1975, J. Crystal Growth 29, 281.

Weiss, G. P. and D. O. Smith,, 1962, J. Appl. Phys. 33, 1166S.

White, R. L., 1969, J. Appl. Phys. 40, 1061.

White, R. L. and T. G. Phillips, 1969, J. Appl. Phys. 39, 579.

Wold, A., B. Post and E. Banks, 1957, J. Amer. Ceram. Soc. 79, 6365.

Wold, A., R. J. Arnott and W. J. Croft, 1963, Inorg. Chem. 2, 972.

Wolf, W. P., 1957, Phys. Rev. 108, 1152.

Wolf, W. P., 1964, Proc. Int. Conf. Magnetism, p. 555.

Wolf, W. P., M. Ball, M. T. Hutchins, M. J. M. Leask and A. F. G. Wyatt, 1962, J. Phys. Soc. Japan 17, Suppl. B-1, 443.

Wolfe, R., M. D. Sturge, F. R. Merritt and L. G. Van Uitert, 1971, Phys. Rev. Lett. 26, 1570.

Wolfe, R., J. C. North and Y. P. Lai, 1973, Appl. Phys. Lett. 22, 683.

Wollan, E. O. and W. C. Koehler, 1955, Phys. Rev. 100, 545.

Wood, D. L. and J. P. Remeika, 1967, J. Appl. Phys. 38, 1038.

Wood, D. L., J. Ferguson, K. Knox and J. F. Dillon, Jr., 1963, J. Chem. Phys. 39, 890.

Wood, D. L., E. D. Kolb and J. P. Remeika, 1968, J. Appl. Phys. 39, 1139.

Wood, D. L., L. M. Holmes and J. P. Remeika, 1969, Phys. Rev. 185, 689.

Wood, E. A., 1951, Acta Crystallogr. 4, 353.

Woodruff, W. O. and H. Ehrenreich, 1961, Phys. Rev. 123, 1553.

Yafet, Y. and C. Kittel, 1952, Phys. Rev. 87, 290.

Yakel, Jr., H. L., 1955, Acta Crystallogr. 8, 394.

Yakel, H. L., W. C. Koehler, E. F. Bertaut and E. F. Forrat, 1963, Acta Crystallogr. 16, 957.

Yamaguchi, T., 1974, J. Phys. Chem. Solids 35, 479.

Yamaguchi, T. and K. Tsushima, 1973, Phys. Rev. B8, 5187.

Yoshida, K. and M. Tachiki, 1957, Progr. Theor. Phys. 17, 331.

Zeyfang, R., 1970, J. Appl. Phys. 41, 3718.

Zonn, Z. N., 1965, Inorganic Mater. 1, 1034.

Zonn, Z. N. and V. A. Joffe, 1968, Growth of Crystals 6A, 112.

Chapter 30

Subject Index

Perovskites and Garnets

Garnets, thermal expansion
Garnets, elastic properties
Garnets, elastic constants
Garnets, ultra-sonic attenuation

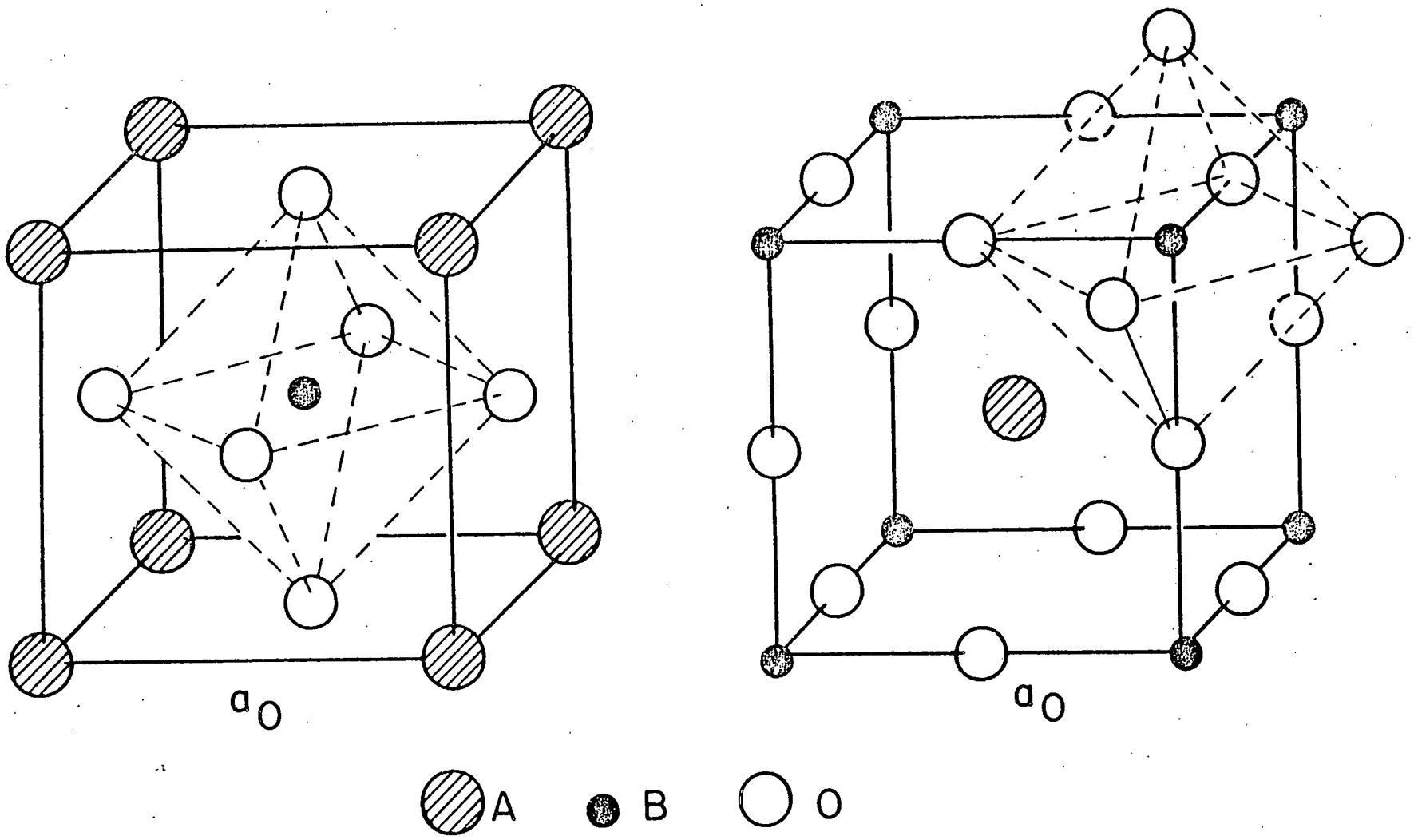

FIG. 30.1

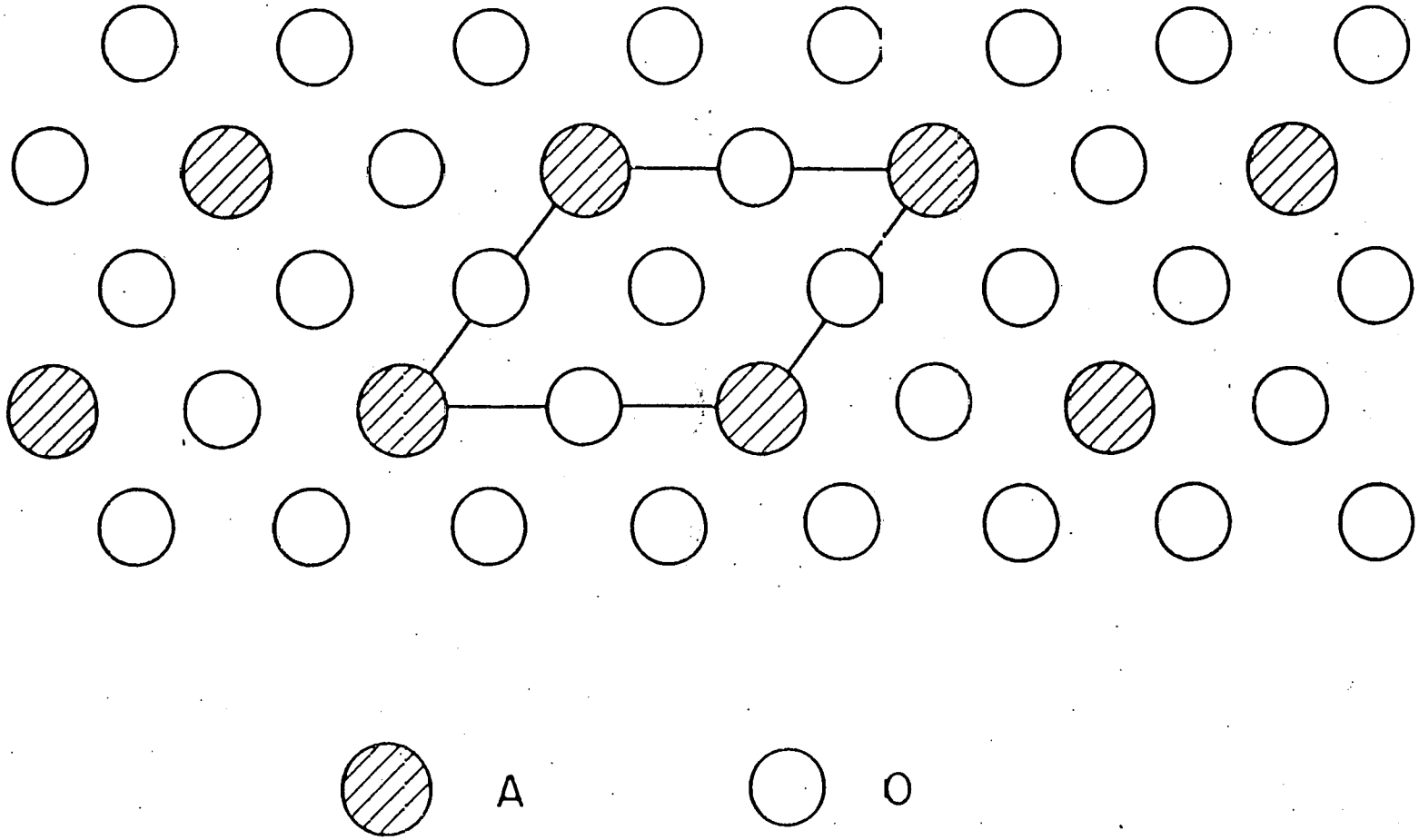

FIG. 30.2

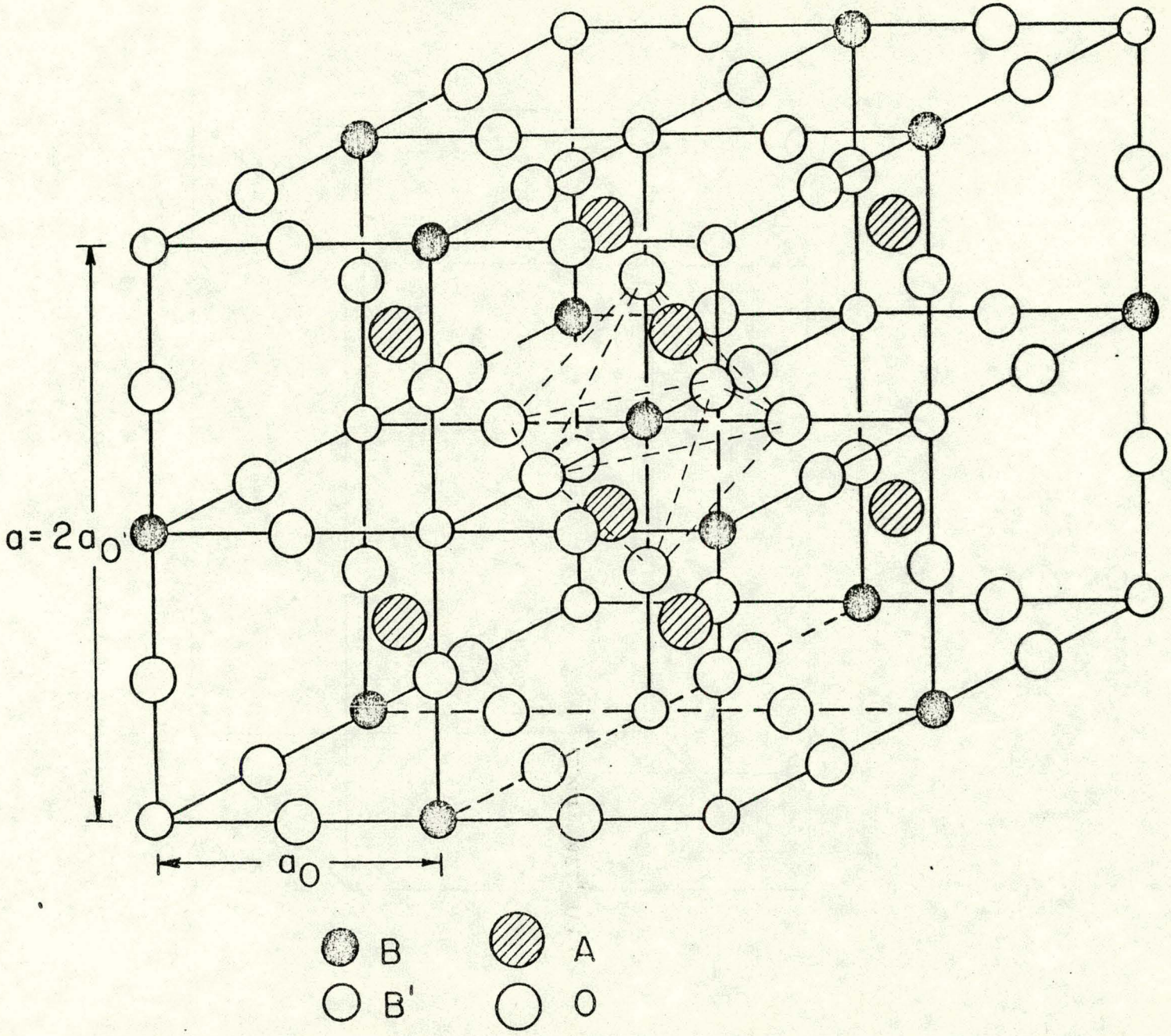

FIG. 30.3

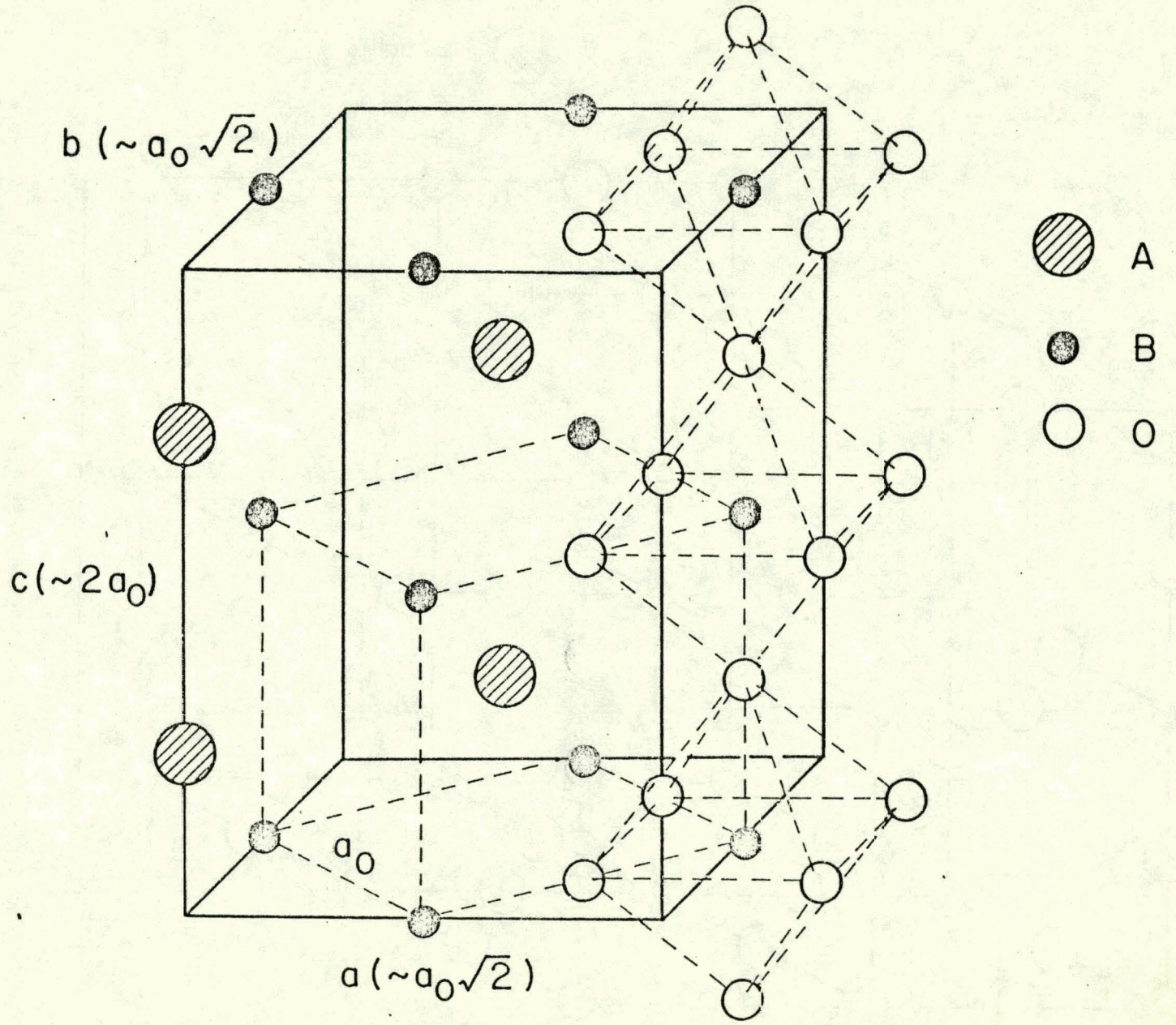

FIG. 30.4

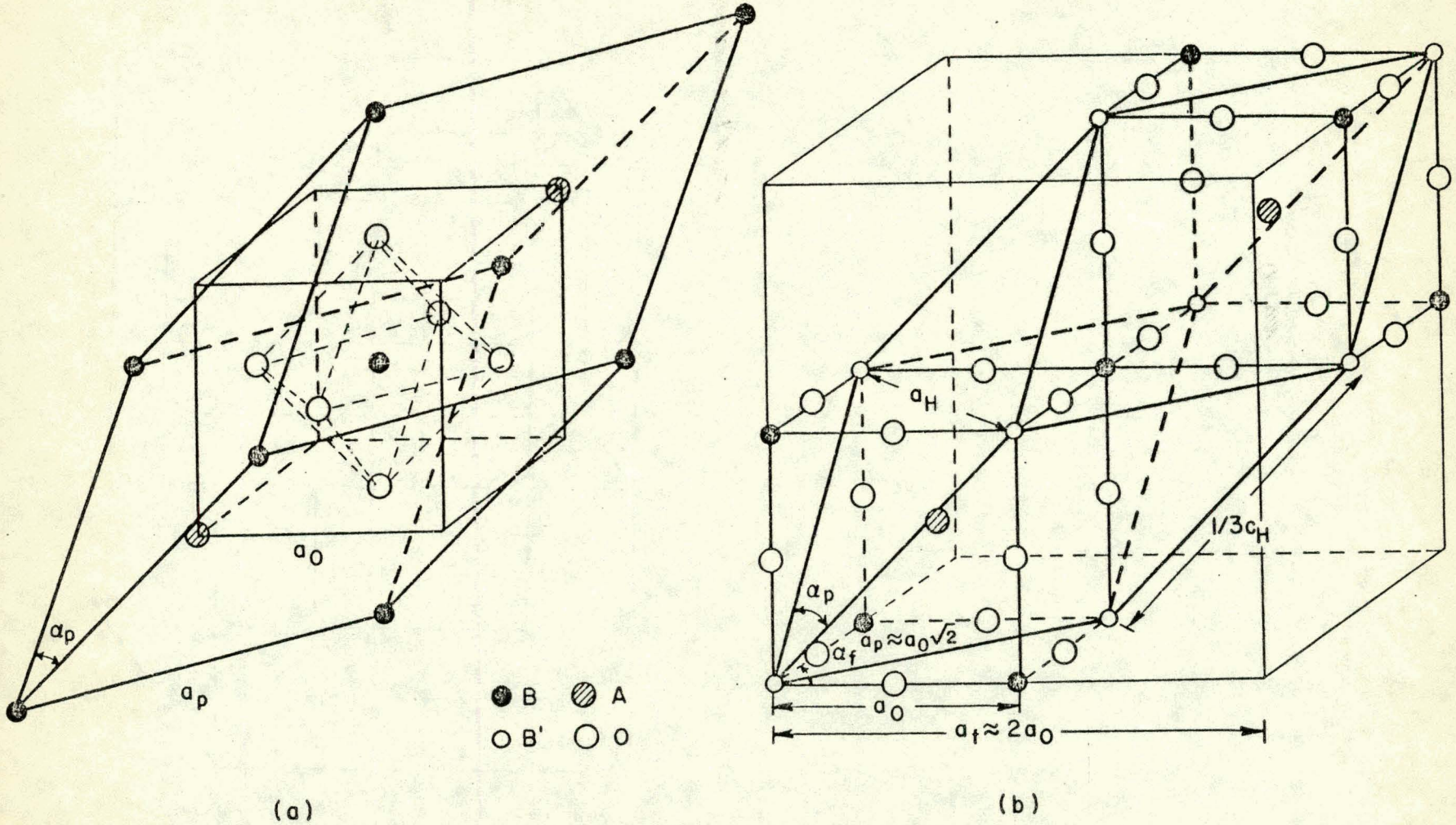
a_0
α_p
a_p
B
A
B'
O
(a)
a_H
$1/3c_H$
α_p
α_f
$a_p \approx a_0\sqrt{2}$
a_0
$a_f \approx 2a_0$
(b)

FIG. 30.5

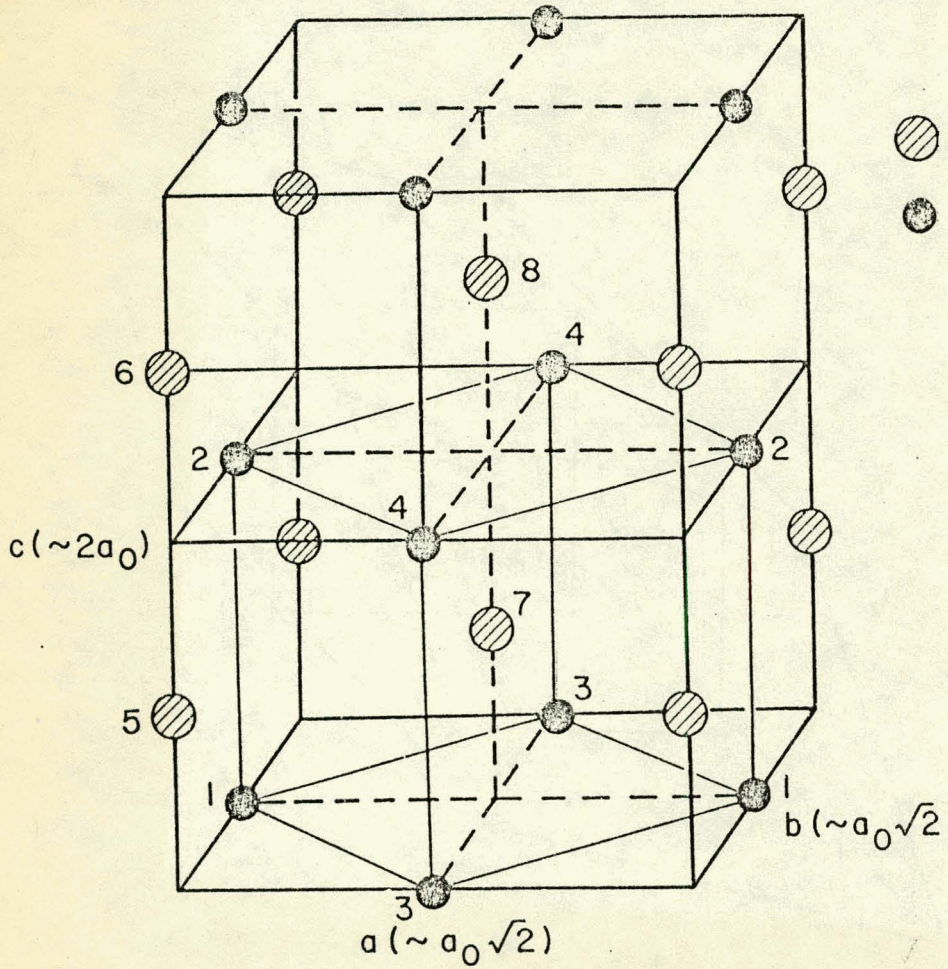

	s_1, s_5	s_2, s_6	s_3, s_7	s_4, s_8
F	+	+	+	+
C	+	+	−	−
A	+	−	+	−
G	+	−	−	+

FIG. 30.6